

Dynamics of cold molecules in electromagnetic fields

by

Sergey Alyabyshev

M.Sc., M.V. Lomonosov Moscow State University, 2005

A THESIS SUBMITTED IN PARTIAL FULFILLMENT
OF THE REQUIREMENTS FOR THE DEGREE OF

Doctor of Philosophy

in

THE FACULTY OF GRADUATE STUDIES
(Chemistry)

The University Of British Columbia
(Vancouver)

October 2012

© Sergey Alyabyshev, 2012

Abstract

The research field of cold and ultracold atoms and molecules is rapidly growing and expanding into different areas of research such as quantum information science and condensed matter physics. The success of this field is due to the possibility of precisely controlling and manipulating atoms and molecules at low temperatures. The progress in this field relies on the development of new methods for controlling collisional dynamics and interactions of particles with electromagnetic fields. This Thesis describes research on modification of the collisional dynamics of ultracold atoms and molecules by external laser and microwave fields as well as new methods for the detection of weak electromagnetic fields.

First, we study the scattering of atoms and molecules confined in a 2D geometry by optical lattices. In particular we develop a theory for scattering in 2D and derive the equations for the threshold dependence of the collision cross sections. We show that inelastic processes and chemical reactions can be suppressed under strong confinement in one dimension and can be controlled by varying the orientation of the external field with respect to the plane of confinement.

Next, we present a rigorous theory of low-temperature molecular collisions in the presence of a microwave field. The microwave field can theoretically be used to trap and control polar molecules. The molecular collisions may lead to trap loss and decoherence. We develop a rigorous quantum theory for molecular scattering in the presence of microwave fields. We study inelastic, spin-changing molecular collisions and Feshbach resonances in the presence of microwave fields. We demonstrate that inelastic collisions accompanied by absorption of microwave photons can be significant.

The detection of weak electromagnetic fields is very important for various ap-

plications ranging from fundamental measurements to biomagnetic imaging, and for tests of microwave chips. We present a method for the detection of weak electromagnetic fields in a wide range of frequencies from sub-kHz to THz with ultracold polar molecules. We show that using ultracold molecules one can achieve the sensitivity of two orders of magnitude larger than with a similar method based on ultracold Rb atoms.

Preface

The research project of Chapter 2 was identified by Roman Krems and lead to the publication in Ref. (I). The author performed the theoretical analysis. The computer code for calculations of the scattering cross sections in 2D was written by Zhying Li and Roman Krems. Numerical calculations were performed by Zhying Li. The theoretical results were analyzed by the author under the supervision of Roman Krems. The manuscript was drafted by the author in collaboration with Roman Krems and Zhying Li.

A part of the material presented in Chapter 3 has been published in Ref. (II). The project was designed by Roman Krems and Timur Tschربول. The author performed the numerical calculations and participated in the preparation of the manuscript.

The material presented in Chapters 4 and 5 has been published in Refs. (III) and Refs. (IV). The projects were identified and designed by the author under the supervision of Roman Krems. The author developed the theory, performed the numerical calculations and analyzed the results. The manuscript in Ref. (III) was written by the author under the supervision of Roman Krems. The manuscript in Ref. (IV) was drafted by Roman Krems.

The research project presented in Chapter 6 was suggested by Roman Krems. The author developed the theory and performed the numerical calculations. The important details and comments that expanded and improved the manuscript were suggested by Mikhail Lemeshko. The project resulted in the manuscript in Ref. (V). The manuscript was drafted by Mikhail Lemeshko in collaboration with the author and Roman Krems.

The following is a list of publications related to the work presented in this

thesis:

- (I) Z.Li, S.V. Alyabyshev, and R.V. Krems, *Ultracold inelastic collisions in two dimensions*, Phys. Rev. Lett. **100**, 073202 (2008)
- (II) S.V. Alyabyshev, T.V. Tscherbul, and R.V. Krems, *Microwave-laser-field modification of molecular collisions at low temperatures*, Phys. Rev. A **79**, 060703(R) (2009)
- (III) S.V. Alyabyshev and R.V. Krems, *Controlling collisional spin relaxation of cold molecules with microwave laser fields*, Phys. Rev. A **80**, 033419 (2009)
- (IV) S.V. Alyabyshev and R.V. Krems, *Greatly enhanced absorption of nonresonant microwave fields by ultracold molecules near a Feshbach resonance*, Phys. Rev. A **82**, 030702(R) (2010)
- (V) S.V. Alyabyshev, M. Lemeshko, and R. V. Krems, *Sensitive imaging of electromagnetic fields with paramagnetic polar molecules*, Phys. Rev. A **86**, 013409 (2012)

Table of Contents

Abstract	ii
Preface	iv
Table of Contents	vi
List of Figures	ix
Acknowledgments	xv
1 Introduction	1
1.1 Cold and ultracold atoms and molecules	2
1.1.1 Development of the field	2
1.1.2 Properties of cold and ultracold gases	3
1.2 Applications of cold and ultracold gases	6
1.2.1 Frequency standards and precision measurements	6
1.2.2 Quantum-degenerate gases	8
1.2.3 Optical lattices and quantum simulation	8
1.2.4 Quantum information processing and quantum computation	9
1.2.5 Detection of weak electromagnetic fields	9
1.3 Key concepts used in Thesis	10
1.3.1 Feshbach resonance	10
1.3.2 Dressed states	11
1.3.3 Low field and high field seeking states	12
1.3.4 Scattering cross section	13
1.4 Thesis outline	14

1.4.1	Quasi 2D confinement of quantum gases	14
1.4.2	Microwave field effects on dynamics of polar molecules	15
1.4.3	Imaging of weak electromagnetic fields with paramagnetic polar molecules	15
2	Ultracold inelastic collisions in two dimensions	17
2.1	Introduction	17
2.1.1	Ultracold collisions and Wigner's threshold laws in 3D	17
2.1.2	Ultracold gases in optical lattices	19
2.2	Scattering theory in 2D	21
2.2.1	Scattering in 2D	21
2.2.2	Wigner's threshold laws in 2D	24
2.2.3	Elastic scattering in 2D	27
2.2.4	Elastic m -changing scattering in 2D	29
2.2.5	Inelastic and reactive scattering	29
2.3	Threshold laws in the Born approximation	30
2.4	Discussion	32
2.5	Conclusion	34
3	Controlling molecular collisions with microwave fields	35
3.1	Introduction	35
3.2	Field-dressed approach	37
3.2.1	Semiclassical Floquet theory	37
3.2.2	Quantum theory	39
3.2.3	$^1\Sigma$ molecules in a microwave cavity	41
3.2.4	Scattering formalism	44
3.2.5	Coupled-channel calculations for atom-molecule scatter- ing in a microwave field	46
3.3	Conclusion	50
4	Controlling spin-changing collisions of $^2\Sigma$ molecules with microwave field	52
4.1	Introduction	52
4.2	$^2\Sigma$ molecules in combined dc magnetic and microwave fields	54

4.2.1	Field-dressed states	54
4.2.2	Avoided crossings of field-dressed states	58
4.3	Scattering calculations	64
4.3.1	Microwave field dependence	64
4.3.2	Resonances near avoided crossings	67
4.3.3	Collision energy dependence	68
4.4	Conclusion	68
5	Feshbach resonances in the presence of a microwave field	70
5.1	Introduction	70
5.2	Feshbach resonances	71
5.2.1	Feshbach resonances in a single scattering channel	71
5.2.2	Feshbach resonances in the presence of multiple open channels	73
5.2.3	Feshbach resonances in the presence of a microwave field	74
5.3	Conclusion	77
6	Sensitive imaging of electromagnetic fields with paramagnetic polar molecules	80
6.1	Introduction	80
6.2	Detection of weak radio-frequency fields with ultracold ⁸⁷ Rb atoms	81
6.3	Detection of weak electromagnetic fields with polar molecules	82
6.3.1	Polar paramagnetic molecule in parallel electric and magnetic field	82
6.3.2	Single-shot sensitivity	86
6.4	Conclusion	90
7	Conclusion	91
7.1	Overall conclusions of the dissertation	91
7.2	Contributions of the dissertation	92
7.3	Future research directions	93
	Bibliography	95

List of Figures

Figure 1.1	Schematic illustration of a Feshbach Resonance.	11
Figure 1.2	Manifolds of field-dressed states.	12
Figure 1.3	Schematic illustration of a magnetic field profile in a magnetic trap. The red and blue arrows indicate the projections of the spin corresponding to the low and high field seeking states. The black arrows indicate the direction of the force acting on particles in a magnetic trap.	13
Figure 2.1	Quasi-2D optical lattice (pancake) formed by interfering of 2 counterpropagating laser beams. The red line shows the ground state wavefunction of the ground state perpendicular to the confinement plane.	21
Figure 2.2	Optical lattices. (a) 2D optical lattice formed by superimposing 2 standing waves (b) 3D optical lattice formed by 3 standing waves. Adapted from Macmillan Publishers Ltd.: I.Bloch, Nature Physics 2005, 1, 23	22
Figure 2.3	Threshold dependence of cross sections for collisions of Li and Cs atoms in 2D: diamonds - 2-wave inelastic collisions; triangles up - p -wave inelastic collisions; triangles down - p -wave elastic collisions; circles - s -to- d -wave transitions. Symbols - numerical calculations; lines - analytical forms. The initial states are $m_{f_{Li}}=-2$ and $m_{f_{Cs}}=2$ the s -to- d wave transitions is calculated for the maximally stretched states.	25

Figure 3.1	Energy levels of a $^1\Sigma$ polar molecule in a microwave laser field as functions of the field-induced coupling strength Ω at a laser frequency $\hbar\omega/B_e = 0.8$. In the limit $\Omega \rightarrow 0$, the field-dressed states for $K = 0$ are: $(\alpha) - N = 0 M_N = 0 n = 0\rangle$, $(\beta) - N = 1 M_N = 0 n = -1\rangle$, $(\gamma) - N = 1 M_N = 1 n = -1\rangle$	43
Figure 3.2	Energy levels of a polar molecule in a microwave cavity as functions of the Rabi frequency at $\hbar\omega/B_e = 1.9$. The levels are grouped in manifolds labeled by K . The initial state for scattering calculations is shown by the dashed line. At $\Omega \rightarrow 0$, the field-dressed states for $K = -1$ are: $ N = 0, n = -1\rangle$ (α), $ N = 4, n = -11\rangle$ (β), $ N = 3, n = -7\rangle$ (γ), $ N = 1, n = -2\rangle$ (ξ), and $ N = 2, n = -4\rangle$ (δ).	47
Figure 3.3	Cross sections for elastic scattering (squares) and inelastic relaxation of CaH molecules induced by collisions with He in a microwave field with $\hbar\omega/B_e = 1.9$ (triangles), 1.1 (diamonds), and 0.01 (circles) as functions of the field intensity. The elastic cross section is for the microwave field frequency of $1.9B_e$. The inelastic cross sections are summed over all energetically accessible field-dressed states except the elastic channel. The collision energy is 0.3 cm^{-1}	48
Figure 3.4	State-resolved cross sections for inelastic relaxation of CaH in a microwave field with $\hbar\omega/B_e = 1.9$ and $\Omega/B_e = 0.5$. The collision energy is 0.3 cm^{-1} . The inelastic channels are labeled according to Fig. 3.2.	49
Figure 3.5	Modification of a shape resonance by microwave laser fields. The elastic cross section is plotted as a function of the collision energy for zero microwave field (full line), $\Delta/B_e = 1.5$ (dashed line), $\Delta/B_e = 0.1$ (dotted line). The Rabi frequency is $0.5B_e$. .	51

Figure 4.1	The field-dressed states of the $\text{CaH}(^2\Sigma)$ molecule as function of magnetic field in a microwave field with photon frequency $\hbar\omega/B_e = 0.7$ and $\Omega/B_e = 0.2$. The initial magnetic low-field seeking state (black dashed curve) correlates with $N = 0$ $n = 0$ $M_S = 1/2$ state at zero Ω . The solid (dashed) arrows show the spin-relaxation transitions corresponding to $\Delta n = 0$ ($\Delta n = -1$).	55
Figure 4.2	Upper panel: The field-dressed states of the $\text{CaH}(^2\Sigma)$ molecule in a magnetic field of 0.1 T and a microwave field with the photon frequency $\hbar\omega/B_e = 0.7$ as functions of Ω . Lower panel: Cross sections for spin relaxation in $\text{CaH}(^2\Sigma)$ -He collisions at a magnetic fields of 0.1 T and mw frequency of $\hbar\omega/B_e = 0.7$. The curves are labeled by the photon number of the final magnetic high-field seeking state at zero Ω . The collision energy is 0.5 K.	57
Figure 4.3	Upper panel: The eigenvalues of \hat{H}_0 (dashed lines) and the Zeeman energy levels of the $\text{CaH}(^2\Sigma)$ molecule in combined magnetic and microwave mw field. The microwave field parameters are $\hbar\omega/B_e = 1.9$ and the field-induced coupling strength $\Omega/B_e = 0.1$. Lower panel: Cross sections for spin relaxation in $\text{CaH}(^2\Sigma)$ -He collisions at a mw frequency of $\hbar\omega/B_e = 1.9$ and the field-induced coupling strength $\Omega/B_e = 0.1$. The curves are labeled by the photon number of the final magnetic high-field seeking state at zero Ω . The collision energy is 0.5 K.	59
Figure 4.4	The dependence of the position of the avoided crossing between the field-dressed states of $\text{CaH}(^2\Sigma)$ molecule in a microwave field with $\hbar\omega/B_e = 1.6$ (upper panel) and $\Omega/B_e = 0.5$ (lower panel).	60

- Figure 4.5 Modification of avoided crossings with changing polarization of the microwave field. The graphs show the magnetic field dependence of the field-dressed states at $\hbar\omega/B_e = 1.9$ and $\Omega/B_e = 1$. The photon polarization is linear $\hat{\mathbf{e}} = \hat{z}$ (upper panel), $\hat{\mathbf{e}} = (\hat{x} + i\hat{y})/\sqrt{2}$ (middle panel), $\hat{\mathbf{e}} = (\hat{x} - i\hat{y})/\sqrt{2}$ (lower panel). 62
- Figure 4.6 The field-dressed states of the CaH($^2\Sigma$) molecule in a magnetic field of 0.1 T and a microwave field with circular polarization $\hat{\mathbf{e}} = (\hat{x} + i\hat{y})/\sqrt{2}$ and $\hbar\omega/B_e = 0.7$ 63
- Figure 4.7 Upper panel: Adiabatic energy levels of the CaH molecule in a microwave field at $\Omega/B_e = 0.5$, $\hbar\omega/B_e = 1.7$ (red) and $\hbar\omega/B_e = 1.3$ (black) correlating with $|N = 0M_S = 1/2n = 0\rangle$ (solid line) and $|N = 1M_N = 1M_S = -1/2n = -1\rangle$ (dashed line) at zero Ω . Lower panel: Magnetic field dependence of the cross sections for spin relaxation in CaH-He collisions near an avoided crossing of the field-dressed states correlating with $|N = 0, n = 0\rangle$ and $|N = 1, n = -1\rangle$ states at zero Ω . $\Omega/B_e = 0.5$, $\hbar\omega/B_e = 1.7$ (circles), $\hbar\omega/B_e = 1.3$ (squares). . . 65
- Figure 4.8 Upper panel: Adiabatic energy levels of the CaH molecule in a microwave field at $\hbar\omega/B_e = 1.9$, $\Omega/B_e = 1$ (black) and $\Omega/B_e = 2$ (red) correlating with $|N = 0, M_S = 1/2, n = 0\rangle$ (solid line) and $|N = 1, M_N = 1, M_S = -1/2, n = -1\rangle$ (dashed line) at zero Ω . Lower panel: Magnetic field field dependence of cross sections for spin relaxation in CaH-He collisions near an avoided crossing of the field-dressed states correlating with $|N = 0, n = 0\rangle$ and $|N = 1, n = -1\rangle$ states at zero coupling. $\hbar\omega/B_e = 1.9$, $\Omega/B_e = 1$ (squares) and $\Omega/B_e = 2$ (circles). . . 66
- Figure 4.9 Collision energy dependence of the cross sections for spin relaxation in CaH-He collisions at a magnetic field of 0.1 T and zero microwave field (diamonds); $\hbar\omega/B_e = 0.7$ and $\Omega/B_e = 0.5$ (triangles up); $\hbar\omega/B_e$ and $\Omega/B_e = 0.5$ (triangles down); $\hbar\omega/B_e = 0.7$ and $\Omega/B_e = 1$ (circles); $\hbar\omega/B_e = 1.9$ and $\Omega/B_e = 1$ (squares). 67

Figure 5.1	Cross sections for elastic collisions (panel a) and collisions accompanied by absorption of microwave photons (panel b) in NH – He scattering as functions of the magnetic field: broken line – no microwave field; solid lines – in the presence of a microwave field with $\Omega = 0.02B_e$ and $\hbar\omega = 0.7B_e$, where $B_e = 16.343 \text{ cm}^{-1}$ is the rotational constants of NH. The line in panel (b) represents a sum of the transitions to all field-dressed states and the symbols represent the cross sections for the dominant single-photon transition $ N = 0, M_S = -1, \bar{N}\rangle \rightarrow N = 0, M_S = 1, \bar{N} - 1\rangle$	75
Figure 5.2	Cross sections for elastic collisions in NH – He scattering as functions of the magnetic field (panel a) and as functions of the microwave field strength (panel b) for different parameters of the microwave field. The magnetic field in panel (b) is $B = 7153.19 \text{ G}$	76
Figure 5.3	Cross sections for elastic collisions (panel a) and collisions accompanied by absorption of microwave photons (panel b) in NH – He scattering as functions of the microwave field frequency. The magnetic field is $B = 7153.19 \text{ G}$	78
Figure 6.1	(a), (b) Energy levels of the $\text{SrF}(^2\Sigma^+)$ molecule ($b_r = 7.53 \text{ GHz}$, $\gamma = 74.7 \text{ MHz}$) in an electric field of $E_0 = 10 \text{ kV/cm}$ as a function of magnetic field B_0 ; (c) Frequency dependence of the ac field sensitivity for SrF in a linearly polarized mw field for different electric fields; the red and black lines correspond to the $2 \rightarrow 3$ and $1 \rightarrow 4$ transitions respectively. The dashed line represents the sensitivity to the magnetic field component of the ac field that can be achieved in experiments with atoms; (d) Same as in (c) but for the $\text{CaH}(^2\Sigma^+)$ molecule ($b_r = 128.3 \text{ GHz}$, $\gamma = 1.24 \text{ GHz}$)	84

Figure 6.2	Sensitivity of the $ 2\rangle \rightarrow 3\rangle$ transition in $\text{SrF}(^2\Sigma^+)$ to electromagnetic fields as a function of the dc electric field E_0 and the frequency of the microwave field. The peaks are labeled by the frequency of the ac field in MHz. The dotted line shows the sensitivity of the $ 2\rangle \rightarrow 3\rangle$ transition in $\text{SrF}(^2\Sigma^+)$ to the magnetic field component of the microwave field.	86
Figure 6.3	The ac electric field sensitivity for $\text{SrF}(^2\Sigma^+)$ as a function of the spatial resolution, for $n = 10^{10} \text{ cm}^{-3}$ (solid lines) and $n = 10^{12} \text{ cm}^{-3}$ (dashed lines). Different colors correspond to different ac field frequencies.	87
Figure 6.4	(a), (b) Energy levels of the $\text{NH}(^3\Sigma^-)$ molecule ($b_r = 490.0 \text{ GHz}$, $\gamma = -1.65 \text{ GHz}$, and $\lambda = 27.6 \text{ GHz}$) as a function of the magnetic field B_0 ; (c) Frequency dependence of the ac field sensitivity. The background electric field $\mathbf{E}_0 = 0$	89

Acknowledgments

I would like to thank my scientific advisor Roman Krems and the Ultracold chemistry group at UBC. Also I would like to thank Timur Tscherbul, Zhying Li, Christopher Chemming, Erik Abrahamson, Yuri Suleimanov and members of the K. Madison, M. Shapiro and V. Milner group for helpful discussions. My family and my friends for support during all this time.

Chapter 1

Introduction

Recent advances in laser technologies have made it possible to study atoms and molecules with high precision and to achieve unprecedented control over their external and internal degrees of freedom. In particular, the development of experimental techniques for laser cooling of atoms and molecules to ultralow temperatures gave rise to the research field of ultracold atoms and molecules. Ultracold atoms and molecules are the simplest controllable quantum systems, which can be manipulated with high precision with available electromagnetic fields and used to study complex quantum phenomena. The progress in the field of ultracold atoms and molecules is expected to have an impact on different areas of science and technology ranging from fundamental measurements and high precision sensing of electromagnetic fields to quantum information processing and quantum simulations [1, 2].

The goal of this chapter is to introduce the field of cold and ultracold quantum gases and to place this thesis in the context of the ongoing research. To give the reader a broad perspective and to position the emergent field of ultracold atoms and molecules in the area of Atomic, Molecular, and Optical physics, we briefly describe the early works on cooling atoms which led to the development of the field. After that, we discuss the properties of cold and ultracold quantum gases, the state of the art in ultracold atom research and some of the applications of cold and ultracold atoms and molecules. Finally, we outline the Thesis and discuss the connection and contribution of our work to the field of ultracold atoms and

molecules.

1.1 Cold and ultracold atoms and molecules

1.1.1 Development of the field

The interest in cooling atoms was inspired by the development of the time and frequency standards and, in particular, atomic clocks in 1940s-1950s [3]. In atomic clocks a laser pulse with duration τ drives transitions between two atomic energy states with the resonant frequency ν . The accuracy of the clock depends on the uncertainty in the measured resonant frequency. The fractional width of the resonance is inversely proportional to the interaction time τ and resonant frequency ν : $\delta\nu/\nu \sim 1/\tau\nu$. Therefore, the relative uncertainty is smaller for longer interaction times and higher frequencies. The thermal motion of atoms limits the interaction times and leads to Doppler broadening of lineshapes and shifts of the resonant frequency. Cooling atoms decreases the Doppler broadening of the atomic transitions, reduces the collisional rate and, therefore, increases the accuracy of the atomic clock. The development of Doppler-free spectroscopy and in particular the Ramsey method of separated oscillatory fields in 1949 [4] and atomic fountains in 1953 [5] allowed experimentalists to diminish the Doppler effect and resulted in the first Cs-based atomic clock with the frequency stability 10^{-9} [6]. The Cs-based atomic clock frequency standard was established in 1968 with the relative inaccuracy in frequency less than 10^{-14} . The further improvement of frequency measurements required further cooling and reducing the effects of thermal motion, which led to the idea of laser Doppler cooling of atoms [7] and ions [8]. The effect of Doppler cooling is based on the absorption of red-detuned photons from counter-propagating laser beams during which an atom decreases its momentum by 'recoil momentum' and re-emission of the photon in a random

with zero momentum gain on average. The first experimental demonstrations of the laser Doppler cooling technique were presented by Wineland [9] and Neuhauser [10] for optically trapped ions. The minimum temperature achievable by the Doppler cooling technique is equivalent to the uncertainty in the energy of the emitted photons, which is determined by the natural linewidth γ of the excited

electronic states: $T_{\text{Doppler}} = \hbar\gamma/2k_B$. With Doppler cooling the micro Kelvin temperatures were reached for alkali atoms ($\sim 240 \mu\text{K}$ for Na and $\sim 130 \mu\text{K}$ for Cs atoms) [11]. Cooling below the Doppler limit relies on an interplay of the polarization gradient created by interfering laser beams, and light shifts experienced by different Zeeman sublevels for different polarizations. Temperatures below the Doppler limit were achieved for Na ($\sim 40 \mu\text{K}$) and Cs ($\sim 700 \text{nK}$) in 1988 [12] by cooling atoms in ‘optical molasses’. The ‘optical molasses’ are created by three pairs of counter-propagated circularly polarized laser beams, generating a periodic potential for atoms. The atomic motion in such a potential is similar to the motion in a viscous medium. The atoms can be trapped if their temperature is less than the depth of the optical potential strength [13, 14]. The atomic motion is quantized in the trapping potential and transitions between the wells occur by tunneling. The ‘optical molasses’ techniques gave rise to the rapidly growing field of optical lattices and quantum simulations with optical lattices. We will discuss the optical lattices in detail in the next chapter. At the same time the methods for both magnetic [15] and optical [16] trapping of atoms were developed. The magneto-optical traps (MOTs) [17] allowed one to trap and to cool atoms simultaneously. Laser cooling followed by magnetic trapping and evaporative cooling led to the observation of the quantum degenerate regime and the demonstration of the Bose-Einstein condensation of atoms. The first ultracold gas of spin polarized hydrogen was obtained in 1979 by I. F. Silvera and J.T.M. Walraven. The BEC of alkali metal atoms was first observed by E.A. Cornell and C.E. Wieman at JILA with ^{87}Rb ($T \sim 170 \text{nK}$), W. Ketterle at MIT with ^{23}Na , and R. Hulet at Rice University with ^7Li in 1995 [18–20]. After that, the field grew rapidly, attracting researchers from atomic physics, quantum optics and condensed matter physics and leading to the emerging research field of ultracold molecules.

1.1.2 Properties of cold and ultracold gases

In this Section, we discuss the unique properties of cold (T between 1 mK and 1 K) and ultracold (below 1 mK) gases in more detail. The long range interaction between particles can be characterized by the effective radius of the interaction R_e depending on the form of the long-range potential. For example, $R_e = (mC_6/\hbar^2)^{\frac{1}{4}}$

for the alkali atoms interacting with a Van der Waals potential $-C_6/r^6$. For sufficiently low densities n , such that the mean interparticle distance in a gas $n^{-1/3}$ is much larger than R_e ($n^{-1/3} \gg R_e$), the motion of atoms is weakly affected by other particles and it is said that the gas is dilute. For dilute gases the probability of three-body and higher order collisions is negligible and one can consider only two body collisions. The thermal motion can be characterised by the de Broglie wavelength $\Lambda_T = \sqrt{\frac{2\pi\hbar^2}{mk_B T}}$. At room temperature the de Broglie wavelength Λ_T is much smaller than the radius of inter-particle interaction R_e and the mean interparticle distance $n^{-1/3}$, so the gas can be described by classical Maxwell-Boltzmann statistics. At lower temperatures the effects of quantum statistics may become important for the description of the macroscopic behavior of the gases. The de Broglie wavelength increases with decrease of the temperature. At low temperatures the size of the de Broglie wavelength is comparable to or larger than the size of the particles. The detailed structure of the short range interaction potential becomes unimportant and the scattering dynamics is governed by the long range part of the interaction potential. The interaction between particles in this regime can be described by an effective potential with a single parameter $V(r) = 4\pi a\delta(r)$, where a - is a scattering length and $\delta(r)$ - is the Dirac delta function. The scattering length is connected with a low energy behaviour of the two body wavefunction. Its meaning and connection to the scattering properties of the particles will be described in the next Chapter. It is important to note that the sign of the scattering length determines the attractive ($a < 0$) or repulsive ($a > 0$) behavior of the potential and it can be tuned in a wide range near a Feshbach resonance using external electromagnetic fields. The gas is considered to be in an ultracold regime if the de Broglie wavelength Λ_T is much bigger than R_e ($\Lambda_T \gg R_e$). For very low temperatures or high densities, such that $\Lambda_T \gg n^{-1/3}$ the gas obeys quantum statistics. Here the difference between particles with integer (bosons) and odd (fermions) composite spins comes into play. Decreasing the temperature in a gas of bosons leads to the formation of a Bose-Einstein condensate (BEC). All particles in a BEC populate a single state of the external potential and can be described by a single wave function. In the case of fermions the Pauli exclusion principle prevents the particles from occupying a single quantum state. Cooling a gas of fermions results in a Fermi sea - a state where there is only one fermion in each quantum state.

The complex structure and strong dipole-dipole interaction between polar molecules promises a lot of interesting applications. The dipole-dipole interaction between polar molecules is long-range and anisotropic. The strength and attraction or repulsion of the dipole-dipole interaction can be tuned by dc electric and microwave fields. The strong dipole-dipole interaction can be used for the creation of exotic quantum phases of dipoles and is a useful tool for simulation of the strongly interacting condensed-matter systems. Ultracold molecules can be used for high-precision spectroscopy tests of fundamental symmetries. For example, cold molecules are used in experiments testing the time variation of fundamental constants, measuring parity-violation in nuclei and for precision measurements of the permanent electric dipole moment (EDM) of the electron [21]. The nonzero value of the electric dipole moment would revolutionize physics, indicating violation of the standard model. The fundamental constants determine the vibrational, rotational and hyperfine structure of molecules, and therefore their temporal and spatial variations can be observed with ultracold molecules.

At room temperature the kinetic energy of the particles is much larger than Stark and Zeeman effects arising in atoms and molecules due to electromagnetic fields available in the laboratory. At cold temperatures, the interaction of atoms and molecules with magnetic, electric and laser field is on the order of the kinetic energy of the particles. Therefore, atoms and molecules cooled down to 1 mK-1 K can be trapped in magnetic, electric or magneto-optical traps. Electric and magnetic fields are used to confine the translational motion of molecules in specific Stark or Zeeman states, resulting in external field traps [22]. According to the Earnshaw theorem, the dc electromagnetic fields can not have a maximum in a free space. Therefore, the atoms and molecules can be confined in a states, whose energy increase from the low to high fields, such states are called low-field seeking states. The collisions of molecules lead to the inelastic relaxation to high-field seeking states which are untrappable. Collision-induced Zeeman and Stark relaxation processes in such traps lead to loss of atoms and molecules from the traps. The ac Stark, radio-frequency and microwave traps on the other hand, can confine atoms and molecules in high-field seeking states, allowing the trapping of the absolute ground state. The inelastic collisions of atoms and molecules in such traps can be suppressed by an appropriate choice of the field parameters. The microwave

traps along with the previously mentioned advantages can have a large depth and size, allowing one to trap larger ensembles of molecules at higher temperatures. The trapping fields modify the molecular energy levels and may affect collisional properties. Therefore, to understand and to control the elastic and inelastic collisions of molecules in traps it is necessary to develop a theory for collisions of molecules in the presence of microwave fields.

Atoms and molecules can generally be cooled to very low temperatures using buffer gas [23, 24], sympathetic [25] and evaporative [26] cooling techniques, all of which rely on the relative efficiency of elastic and inelastic collisions in electromagnetic traps. The effective interactions between molecules can be manipulated using scattering resonances induced by dc- magnetic [27], electric [28] or laser fields [29], allowing for realization and simulation of strongly correlated quantum systems with ultracold atoms and molecules [30]. Electromagnetic fields can also be used to orient and align polar molecules [31] and induce molecular predissociation [32]. The orientation of molecules with external fields allows for the study of the anisotropy of intermolecular interactions. It is therefore very important to understand the effects of static and laser electromagnetic fields on collision dynamics of molecules at subKelvin temperatures and develop mechanisms for external field control of elastic and inelastic collisions of cold molecules.

1.2 Applications of cold and ultracold gases

In this Section we discuss ongoing research in the field of cold and ultracold quantum gases ranging from precision spectroscopy and metrology to quantum information processing and simulations of various condensed matter systems.

1.2.1 Frequency standards and precision measurements

As discussed before, confinement and cooling of particles to the ground state of their center-of-mass motion allowed for the possibility to eliminate such unwanted effects as Doppler shifts, relativistic time dilation and increase the interrogation time and, therefore, in general increase the accuracy and precision of the spectroscopic measurements.

The current frequency and time standards are based on the atomic fountain

clock which was proposed by Zacharias in 1953 [5] and received a wide practical implementation [33, 34] only after the development of sub-Doppler laser cooling methods. The Cs atoms in an atomic fountain are cooled down to $1 \mu\text{K}$ and launched up by a laser kick with a velocity of 4 ms^{-1} . The atoms in the atomic beam are prepared in the $|F = 3M_F = 0\rangle$ state by a combination of optical pumping and resonant laser excitation. The atoms then traverse the microwave cavity and the number of atoms in the $|F = 4M_F = 0\rangle$ state is detected. The best atomic fountain clocks have a fractional uncertainty of $< 5 \times 10^{-16}$ limited by collisions and light-shifts from blackbody radiation.

Using optical instead of microwave transitions increases the stability of the atomic clocks. The other component which is required for atomic clocks is an ultra-stable laser system. The first system used as an optical standard was based on trapped ions because the tight confinement and low temperature eliminate the Doppler effects and allow for long interrogation times. The main disadvantage of ions is the strong ion-ion repulsion and therefore a low total number of ions that can be trapped, leading to a weak signal. Larger ensembles of neutral atoms are trappable with current technologies, providing a stronger signal. The main disadvantages of atoms are the residual Doppler shifts, collisional shifts, and a limited interaction time ($\sim 1\text{s}$). By confining larger ensembles of atoms in tight optical lattices one can increase the interrogation times, perform Doppler-free interrogation and achieve a high signal-to-noise ratio. The spin-forbidden 1S_0 - 3P_0 transition in alkaline-earth atoms of Sr and Yb has a narrow linewidth making them favorable for using as optical lattice clocks. The lowest systematic uncertainties for optical lattice clocks are $\sim 10^{-16}$ with Sr [35]. The frequency standards find applications far beyond simple time keeping. For example, the more accurate determination of the electron-to-proton mass ratio [36], measurement of fundamental constants and their possible variations with time [37, 38], optical communication and gravitational wave detection [39] have become possible with the development of the optical frequency standards.

The current efforts in the field focus on the development of chip-scale atomic vapor-based instruments with a size less than 10 mm^3 that could run in portable AA battery-operated systems. These devices potentially have a lot of promising applications from chip-scale atomic magnetometers monitoring signals produced

by human body (heart and brain) to gyroscopes and atomic clocks [40–42].

1.2.2 Quantum-degenerate gases

The BEC is an example of a weakly interacting many-body system, usually studied in the condensed matter field. The realization of a BEC with ultracold alkali metal atoms merged condensed-matter and AMO physics. Since then, the ultracold atoms were extensively used to study various condensed matter phenomena. For example, the Mott insulator to superfluid phase transition [43], BEC-BSC crossover [44] and fractional quantum Hall effect [45] were observed with ultracold atoms in optical lattices to study the behaviour of strongly correlated systems. The mixtures of bosons and fermions were realized and used to probe the behavior of strongly interacting mixtures in order to understand the detailed physics behind the Feshbach resonance and Fermi gas superfluidity [46, 47]. The interatomic interactions in BEC can be used to create entanglement and squeezing of the wavefunction. Such systems can be used, for example, to enhance the sensitivity of precision measurements and in atomic interferometers [48]. There is a phase coherence between two parts of the spatially separated condensate, which is an example of the Josephson effect. The atomic population in a such system oscillates between two parts due to tunneling through the potential well. The parameters of the well and the interatomic interaction strength can be varied to study different regimes [49].

1.2.3 Optical lattices and quantum simulation

The optical lattices of atoms and molecules find numerous applications. The creation, manipulation and underlying physic of the optical lattices is discussed in next Chapter. Here we provide examples of some of the applications of optical lattices. Optical lattices can be used to confine atoms and molecules in lower dimensions. The motion of atoms and molecules can be confined in 2D plane or in 1D by confining the motion along other directions to the ground state of the harmonic potential. Atoms and molecules confined in lower dimensions have properties different from 3D. For example, Bose-Einstein condensation in an ideal 1D and 2D is impossible, but can occur in atomic traps [50]. The Bose-Einstein condensation in lower dimensions was experimentally studied by confining atoms in pancake and cigar-

shaped traps [49, 51]. Confining polar molecules to a plane can be used to study strongly-correlated quantum phases such as Wigner crystals [52]. Trapping polar molecules in a 3D lattice and tuning interactions with microwave fields may help to realize different spin-lattice models [53]. Chemical reactions and inelastic collisions can lead to decoherence, heating of gas and losses of the particles from the trap. To have a clear picture of these phenomena one needs to understand the cold and ultracold collision dynamics in low dimensions. For this reason, it is important to develop a quantum mechanical scattering theory in low dimensions.

1.2.4 Quantum information processing and quantum computation

The other promising area of application of cold and ultracold atoms and molecules is quantum information processing, quantum simulations and quantum computation. The permanent dipole moment makes polar molecules promising candidates for quantum information processing. The first scheme for quantum computation consisted of the 1D lattice of polar molecules combined with inhomogeneous electric fields [54]. The dipoles constituted qubits, individually addressable due to the different Stark shifts in an inhomogeneous electric field. The entanglement is achieved via interaction between the dipoles. The polar molecules can be coupled to the superconducting stripline microwave resonators [55]. The exchange of virtual photons can mediate the coupling between different polar molecules, which can be achieved by adjusting the detuning of each molecule, for instance by varying the voltage for each traps.

1.2.5 Detection of weak electromagnetic fields

Sensitive detection of weak electromagnetic fields finds numerous applications from fundamental physical measurements to biomagnetic imaging and materials characterization. The atom based spin exchange relaxation-free (SERF) magnetometers offer the sensitivity of $1 \text{ fT}/\sqrt{\text{Hz}}$ and have a theoretical limit less than $0.01 \text{ fT}/\sqrt{\text{Hz}}$ for 1 cm^3 sensor [56]. The sensitivity of the atomic magnetometers depends on a large set of parameters. In general, the sensitivity of the atomic magnetometer is proportional to the interaction of the atomic magnetic moment with the magnetic component of the field. Polar molecules have a permanent electric

dipole moment. The interaction of the molecular permanent dipole moment with the electric field component of electromagnetic field is approximately two orders of magnitude stronger and therefore potentially can increase the sensitivity.

1.3 Key concepts used in Thesis

1.3.1 Feshbach resonance

Magnetic Feshbach resonances play an important role in experiments with ultracold atoms and molecules. The Feshbach resonance occurs when the kinetic energy of the colliding particles in the entrance channel matches the energy of the bound state in a closed channel. Figure 1.1 shows the potential energy curves of a typical collision complex as a function of the interparticle distance. The red and black curves correspond to the open and closed channels. The dashed line shows the total energy of the system. The open and closed channels often have different magnetic or electric moments, therefore the energy separation between the open and closed channels can be changed by applying an external magnetic or electric field. In experiments, the magnetic Feshbach resonances are observed by scanning magnetic fields. The Feshbach resonances manifest themselves as strong narrow peaks in the elastic scattering cross sections.

Feshbach resonances provide a mechanism to tune the scattering length of ultracold atoms. The sign and magnitude of the scattering length determine the dynamical properties of ultracold gases [27, 57, 58]. The effective interparticle interaction potential in ultracold quantum gases is proportional to the scattering length. Feshbach resonances thus provide a method to control an effective interaction in ultracold gases [27, 57, 58]. Magnetic Feshbach resonances have been used, for example, for the creation of ultracold molecules [59], the production of Bose-Einstein condensates (BEC) of fermionic dimers [58, 60], the study of the BEC-BSC crossover in dilute gases [61] and the observation and tuning of dynamical instabilities in atomic BEC [62].

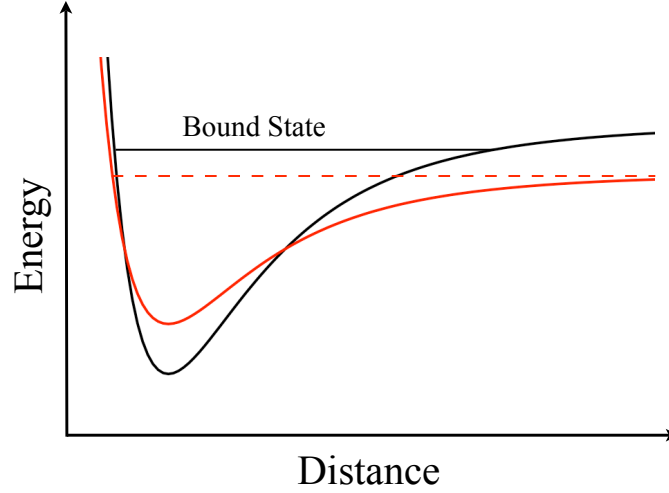


Fig. 1.1: Schematic illustration of a Feshbach Resonance.

1.3.2 Dressed states

Consider a two level quantum system (atom or molecule) placed in a single-mode electromagnetic field with a frequency ω . The Hamiltonian for this problem is as following

$$\hat{H} = E_a|a\rangle\langle a| + E_b|b\rangle\langle b| + \hbar\omega(\hat{a}^\dagger\hat{a} + 1/2) + g(|a\rangle\langle b| + |b\rangle\langle a|)(\hat{a}^\dagger + \hat{a}), \quad (1.1)$$

where \hat{a}^\dagger and \hat{a} are operators of photon creation and annihilation, and g is the atom-field coupling constant. The eigenstates of such coupled atom-field system are called field-dressed states. The field-dressed states group into manifolds $E(N)$ which can be characterized by the number of photons N . In the absence of the atom-field coupling each eigenstate of the Hamiltonian 1.1 is a direct product of atom and field states $|a, N\rangle = |a\rangle|N\rangle$. In the presence of the coupling the eigenstate of 1.1 is a linear combination of such products, with coefficients depending on the coupling strength. It is convenient to keep the notation $|a, N\rangle$ for the field dressed states adiabatically connected to $|a\rangle|N\rangle$. Figure 1.2 shows the scheme for the field dressed states for the case of small detuning $\omega - (E_b - E_a)/\hbar \ll \omega$. Such concept is especially convenient for describing particle-field interactions and absorption and emission of photons.

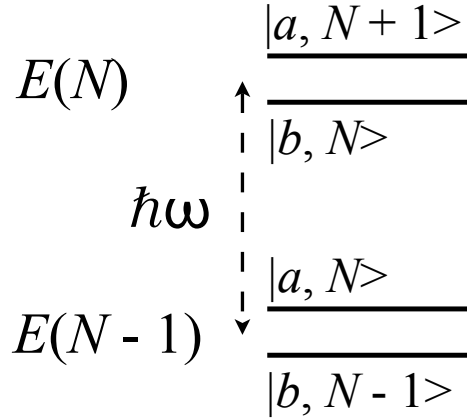


Fig. 1.2: Manifolds of field-dressed states.

1.3.3 Low field and high field seeking states

The atoms and molecules with unpaired electrons can be trapped in a dc magnetic field. Figure 1.3 shows the magnetic field profile and the relative energy of particles inside the magnetic trap. The magnetic field profile has a minimum in the center of the trap. The energy of atoms or molecules inside the trap depends on the projection of the spin angular momentum along the magnetic field direction and can be described by the following expression

$$\hat{H}_{\text{Zeeman}} = 2\mu_B \mathbf{B} \cdot \hat{\mathbf{S}}, \quad (1.2)$$

where μ_B is the Bohr's magneton, \mathbf{B} is the magnetic field vector and $\hat{\mathbf{S}}$ is the spin angular momentum operator. For the states with positive projection of the spin angular momentum along \mathbf{B} , the energy of the particle increases with increasing magnetic field. Such states are called low-field seeking states. The potential energy of the particle in a magnetic trap has a minimum in the center, and therefore the particle can be trapped in a magnetic trap. The states with negative projection of the spin angular momentum have a maximum in the center of the trap, and therefore such states are not trappable. The collisions of trapped atoms or molecules may change the projection of the spin, and result in trap loss of the particles. Such process are called spin-relaxation.

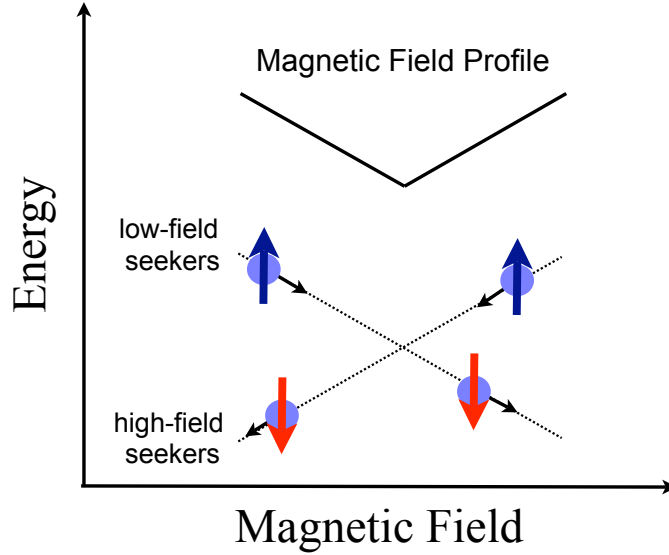


Fig. 1.3: Schematic illustration of a magnetic field profile in a magnetic trap. The red and blue arrows indicate the projections of the spin corresponding to the low and high field seeking states. The black arrows indicate the direction of the force acting on particles in a magnetic trap.

1.3.4 Scattering cross section

The last concept we will often use in the Thesis is that of a scattering cross section. The collision process treated in the center of mass frame is equivalent to scattering of particles by the potential located at origin of the coordinate frame. We assume that particles approach the target along one of the coordinate axes (x or z). One can define the incoming flux J_{inc} of particles i as a number of particles crossing the plane $x = a$ ($z = a$) in the direction of origin of the coordinate system per unit time. The particles can be scattered by the potential in different directions and can change their internal state or react to form other species during the scattering process. The number of particles of type j scattered in a direction defined by spherical coordinates (θ, ϕ) per unit time is the scattered flux $J_{\text{scat}}(\theta, \phi)$. The differential cross section is defined as a ratio between the scattered and incoming fluxes $d\sigma_{i,j}/d\Omega = r^2 J_{\text{scat}}(\theta, \phi)/J_{\text{inc}}$. Upon integration over $d\Omega$ one gets a total cross section for particles of type j conventionally denoted by $\sigma_{i,j}$, which can be considered as probability of forming particle j from particle i during the collision

process.

1.4 Thesis outline

In this section we briefly discuss the results presented in the following chapters. Chapter 2 describes an ultracold gas confined to a plane and presents the derivation of Wigner's threshold laws for 2D collisions. Chapter 3 discusses molecular collisions in the presence of a microwave field. In particular, the particle-field interactions and the dressed field formalism are briefly reviewed and the collisions of $^1\Sigma$ molecules with He atoms in a microwave cavity are studied within this approach. The spin-changing collisions of $^2\Sigma$ molecules in the presence of superimposed magnetic and microwave fields are explored in Chapter 4. The effects of microwave fields on Feshbach resonances in collisions of polar molecules are described in Chapter 5. In Chapter 6, we discuss the application of paramagnetic molecules to sensitive imaging of electromagnetic fields. In particular we show that experiments using cold molecules can be used to detect electromagnetic fields with sensitivity >100 times that of experiments with ultracold atoms. Chapter 7 concludes the Thesis.

1.4.1 Quasi 2D confinement of quantum gases

The motion of ultracold particles can be confined in one, two or three directions upon application of the strong laser field. The confined gases have unusual properties and allow one to study various interesting phenomena. The scattering properties of atoms and molecules at vanishing kinetic energies have universal character and in 3D are governed by Wigner's threshold laws. The collision properties of confined particles are different from those in 3D. In Chapter 2 we derive the threshold laws for inelastic collisions in 2D. We show that collisions accompanied by a change of relative angular momentum of the particles are suppressed in 2D. Our analysis suggests a new method of control of 2D collisions by varying the direction of the external fields. For example, the spin-changing collisions of ultracold atoms confined in 2D are suppressed in the presence of a weak dc electric or magnetic field perpendicular to the plane of confinement.

1.4.2 Microwave field effects on dynamics of polar molecules

The dynamics of cold and ultracold molecules is extremely sensitive to external fields. Ultracold molecules in a microwave field can potentially be used for various applications ranging from simulation of spin-lattice models to creation of a microwave trap for polar molecules, which would trap large ensembles of polar molecules at sufficiently high temperatures, up to 1K. Polar molecules in such traps can be confined in the absolute ground state, thus being stabilized against various trap losses. In Chapter 3, we explore collisions of ground state molecules in the presence of a microwave field. We describe the microwave field and the molecules-field coupling using a field-dressed formalism. We show that the anisotropy of the interaction potential drives transitions between different field-dressed states. Such transitions can be considered as collision-induced absorption of the microwave photons and lead to excitations of molecules and therefore to trap loss. We show that inelastic collisions of ground state molecules in the presence of microwave fields are very significant and should be taken into account for designing the mw traps. Molecules with unpaired electron spin can be trapped in a magnetic trap. The application of microwave fields to the magnetically trapped polar molecules can be used for inducing spin-forbidden reactions and modification of elastic and inelastic collisions, e.g through the creation or modification of Feshbach resonances. In Chapters 4 and 5 we analyse the effects of microwave fields on collisions of $^2\Sigma$ and $^3\Sigma$ molecules in the presence of magnetic fields. In particular we consider spin relaxation of the rotational ground state CaH molecules from a magnetic low-field seeking state to the high field seeking state, which is the main source of trap loss in magnetic traps, and modification of magnetic Feshbach resonances in NH-He collisions by an external microwave field.

1.4.3 Imaging of weak electromagnetic fields with paramagnetic polar molecules

In Chapter 6, we discuss the possibility of using paramagnetic polar molecules for the detection of weak electromagnetic fields. We propose a method for measuring weak electromagnetic fields ranging from sub-kHz to THz frequencies with polar molecules. This method is similar to the technique used by Böhi [63] to image

the distribution of the magnetic field amplitude and the phase of the electromagnetic field created by the chip with ultracold Rb atoms. We show that molecule based sensors would increase the sensitivity of the imaging up to two orders of magnitude. Various applications of the molecular sensors are discussed.

Chapter 2

Ultracold inelastic collisions in two dimensions

2.1 Introduction

2.1.1 Ultracold collisions and Wigner's threshold laws in 3D

The ability to control atomic and molecular collisions at low temperatures is important for many applications. It is often required to enhance elastic and/or to suppress inelastic collision processes. For example, a high ratio of elastic to inelastic cross section ($\sigma_{\text{el}}/\sigma_{\text{inel}} > 150$) is necessary for the experimental realization of evaporative and sympathetic cooling [64]. Finding the parameters of external fields that give large elastic-to-inelastic ratio is therefore essential for planning and performing evaporative cooling experiments. Tuning the system near a Feshbach resonance allows one to change the sign and magnitude of the scattering length, and therefore, to modify the effective interactions in the gas. This is especially important for the realization of the strongly interacting quantum gases. Spin-changing collisions are one of the main sources of decoherence in atomic magnetometers. The development of spin-exchange relaxation free (SERF) technique allowed experimentalists to improve the sensitivity and made the SERF magnetometer one of most sensitive magnetic field detectors [56]. In this chapter we investigate the

effects of tight external confinement on the collisional properties of the ultracold atoms and molecules. In particular, we explore the energy dependence of the elastic, inelastic and reaction cross sections in a confined 2D geometry. We derive analytic expressions corresponding to Wigner’s threshold laws for collisions in 2D and analyse the effects of the long-range potential on the scattering phase shift in the Born approximation. We show that inelastic Zeeman and Stark relaxation can be suppressed by application of a weak dc magnetic or electric field perpendicular to the plane of confinement.

The dynamics of cold and ultracold collisions is different in many aspects from room temperature dynamics. The rotational motion of the collisional complex give rise to a centrifugal force that suppresses collisions with high angular momenta at low temperatures. The wavefunction and the scattering cross section is a sum of contributions from different angular momenta. The elastic cross section is strongly dominated by a few lowest partial waves for cold collisions and by the single s - or p -wave for ultracold collisions. The spin statistics of the particles play very important role. For example, in collisions of identical bosons only even partial waves are possible. The dominant contribution comes from the s -wave scattering ($L=0$). The collisions of bosons are isotropic and can be very efficient at ultracold temperatures. The evaporative cooling is therefore possible. Fermions allow only odd partial waves. The cross section for ultracold scattering of fermions is dominated by p -wave scattering, which is anisotropic and vanishes with decreasing temperature. The evaporative cooling of fermions is therefore impossible.

The energy dependence of the two-body collision cross sections in the limit of low collision energy was analyzed by Wigner [65]. He showed that the cross section as a function of the energy depends mainly on the longest-range part of the interaction potential of reacting particles. The rotational angular momentum of the collisional complex gives rise to the term $-\hbar^2 L(L+1)/2\mu r^2$, where L is the angular momentum quantum number and r is the inter-particle distance, which dominates at large distances and governs the dynamics of slow collisions of neutral particles. In particular, he demonstrated that the elastic cross section varies as k^{4L} , where k is the collision wave number defined by $E_{\text{kin}} = \hbar^2 k^2 / 2\mu$ and L is the orbital angular momentum before collision. He also showed that the cross sections for inelastic and reactive collisions vary as $k^{2L+2L'}$ (L' - is the angular momentum

of the products) and k^{2L-1} correspondingly. Applying these results to ultracold s -wave collisions ($L = 0$) we obtain that the elastic cross section is finite at very low energies $\sigma = 4\pi a^2$, where a is the scattering length. The inelastic collisions (e.g spin-depolarization) are suppressed by the factor $k^{2L'}$ and the cross sections of the exothermic reactions increase as k^{-1} with decreasing kinetic energy.

Landau and Lifshits [66] showed that in the Born approximation the dispersion potentials ($1/r^s$, $s > 3$) introduce an additional “anomalous” phase shift proportional to k^{s-2} and the scattering amplitude for s -wave scattering in the $1/r^3$ potential diverges as $\ln k$. The dispersion potentials modify the Wigner’s threshold laws for elastic scattering for the partial waves L such that $2L < s - 3$, but do not change the energy dependence of the inelastic and reactive scattering cross section. The same results were obtained in a number of other articles [67–70].

2.1.2 Ultracold gases in optical lattices

The optical lattice is a periodic potential energy surface, created by interfering optical laser beams. Oscillations of the electric field of the light induce oscillations of the dipole moments, which interact with the electric field providing the trapping potential in the optical lattice. In other words the laser field creates the AC Stark shift, which acts as a trapping potential for atoms and molecules:

$$\hat{V}_{\text{dip}}(\mathbf{r}) = -\langle \mathbf{d}(t) \cdot \mathbf{E}(\mathbf{r}, t) \rangle = \sum_{i,j} a_{i,j}(\omega_L) \langle E_i(\mathbf{r}, t) E_j(\mathbf{r}, t) \rangle^2, \quad (2.1)$$

where $a(\omega_L)$ is the dynamic polarizability of the particle at the laser frequency ω_L and the brackets denote the average over time. The laser frequency below $\omega_L < \omega_0$ (above $\omega_L > \omega_0$) the atomic or molecular resonance ω_0 creates an attractive (repulsive) potential. The product of the electric field components is proportional to the intensity of the laser light. The overlap of two counter-propagating laser beams creates a periodic modulation of the laser intensity and therefore the particle feels the periodic potential with periodicity $\lambda_L/2$ along the laser beam propagation axis. The Gaussian profile of the laser beam creates a weak confining force in the direction perpendicular to the laser beam propagation. If the kinetic energy of the atoms or molecules is sufficiently small ($\sim 1\mu\text{K}$) they can be trapped in this potential.

The single potential well in a 1D optical lattice has a pancake shape and for small kinetic energies of the particles it can be described as a three dimensional harmonic oscillator with one of the frequencies (transverse frequency) much higher than the other two. At elevated temperatures of the gas, the kinetic energy may be comparable to or larger than the harmonic frequencies of the trapping potential and therefore the transitions between the quantized energy levels in the transverse direction occur frequently and the motion of the atoms in the direction of the laser beam can be considered as free. In the limit of tight transverse confinement or small kinetic energy of the particles, in particular when $E_{\text{kin}} \ll \hbar\omega_z$, the transitions between different harmonic states are strongly suppressed. The gas of atoms can be prepared in a state, where the transverse motion of the center of mass of the particles is well described by the lowest energy wavefunction of the harmonic potential. The gas of atoms confined to the ground state of the harmonic potential of the 1D optical lattice and moving relatively free in the other two dimensions is called a quasi-2D gas (2.1). By superimposing two standing waves perpendicular to each other, the creation of tight confinement in two directions is possible. The motion of particles in two direction in such potential can be well described by the eigenfunctions of the ground state of the harmonic oscillator and free motion in the other direction. Such potential is periodic in two dimensions and the single well has a cigar shape. The addition of a third laser beam allows one to create strong 3D periodic potentials (2.2), in which atoms can be trapped in the ground state of the 3D harmonic potential of a single well and these wells form a 3D periodic lattice. By varying the angles between the laser standing waves, different forms of the lattices can be created, e.g. hexagonal, Kagome [71, 72].

The development of these methods of the production of low-dimensional quantum gases and the creation of periodic lattices for trapping atoms and molecules has opened up an opportunity for studying physics and chemistry of low dimensional gases [1, 2]. Confining the motion of gas particles to lower dimensions usually enhances quantum effects and gives rise to new phenomena. For example, confining atoms in an optical lattice may result in interesting decoherence dynamics of quantum gases [49, 51, 73–76], and may be used for investigation of a variety of phenomena in condensed-matter physics, such as Bose-Einstein condensation in low dimensions. The dipolar gases, i.e polar molecules confined in two dimen-

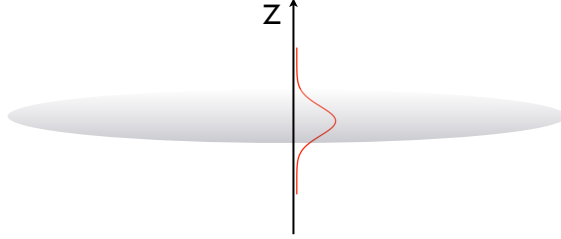


Figure 2.1: Quasi-2D optical lattice (pancake) formed by interfering of 2 counterpropagating laser beams. The red line shows the ground state wavefunction of the ground state perpendicular to the confinement plane.

sions (2D) may repel each other at long range, which leads to the formation of self-organizing crystals at ultracold temperatures [52]. The strong dipole-dipole interactions of polar molecules give rise to new and exotic quantum phases [53]. The confinement modifies the symmetry of the long range potential and, therefore modifies the collisional properties of atoms and molecules at low temperatures [77]. For example, the s -wave scattering cross section and the dipole-dipole potential in 2D are not averaged to zero as in 3D. The stability of the gas can be enhanced by confinement. For example, 2D optical lattices can stabilize cold polar molecules against inelastic and reactive collisions, if the molecules are polarized in the direction perpendicular to the plane of confinement.

2.2 Scattering theory in 2D

2.2.1 Scattering in 2D

In this section we describe the theory of atomic and molecular scattering in 2D. We show that it is possible to describe the scattering wavefunction in terms of S - and T - matrices in a way similar to collision properties in 3D and derive expressions for the scattering cross sections at small collision energies

After the separation of the center of mass motion, the two-body problem reduces to the problem of the motion of one particle with the mass equal to the reduced mass of the system $\mu = \frac{m_1 m_2}{m_1 + m_2}$. The quantum mechanical Hamiltonian

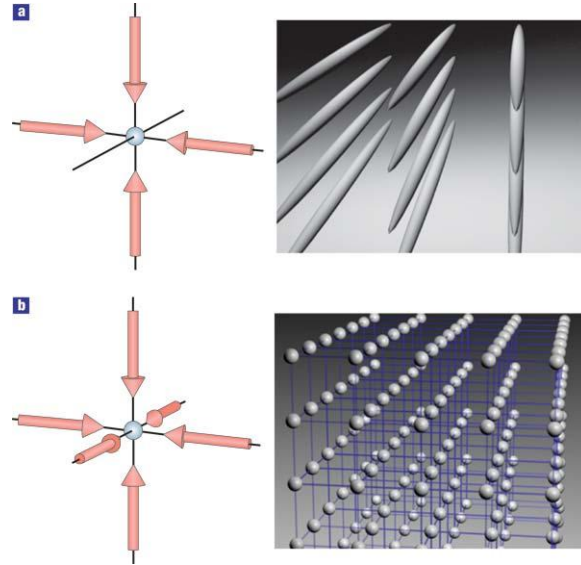


Figure 2.2: Optical lattices. (a) 2D optical lattice formed by superimposing 2 standing waves (b) 3D optical lattice formed by 3 standing waves. Adapted from Macmillan Publishers Ltd.: I.Bloch, Nature Physics 2005, 1, 23

corresponding to this problem has the following form

$$\hat{H} = -\frac{\hbar^2}{2\mu}\Delta + \hat{H}_{\text{as}} + \hat{V}, \quad (2.2)$$

where first term is the kinetic energy of the particles, μ is the reduced mass of the colliding complex, the asymptotic Hamiltonian H_{as} describes the separated atoms or molecules and V is the inter-particle interaction potential. To describe the motion of the particles confined in the 2D plane, it is convenient to direct the quantization axis along the normal to the confinement plane and introduce the polar coordinates (r, θ) , defined by $x = r \cos \theta$ and $y = r \sin \theta$, where θ changes from 0 to 2π . The variable r describes the separation between the centers of mass of the particles and θ the angular motion of the collision complex. The Laplace operator

in polar coordinates is

$$\Delta = \frac{\partial^2}{\partial x^2} + \frac{\partial^2}{\partial y^2} = \frac{1}{r} \frac{\partial}{\partial r} r \frac{\partial}{\partial r} + \frac{1}{r^2} \frac{\partial^2}{\partial \theta^2}. \quad (2.3)$$

The radial and angular dependence of the Hamiltonian is separable and the wavefunction can be written as a product of functions depending only on radial and angular coordinates. For the angular dependence one can introduce the 2D rotational angular momentum operator as $\hat{l}_z^2 = -\hbar^2 \partial^2 / \partial \theta^2$. The eigenvalues and normalized eigenfunctions of the rotational angular momentum operator \hat{l}_z^2 are $\hbar^2 m^2$ and $\frac{1}{\sqrt{2\pi}} e^{im\theta}$ correspondingly, where m is an integer number. The Hamiltonian describing the relative motion of two particles confined in a plane takes on the following form

$$\hat{H} = -\frac{\hbar^2}{2\mu r} \frac{\partial}{\partial r} r \frac{\partial}{\partial r} + \frac{\hat{l}_z^2(\theta)}{2\mu r^2} + \hat{H}_{\text{as}} + \hat{V}. \quad (2.4)$$

The total wavefunction can be written as a sum over channel functions $\Psi^i = \sum_j \Psi_j^i = \sum_j \psi_j^i \phi_j$, where ϕ_j represents the eigenfunction of H_{as} with eigenvalue ε_j corresponding to the energies of noninteracting particles. The scattering function can be expanded in eigenfunctions of the angular momentum operator as

$$\psi_j^i(r) = \sum_m \frac{A_m^i}{\sqrt{2\pi}} \psi_{jm}(k_j r) e^{im\theta}, \quad (2.5)$$

where A_m^i do not depend on the index of the outgoing channel j and the upper index i indicates that the incoming flux is in channel i , $\psi_{jm}(k_j r)$ is a radial wavefunction in channel jm and $\frac{1}{\sqrt{2\pi}} e^{im\theta}$ is the eigenfunction of the angular momentum operator \hat{l}_z^2 .

The following system of coupled differential equations can be obtained upon substitution of the total wavefunction Ψ^i in the Hamiltonian, multiplication by $\phi_j^* \frac{1}{\sqrt{2\pi}} e^{-im\theta}$ and integration over the angular and internal degrees of freedom of colliding particles

$$\left(\frac{1}{r} \frac{\partial}{\partial r} r \frac{\partial}{\partial r} - \frac{m^2}{r^2} + k_j^2 \right) A_m^i \psi_{jm}(k_j r) = \frac{2\mu}{\hbar^2} \sum_{j'm'} V_{jm;j'm'} A_{m'}^i \psi_{j'm'}(k_j r), \quad (2.6)$$

where $k_j^2 = \frac{2\mu}{\hbar^2}(E - \varepsilon_j)$, E is the total energy of the system and $V_{jm,j'm'} = (2\pi)^{-1} \int V(r, \theta, \tau) e^{i(m'-m)\theta} \phi_j(\tau) \phi_{j'}^*(\tau) d\theta d\tau$. The interaction potential between neutral atoms or molecules vanishes faster than $1/r^3$ (or as $1/r^3$ for dipole-dipole interactions of polarized molecules or atoms) as $r \rightarrow \infty$. Neglecting the interaction potential V at large r , we obtain the free particle Schrödinger equation corresponding to the asymptotic solution of Eq. 2.6

$$\left(\frac{1}{r} \frac{\partial}{\partial r} r \frac{\partial}{\partial r} - \frac{m^2}{r^2} + k_j^2 \right) \psi_{jm}(k_j r) = 0. \quad (2.7)$$

This equation can be transformed to the Bessel equation for the argument $x = k_j r$ [78]. The wavefunction $\psi_{jm}(k_j r)$ can be written as a linear combination of Bessel or Hankel functions of argument $k_j r$.

The unit normalized flux of particles moving in the positive x direction with velocity $v_i = \hbar k_i / \mu$ can be described by the plane wave $v_i^{-\frac{1}{2}} e^{ik_i x}$. Using the Jacobi-Anger expansion [78], one can express the plane wave in terms of the solutions of Eq.2.7

$$v_i^{-\frac{1}{2}} e^{ik_i x} = v_i^{-\frac{1}{2}} \sum_m i^m J_m(k_i r) e^{im\theta} = v_i^{-\frac{1}{2}} \sum_m i^m \frac{1}{2} [H_m^1(k_i r) + H_m^2(k_i r)] e^{im\theta}, \quad (2.8)$$

where m is an integer number, and $J_m(k_i r)$ and $H_m^{1/2}(k_i r)$ are Bessel and Hankel functions of the first and second order [78].

2.2.2 Wigner's threshold laws in 2D

In this section we analyse the threshold laws for slow collisions of particles confined in 2D. We follow the works of Wigner and Eisenbud [65, 79] and define the internal and external regions of configurational space separated by the surface S at $r = a$. We choose the boundary $r = a$ in such a way that the interaction potential in the external region has the form $1/r^n$. Wigner showed [65] that in 3D the potentials dropping faster than $1/r^2$ give the same energy dependence of the cross section as in the case when there is no interaction ($V = 0$) in the external region. We assume our potential drops faster than $1/r^3$ and neglect its dependence in the external region. The case $1/r^3$ we treat separately in the next section.

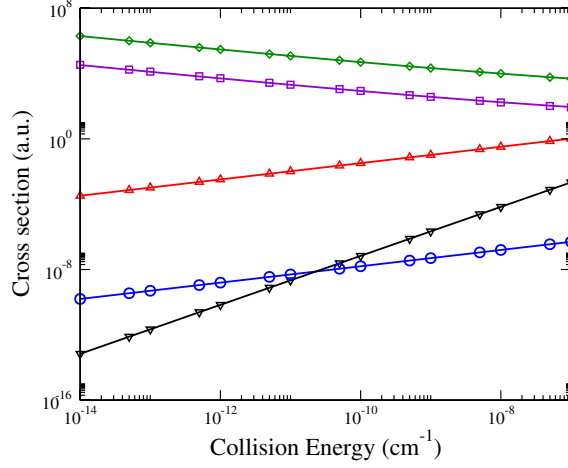


Figure 2.3: Threshold dependence of cross sections for collisions of Li and Cs atoms in 2D: diamonds - 2-wave inelastic collisions; triangles up - p -wave inelastic collisions; triangles down - p -wave elastic collisions; circles - s -to- d -wave transitions. Symbols - numerical calculations; lines - analytical forms. The initial states are $m_{f_{Li}}=-2$ and $m_{f_{Cs}}=2$ the s -to- d wave transitions is calculated for the maximally stretched states.

Following Wigner we use linearly independent solutions I_{jm} and E_{jm} ($E_{jm}^* = I_{jm}$) of Eq.(2.7) with asymptotics of the incident and emerging waves to expand the wavefunction in the external region. We chose the following form for the emergent wavefunction E_{jm}

$$E_{jm} = a^{\frac{1}{2}} \sqrt{\frac{\pi\mu}{2\hbar}} (i)^m e^{i\frac{\pi}{4}} H_m^{(1)}(k_j r) \propto a^{\frac{1}{2}} v_j^{-\frac{1}{2}} \frac{e^{ik_j r}}{\sqrt{r}}, r \rightarrow \infty, \quad (2.9)$$

where $v_j = \hbar k_j / \mu$ is the velocity of the particles in state j . The E_{jm} is normalized to give a unit flux at $r = a$

$$J_{\text{out}} = \frac{\hbar}{\mu} \text{Im} \left(E_{jm}^* \frac{\partial}{\partial r} E_{jm} \right) = a/r. \quad (2.10)$$

The plane wave 2.8 has the following expression in terms of the incident and

emergent 2.9 waves

$$v_i^{-\frac{1}{2}} e^{ik_i x} = a^{-\frac{1}{2}} k_i^{-\frac{1}{2}} \sum_m (-1)^m \frac{e^{im\theta}}{\sqrt{2\pi}} e^{i\frac{\pi}{4}} \left(I_{im} + (-1)^m e^{-i\frac{\pi}{2}} E_{im} \right). \quad (2.11)$$

If the incoming collision flux is prepared in a single quantum channel (im), the collision wavefunction has the form

$$I_{im} \frac{e^{im\theta}}{\sqrt{2\pi}} \phi_i - \sum_{jm'} U_{im;jm'} E_{jm'} \frac{e^{im'\theta}}{\sqrt{2\pi}} \phi_j, \quad (2.12)$$

where \mathbf{U} is the collision matrix [79]. We construct the scattering wavefunction of the form 2.12 with the plane wave 2.11 in the incoming channel i as

$$\begin{aligned} & a^{-\frac{1}{2}} k_i^{-\frac{1}{2}} e^{i\frac{\pi}{4}} \sum_m (-1)^m \left(I_{im} \frac{e^{im\theta}}{\sqrt{2\pi}} \phi_i - \sum_{jm'} U_{im;jm'} E_{jm'} \frac{e^{im'\theta}}{\sqrt{2\pi}} \phi_j \right) = \\ & v_i^{-\frac{1}{2}} e^{ik_i x} \phi_i - a^{-\frac{1}{2}} k_i^{-\frac{1}{2}} e^{-i\frac{\pi}{4}} \sum_{m,j,m'} (-1)^m \left(\delta_{im,jm'} + (-1)^{m'} e^{i\frac{\pi}{2}} U_{im;jm'} \right) E_{jm'} \frac{e^{im'\theta}}{\sqrt{2\pi}} \phi_j \end{aligned} \quad (2.13)$$

From 2.13 the integral cross sections for elastic and inelastic scattering in terms of the matrix elements of \mathbf{U} can be calculated. The inelastic cross section is given by the Wigner's R -matrix

$$\sigma_{im,jm'} = \frac{1}{k_i} \left| \delta_{im,jm'} + (-1)^{m'} e^{i\frac{\pi}{2}} U_{im;jm'} \right|^2 \quad (2.14)$$

The formulation of the collision problem as described above allows us to determine the dependence of the 2D scattering cross sections on the collision energy in the limit of small collision velocities using the formalism of Wigner [65] directly. He introduced the R -matrix connecting the expansion coefficients of the wavefunction and its normal derivative on S . The matrix elements of the collision matrix \mathbf{U} can be expressed through the matrix elements of the Wigner's R -matrix and logarithmic derivatives of E_{jm} . We define e_{jm} and q_{jm} - the derivative and reciprocal logarithmic derivative of E_{jm} as $e_{jm} = (\hbar/2\mu) \partial E_{jm} / \partial r$ and $E_{jm} = q_{jm} e_{jm}$ correspondingly. The j_{jm}^2 is the imaginary part of $2q_{jm}^*$ defined by

$j_{jm}^2 = -2Im(q_{jm}) = a/re_{jm}e_{jm}^*$. The U -matrix entering Eq. (2.12 and 3.32) can be represented as

$$\mathbf{U} = \boldsymbol{\omega} [1 + i\mathbf{j}(\mathbf{q} - \mathbf{R})^{-1}\mathbf{j}] \boldsymbol{\omega}, \quad (2.15)$$

where \mathbf{R} , \mathbf{q} and \mathbf{j} are a diagonal matrices with diagonal elements q_{jm} and j_{jm} evaluated at $r = a$ and $\boldsymbol{\omega}$ is a unitary diagonal matrix defined by $\mathbf{e} = |\mathbf{e}\boldsymbol{\omega}^*$. The R -matrix is assumed to be energy independent near threshold, so all energy dependence of the U -matrix is contained in the matrix elements of \mathbf{j} , $\boldsymbol{\omega}$ and \mathbf{q} . The threshold dependence of the U -matrix on the collision energy can thus be found analytically by analyzing the form of the scattering waves (2.9) at small collision velocities.

2.2.3 Elastic scattering in 2D

The elastic scattering cross section can be written from the general expression for cross section(3.32) and collision matrix (2.12) as

$$\sigma_{j_{m,jm}} = \frac{1}{k_j} |1 + i\omega_{jm}^2 - \omega_{jm}^2 j_{jm}^2 [(\mathbf{q} - \mathbf{R})^{-1}]_{jm,jm}|^2. \quad (2.16)$$

The case of s -wave scattering ($m = 0$) is of the major importance for low energy collisions, so we consider it first. The argument of the wavefunction $x = k_j r$ evaluated at the surface S ($r = a$ and $x = k_j a$) goes to zero as the kinetic energy goes to zero. The asymptotic form of the Hankel function $H_0^{(1)}$ at small x is

$$H_0^{(1)}(x) = 1 - \frac{x^2}{4} + \frac{2i}{\pi} \left\{ \ln\left(\frac{x}{2}\right) + \gamma \right\} + \bar{o}(x^2), \quad (2.17)$$

and the derivative of the Hankel function with respect to x is

$$\left(H_0^{(1)}(x) \right)' = -\frac{x}{2} + \frac{2i}{\pi x} + \bar{o}(x). \quad (2.18)$$

The matrix element e_{j0} and can be evaluated using 2.9, 2.18 and the chain rule

$$e_{j0} = \frac{\hbar}{2\mu} a^{\frac{1}{2}} \sqrt{\frac{\pi\mu}{2\hbar}} e^{i\frac{\pi}{4}} k_j \left(-\frac{k_j a}{2} + \frac{2i}{\pi k_j a} + \bar{o}(k_j) \right). \quad (2.19)$$

The ω_{j0} can be calculated from 2.19 leading to

$$\omega_{j0} = e^{-i\frac{\pi}{4}} \left(-\frac{\pi a^2 k_j^2}{4} - i + \bar{o}(k_j^2) \right). \quad (2.20)$$

The term $(1 + i\omega_{j0}^2)$ in the elastic s -wave cross section is equal to $i\frac{\pi^2 a^2 k_j^2}{2} + \bar{o}(k_j^2)$ at small energies. The j_{j0}^2 term equal to $\frac{2\pi\mu a}{\hbar} + \bar{o}(k_j^2)$ and $\omega_{j0} = i + \bar{o}(k_j^2)$. The q_{j0} term diverges as $a \ln(k_j a)$ and therefore the matrix element $[(\mathbf{q} - \mathbf{R})^{-1}]_{j0,j0} \sim [\ln k_j]^{-1}$. Therefore the energy dependence of the elastic cross section for the s -wave scattering is given by

$$\sigma_{j0,j0} \propto \frac{1}{k_j \ln k_j^2} \quad (2.21)$$

This result agrees with the expression for the scattering amplitude presented by Landau and Lifshitz [66] and by Petrov and Shlyapnikov [77].

The threshold behavior for elastic scattering for higher partial waves $|m| > 0$ can be calculated in a similar way. Using asymptotic expansion for Bessel and Neuman functions at small argument [78] one can show that

$$q_{jm} = \frac{2\mu}{\hbar} \left(-\frac{a}{m} - i \frac{4\pi}{(m!)^2} \left(\frac{a}{2}\right)^{2m+1} k_j^{2m} \right) + \bar{o}(k_j^2). \quad (2.22)$$

The j_{jm}^2 term has the following form

$$j_{jm}^2 = \frac{16\pi\mu}{\hbar(m!)^2} \left(\frac{a}{2}\right)^{2m+1} k_j^{2m} + \bar{O}(k_j^2). \quad (2.23)$$

The elastic cross section for $m > 0$ has the following energy dependence

$$\sigma_{jm,jm} \propto k_j^{4|m|-1}. \quad (2.24)$$

2.2.4 Elastic m -changing scattering in 2D

For collision processes that change the 2D orbital angular momentum ($jm \rightarrow jm'$), the cross section can be written as

$$\sigma_{jm,jm'} = \frac{1}{k_j} |j_{jm} j_{jm'} [(\mathbf{q} - \mathbf{R})^{-1}]_{jm,jm'}|^2. \quad (2.25)$$

To determine the threshold behavior of the cross sections for scattering in collision channels with $|m| > 0$, we express the Hankel functions in terms of the Bessel and Neuman functions. Using the asymptotic expansions of the Bessel and Neuman functions [78], we find that $j_{jm}^2 \propto k_j^{2|m|}$ as $k_j \rightarrow 0$. This yields the following energy dependence of the cross section near threshold:

$$\sigma_{j0,jm} \propto k_j^{2|m|-1} \frac{1}{\ln^2 k_j}. \quad (2.26)$$

Processes described by Eq. (2.26) are particularly important for inelastic collisions and angular momentum depolarization of molecules trapped in 2D at ultracold temperatures.

It is also necessary to consider transitions between states of non-zero angular momentum m . Such transitions determine collision properties of fermionic atoms and molecules confined in 2D. Using the above result $j_{jm}^2 \propto k_j^{2|m|}$ and noting that $[(\mathbf{q} - \mathbf{R})^{-1}]_{jm,jm'} \propto \text{const}$ as $k_j \rightarrow 0$, we find the following energy dependence of the scattering cross sections

$$\sigma_{jm;jm'} \propto k_j^{2|m|+2|m'|-1}. \quad (2.27)$$

2.2.5 Inelastic and reactive scattering

When collisions release energy, the energy dependence of the scattering cross sections near threshold does not depend on the angular momentum in the final collision channel. For example, the cross section for inelastic energy transfer in 3D collisions is proportional to $k_j^{(2l-1)}$ [65]. For reactive or inelastic collisions changing

the quantum number j , Eq. (2.25) transforms into

$$\sigma_{jm,j'm'} = \frac{1}{k_j} \left| j_{jm} j_{j'm'} [(\mathbf{q} - \mathbf{R})^{-1}]_{jm,j'm'} \right|^2. \quad (2.28)$$

According to Wigner [65], the off-diagonal matrix elements $[(\mathbf{q} - \mathbf{R})^{-1}]_{jm,j'm'}$ are then independent of energy at small collision energies if $m \neq 0$. For $m = 0$, we obtain

$$[(\mathbf{q} - \mathbf{R})^{-1}]_{jm,j'm'} \propto \frac{1}{\ln k_j} \quad (2.29)$$

so the energy dependence of the inelastic s -wave scattering cross section is the same as that of the elastic cross section given by Eq. (2.21):

$$\sigma_{j0,j'm'} \propto \frac{1}{k_j \ln^2 k_j} \quad (2.30)$$

This result is consistent with the analysis of Petrov and Shlyapnikov [77], who concluded that the frequency of inelastic collisions between atoms confined in a quasi-2D geometry has the same temperature dependence as the mean frequency of elastic collisions. The reader may observe that their Eq. (52) also yields the inverse logarithmic dependence on the collision velocity in the limit of extremely low temperatures.

When $|m| > 0$, the energy dependence of the scattering amplitude is determined by the term $j_{jm}^2 \propto k_j^{2|m|}$ so the inelastic scattering cross section for collisions with angular momentum m is given by

$$\sigma_{jm,j'm'} \propto k_j^{2|m|-1}. \quad (2.31)$$

2.3 Threshold laws in the Born approximation

As was discussed in the Introduction, the threshold laws for collisions in 3D depend on both the centrifugal $\sim 1/r^2$ and dispersion $\sim 1/r^s$ potentials. For the dipole-dipole interaction ($s=3$) for $L > 0$ the dispersive term ($\delta \sim k$) dominates over the centrifugal term ($\delta \sim k^{2L+1}$) and therefore has significant effect on collision dynamics. To explore the effects of dispersive potential ($C/r^s, s > 2$) on the

energy behavior of the 2D cross sections near threshold we use the Born approximation (described e.g in [66, 80]). The Born approximation is valid at low energies (if $kr_0 \ll 1$, where r_0 is the effective radius of the potential), provided that the potential is strong enough to support bound states, which is satisfied for the $1/r^3$ potential and the low collision energy considered here.

In the Born approximation the T -matrix element is $T_{j,j'} \sim V_{j,j'}$. The Green's function corresponding asymptotically to the outgoing wave has the following form

$$G_{jm}^+(r, r') = \frac{\pi r'}{2i} J_m(k_j r') H_m^{(1)}(k_j r), r > r'. \quad (2.32)$$

The wavefunction in channel (j', m') and correction due to scattering off the C/r^s potential can be written in terms of the Green's function $G^+(r, r')$

$$\psi_{j'm'}^0 = J_m(k_j r) \delta_{j,j'} + \frac{\pi}{2i} H_{m'}^{(1)}(k_{j'} r) C \int_0^\infty J_{m'}(k_{j'} r) J_m(k_j r) r^{1-s} dr. \quad (2.33)$$

Comparing its asymptotic form with the expression for T -matrix, we can obtain the T -matrix elements as

$$T_{jm,j'm'} = \frac{\pi C \mu}{2i} \int_0^\infty J_m(k_j r) J_{m'}(k_{j'} r) r^{1-s} dr. \quad (2.34)$$

The elastic case ($k_j = k_{j'}$) can be solved for $m + m' - s + 2 > 0$ and gives the result

$$\int_0^\infty J_m(k_j r) J_{m'}(k_j r) r^{1-s} dr = \frac{k_j^{s-2} \Gamma(s-1) \Gamma(\frac{m+m'-s+2}{2})}{2^{s-1} \Gamma(\frac{-m+m'+s}{2}) \Gamma(\frac{m+m'+s}{2}) \Gamma(\frac{m-m'+s}{2})}. \quad (2.35)$$

Therefore $T_{j,j} \sim k_j^{s-2}$ and the elastic cross sections vanish as k_j^{2s-5} in the zero-energy limit. For inelastic processes ($k_j < k_{j'}$) the integral has the following solution ($m + m' - s + 2 > 0$)

$$\begin{aligned} & \int_0^\infty J_m(k_j r) J_{m'}(k_{j'} r) r^{1-s} dr = \\ & \frac{k_j^m \Gamma(\frac{m+m'-s+2}{2})}{2^{s-1} k_{j'}^{m'-s+2} \Gamma(\frac{-m+m'+s}{2}) \Gamma(m+1)} \\ & \times {}_1F_0\left(\frac{m+m'-s+2}{2}, \frac{m-m'-s+2}{2}; m+1; \frac{k_j^2}{k_{j'}^2}\right). \end{aligned} \quad (2.36)$$

The hypergeometric function ${}_1F_0$ is independent on k_j in first approximation (the leading term in series expansion in k_j is constant). Therefore, neglecting the energy dependence in the final state and in ${}_1F_0$ we obtain $T_{j,j'} \sim k_j^{2m}$ and recover the $k_j^{2m_1-1}$ dependence for the inelastic cross section which is the same as in Wigner's theory.

2.4 Discussion

In order to numerically verify the analytical results presented in this Chapter, we calculated [81] the cross sections for elastic and inelastic Zeeman relaxation transitions induced by the $1/r^3$ magnetic dipole-dipole interaction in 2D collisions of Li and Cs atoms (2.3) in a magnetic field of 100G. The symbols in Fig. 2.3) represent the results of the numerical calculation of the cross sections and the solid lines represent the results calculated from the analytical expressions. The analytical and numerical results are in good agreement exhibiting small deviations for s -wave cross sections, where an additional constant term in the denominator, as in the Problem Set to §132 of [66] or [77], is important for collisional energies considered.

Quemener and Bohn analyzed the electric field dependence of inelastic collisions of molecules in 3D and 2D geometries [82]. The energy dependence for the inelastic quenching transitions in 2D is in agreement with our results. Micheli et al [83] and Quemener and Bohn [84] analyzed the reactive and elastic collisions of polar molecules in traps for different regimes of confinement; their results for quasi 2D reactions and elastic collisions are in agreement with our predicted threshold laws.

Eqs. (2.21) and (2.26) demonstrate that s -wave collisions of ultracold molecules in a 2D gas accompanied by angular momentum change are suppressed by a factor $k_j^{2|m|}$. Typical temperatures of ultracold gases are about 10^{-7} K so collisions involving transitions to $m = 1$ channels should be several orders of magnitude less probable than collisions conserving m . Certain collision processes are, however, forbidden unless the angular momentum of the collision complex changes. Consider, for example, the s -wave collisions of spin- $\frac{1}{2}$ Σ molecules in the rotationally ground state. In the presence of a magnetic field, molecular energy states split into Zeeman sublevels. We assume that the magnetic field is weak so that the

release of Zeeman energy into the translational motion of the molecules does not result in loss of molecules from the 2D confinement. If the magnetic field axis is directed along the z -axis, i.e. perpendicularly to the confinement plane, and the molecules are prepared in a state with the maximum electron spin projection, collisions may change the population of the Zeeman levels, only if they change the angular momentum m of the collision complex. This follows from the conservation of the total angular momentum projection on the quantization axis. Before the collision, the projection of the total electron spin of the combined system on the z -axis is 1 and after the collision it is -1 . The sum of the electron spin projection and m cannot change so m must change from 0 to 2. According to Eqs. (2.21) and (2.26), such process at zero magnetic field is suppressed by a factor k_j^4 . The threshold laws for transitions changing energy are modified (*cf.*, Eq. (2.31)); however, the limiting zero-field value determines the absolute magnitude of the cross section in weak fields and Eqs. (2.21) and (2.26) indicate that collisional spin relaxation of ultracold molecules initially in a maximum spin state will be strongly suppressed. This suppression of collisional energy transfer in 3D has been observed by Volpi and Bohn [85].

The symmetry of the problem will dramatically change, if the magnetic field axis is rotated with respect to the confinement plane normal. The interaction potential matrix that drives the spin-depolarization transitions remains diagonal in the total angular momentum projection [86]. The electron spin is, however, no longer projected on the quantization axis. The Zeeman states can be written in terms of the spin states projected on the z -axis as follows:

$$\begin{aligned} \left|\frac{1}{2}\right\rangle_B &= \cos(\gamma/2)\left|\frac{1}{2}\right\rangle_z - \sin(\gamma/2)\left|-\frac{1}{2}\right\rangle_z \\ \left|-\frac{1}{2}\right\rangle_B &= \sin(\gamma/2)\left|\frac{1}{2}\right\rangle_z + \cos(\gamma/2)\left|-\frac{1}{2}\right\rangle_z \end{aligned} \quad (2.37)$$

where the subscripts indicate the axis of projection and γ is the angle between the magnetic field axis and the confinement plane normal. The Zeeman levels are thus superpositions of different projection states in the coordinate system defined by the confinement and transitions from the Zeeman state $\left|\frac{1}{2}\right\rangle_B$ no longer have to change the orbital angular momentum m . We conclude that Zeeman transitions in

collisions of molecules or atoms in states with maximum spin projections on the magnetic field axis must be suppressed if the magnetic field axis is perpendicular to the plane of confinement and enhanced if the magnetic field axis is directed at a non-zero angle with respect to the confinement plane normal.

2.5 Conclusion

We have presented an analysis of elastic and inelastic collisions of ultracold atoms or molecules confined in 2D geometry. Our derivations demonstrate that the ultracold collisions accompanied with changes of the angular momentum m in 2D must be suppressed by the same factor as in 3D. This has important consequences for angular momentum transfer in 2D collisions. For example, this indicates that Zeeman and Stark transitions in collisions of atoms and molecules in maximally stretched states will be suppressed at low external fields as in 3D collisions, if the external field is oriented perpendicularly to the plane of confinement. The symmetry of the collision problem in 2D may, however, be broken by tilting the external field axis with respect to the confinement plane normal, which should result in dramatic enhancement of angular momentum transfer at extremely low collision energies.

Chapter 3

Controlling molecular collisions with microwave fields

3.1 Introduction

Controlling molecular interactions with lasers has been an important goal in chemical dynamics research for the past five decades [87–91]. This goal stimulated the development of the research fields of coherent and optimal control of molecular processes [87], attosecond spectroscopy [89, 90] and stereodynamics [91]. Many experiments demonstrated that laser fields can be used to selectively induce or suppress uni-molecular dynamical processes such as photodissociation [87, 89, 90, 92]. Controlling molecular collisions has, however, proven to be much more difficult. The effects of external laser fields are usually negated by thermal motion of molecules and perturbative molecule - field interactions do not affect molecular collisions in a thermal gas [93]. In order to achieve external field control over molecular collision processes, it is necessary to create molecular ensembles with the temperature smaller than the energy of molecule - field interactions. Recent technological advances in cooling molecules enable the production molecular gases at ultracold temperatures with densities up to 10^{12} cm^{-3} [94–97].

In the previous chapter we discussed the effects of laser fields with frequencies in the visible region of electromagnetic spectrum on collisions of atoms and molecules. In particular, we showed that strong laser fields of the optical lattices

can confine the motion of the center of mass and modify the collisional threshold laws of atoms and molecules. In this chapter we investigate the effects of the microwave field on collisional dynamics of atoms and molecules. Microwave fields operate in the frequency of fine structure atomic and rotational molecular transitions and they are especially important for operation with polar molecules due to strong electric dipole induced couplings. For example, a proper choice of parameters of static electric and microwave fields can cancel the leading dipole-dipole interaction term in the intermolecular potential [98]. The remaining van der Waals term (C_6/R^6) is repulsive in 3D. Thus, inelastic collisions can be suppressed and simultaneously elastic collisions enhanced, which is important for stabilization and evaporative cooling of polar molecules. A strong intermolecular interaction with a C_3/R^3 potential and three-body interaction terms can be created by application of dc electric and mw fields to polar molecules trapped in 2D optical lattices, which can be used for the realization of strongly correlated and exotic quantum phases such as Wigner crystals [52], spin liquids and topological phases [99]. A microwave magnetic dipole force trap for neutral atoms was suggested by Agosta et al [100]. The atoms in a microwave trap can be trapped in the low energy spin state, and therefore spin-relaxation processes leading to trap loss are suppressed in a microwave traps. Low rates of spontaneous emission for microwave transitions and the suppression of the spin-changing collisions result in large lifetimes for atoms in a trap, which allows the creation of ultracold atomic ensembles with larger densities. Furthermore, due to a large trapping volume and high trap depth, microwave traps should allow for evaporative cooling of large ensembles of atoms. The first experimental demonstration of Cs atom trapping with microwave fields was reported by Spreuw et al [101]. They obtained the ~ 0.1 mK deep trap for laser cooled Cs atoms in a spherical microwave cavity.

DeMille, Glenn, and Petricka have recently proposed a scheme to trap polar molecules in a microwave cavity [102]. This approach has several advantages over optical, dc Stark and magnetic traps. The trapping potential of the microwave cavity is based on the interaction of the molecular electric permanent dipole moment with the electric field so it is deeper than those of the magnetic and optical [1] traps, which makes the trap loading easier. Molecules in microwave cavities can potentially be confined in their absolute ground state, which suppresses the prob-

ability of inelastic collisions leading to trap loss. Microwave traps can potentially hold a large number of molecules at temperatures as high as 0.5 - 1 K. However, further cooling may be required to reach the ultracold temperature regime. This can be achieved by evaporative or sympathetic cooling inside the trapping area, which relies on the relative efficiency of elastic and inelastic collisions. It is, therefore, particularly important to analyze the collision dynamics of polar molecules in the presence of microwave fields. In this chapter we discuss collisions of polar molecules in a microwave cavity using the dressed-state formalism [103] to describe molecule-field interactions. We perform accurate coupled-channel calculations of cross sections for low-temperature elastic and inelastic collisions of CaH molecules with He atoms. We neglect the spin structure of CaH molecule, so it is used as a simple $^1\Sigma$ molecule. The CaH-He potential is slightly anisotropic, for more complicated systems such as molecule - P atom or molecule-molecule the potential should be more anisotropic and, therefore, the overall effects are expected to be more pronounced.

3.2 Field-dressed approach

The idea to use the dressed-state formalism for quantum scattering calculations of slow atom-atom collisions in an intense near-resonant laser field of the optical trap was proposed by Julienne [104]. He showed that the couplings with the radiation field largely modify the long-range part of the interaction potential between two atoms, accelerating them towards each other in the intermediate region and, therefore, increasing the scattering cross section. The coupled-channel calculations for atoms dressed by optical [105] and microwave and rf field [106, 107] were carried out. In this section we introduce the dressed-field approach and its connection to the Floquet and quantum mechanical description of atoms in an electromagnetic field.

3.2.1 Semiclassical Floquet theory

Consider an atom in the presence of a strong laser field varying periodically in time, treated semiclassically. Shirley showed [108], that the Hamiltonian of this system can be replaced by a time-independent Hamiltonian represented by an infinite ma-

trix. He also showed that this approach is equivalent to a purely quantum approach in the limit of strong laser fields [108]. For a two-level atom, the exact solution of this problem can be obtained upon application of the rotating-wave approximation. The rotating wave approximation is valid near resonance or when the intensity of the laser field, or coupling to the laser field is weak. We are interested in obtaining the approximation to the exact solution of this system, which is beyond the rotating-wave approximation, since the coupling of the permanent dipole moment of the molecule to the electric field component of the microwave field can be made very strong. Following Shirley [108], we consider the time-dependent Schrödinger equation for the matrix of expansion coefficients of the total wave function in some atomic basis:

$$i\frac{d}{dt}\mathbf{F}(t) = \mathbf{H}_C(t)\mathbf{F}(t), \quad (3.1)$$

where $\mathbf{H}_C(t) = \mathbf{H}_a + \mathbf{H}_{\text{int}}^c(t)$ is a composite periodic semiclassical Hamiltonian describing the interaction of the atom with the laser field $\mathbf{E}(\mathbf{r}, t) = E_0(\mathbf{r})\boldsymbol{\epsilon}\cos(\omega t)$ ($T=2\pi/\omega$) and $F(t)$ is a time-dependent matrix of the expansion coefficients giving the total wave function in atomic basis $|\alpha\rangle$. The \mathbf{H}_a is a Hamiltonian matrix describing atom in the absence of field. The Hamiltonian for the interaction of the atom with the laser field $\mathbf{H}_{\text{int}}^c(t)$ in dipole approximation can be expressed as

$$\mathbf{H}_{\text{int}}^c(t) = -\mathbf{d} \cdot \mathbf{E}(\mathbf{r}, t) = -E_0(\mathbf{r})\mathbf{d} \cdot \boldsymbol{\epsilon}\cos(\omega t) \quad (3.2)$$

The general form of the solution of Eq.(3.3) according to the Floquet's theorem can be written:

$$\mathbf{F}(t) = \boldsymbol{\Phi}(t)e^{-i\mathbf{Q}t}, \quad (3.3)$$

where $\boldsymbol{\Phi}(t)$ is a periodic solution with period T , and \mathbf{Q} is a Hermitian matrix, the diagonal elements q_α of which satisfy [108]

$$\sum_{\alpha} q_{\alpha} = \frac{1}{T} \int_0^T \text{Tr}\mathbf{H}_C(t)dt(\text{mod}\omega). \quad (3.4)$$

Expanding the Hamiltonian:

$$\mathbf{H}_C = \sum_n \mathbf{H}_C^n e^{-in\omega t}, \quad (3.5)$$

and the general form of the solution:

$$\mathbf{F}(t) = \sum_n \mathbf{F}^n(t) e^{-in\omega t} e^{-i\mathbf{Q}t}, \quad (3.6)$$

in Fourier series and substituting into the time dependent Shrodinger equation 3.1, one gets the following matrix equation:

$$\sum_{\gamma m} [(\mathbf{H}_C^{n-m})_{\alpha,\gamma} + n\omega \delta_{\alpha,\gamma} \delta_{m,n}] \mathbf{F}_{\gamma,\beta}^m = \sum_{\gamma m} (\mathbf{H}_F)_{\alpha n, \gamma m} \mathbf{F}_{\gamma,\beta}^m = q_\beta \mathbf{F}_{\alpha,\beta}^n, \quad (3.7)$$

where $(\mathbf{H}_F)_{\alpha n, \gamma m} = \langle \alpha n | \mathbf{H}_F | \gamma m \rangle$ is an infinite matrix representation of the Floquet Hamiltonian in basis $|\alpha n\rangle$, α denotes the atomic state and n is the Fourier component. In our case the Fourier components of the \mathbf{H}_C matrix are given by

$$(\mathbf{H}_C^{n=0})_{\alpha,\gamma} = (\mathbf{H}_a)_{\alpha,\gamma}, \quad (3.8)$$

$$(\mathbf{H}_C^{n=\pm 1})_{\alpha,\gamma} = -\frac{E_0}{2} \langle \alpha | \mathbf{d} \cdot \boldsymbol{\epsilon} | \gamma \rangle \quad (3.9)$$

The matrix \mathbf{H}_F has an infinite number of eigenvalues $\{\varepsilon_{\alpha n}\}$ of the form $\varepsilon_{\alpha n} = \lambda_\alpha + n\omega$, where n is an integer and $1 \leq \alpha \leq \dim(\mathbf{H}_C)$, where $\dim(\mathbf{H}_C)$ is the dimension of the Hamiltonian matrix \mathbf{H}_C . It is obvious that the spectrum consists of the n ($n = \dim(\mathbf{H}_C)$) different eigenvalues shifted by the integer amount of laser frequencies $n\omega$. These energies are called dressed-states of the atom in the field. To clarify the meaning of n , we briefly review the quantum mechanical description of the electromagnetic field.

3.2.2 Quantum theory

Consider an atom in a single mode microwave cavity. The quantum Hamiltonian (\hat{H}_Q) describing the atom and the laser field is given by

$$\hat{H}_Q = \hat{H}_a + \hat{H}_{\text{int}}^q + \hat{H}_f, \quad (3.10)$$

where $\hat{H}_a, \hat{H}_f, \hat{H}_{\text{int}}^q$ are the Hamiltonians for the atom, the field and the atom-field interaction. We consider the single mode microwave cavity with volume V . The

electric field inside the cavity [103] is given by

$$\hat{\mathbf{E}}_T(\mathbf{r}) = \sqrt{\frac{\hbar\omega}{2\epsilon_0 V}} \boldsymbol{\epsilon}(\hat{a} + \hat{a}^\dagger) = \frac{E_0(\mathbf{r})}{2\sqrt{\bar{n}}} \boldsymbol{\epsilon}(\hat{a} + \hat{a}^\dagger), \quad (3.11)$$

where \hat{a}^\dagger and \hat{a} are the photon creation and annihilation operators defined in the basis of the Fock photon number states, $\boldsymbol{\epsilon}$ is the polarization of the laser mode, E_0 is the electric field amplitude, and $\bar{n} = E_0^2 \frac{\epsilon_0 V}{2\hbar\omega}$ is a mean number of photons in the cavity.

The field Hamiltonian \hat{H}_f of such system can be written as

$$\hat{H}_f = \hbar\omega \left(\hat{a}\hat{a}^\dagger + \frac{1}{2} \right). \quad (3.12)$$

The matrix elements of the \hat{H}_f in the basis of the product states $|\alpha n\rangle = |\alpha\rangle|n\rangle$ are $(\hat{H}_f)_{\alpha n, \beta m} = \delta_{\alpha, \beta} \delta_{n, m} (\hbar\omega n + \frac{1}{2})$.

The Hamiltonian for the atom-electric field interaction in the dipole approximation can be written as

$$\hat{H}_{\text{int}}^q = -\mathbf{d} \cdot \hat{\mathbf{E}}_T(\mathbf{r}) = -\frac{E_0(\mathbf{r})}{2\sqrt{\bar{n}}} \mathbf{d} \cdot \boldsymbol{\epsilon} (\hat{a} + \hat{a}^\dagger). \quad (3.13)$$

The matrix elements of the operator \hat{H}_{int}^q are

$$\langle \alpha \bar{n} + n | \hat{H}_{\text{int}}^q | \beta \bar{n} + m \rangle = -\frac{E_0(\mathbf{r})}{2\sqrt{\bar{n}}} \langle \alpha | \mathbf{d} \cdot \boldsymbol{\epsilon} | \beta \rangle \left(\sqrt{\bar{n} + m - 1} \delta_{n, m-1} + \sqrt{\bar{n} + m + 1} \delta_{n, m+1} \right). \quad (3.14)$$

In the limit of a large photon number $\bar{n} \gg n \geq 1$, the square root can be approximated as $\sqrt{\bar{n} + m \pm 1} \sim \sqrt{\bar{n}}$, and the matrix elements of \hat{H}_{int}^q take on the following form

$$\langle \alpha \bar{n} + n | \hat{H}_{\text{int}}^q | \beta \bar{n} + m \rangle = -\frac{E_0(\mathbf{r})}{2} \langle \alpha | \mathbf{d} \cdot \boldsymbol{\epsilon} | \beta \rangle (\delta_{n, m-1} + \delta_{n, m+1}). \quad (3.15)$$

Now, one can see, that in the limit of large mean photon number states \bar{n} the matrix elements of the quantum Hamiltonian \hat{H}_Q are the same as the matrix ele-

ments of the Floquet Hamiltonian up to a constant total energy shift

$$(\hat{H}_Q)_{\alpha\bar{n}+n,\beta\bar{n}+m} = (\mathbf{H}_F)_{\alpha n,\beta m} + \hbar\omega(\bar{n} + 1/2)\delta_{\alpha,\beta}\delta_{n,m}. \quad (3.16)$$

We see that the integer n in the Floquet theory is equivalent to the number of absorbed or emitted photons in quantum theory and the Floquet state $|\alpha n\rangle$ is equivalent to the quantum state $|\alpha\bar{n} + n\rangle$. For convenience we treat the laser field quantum mechanically assuming a large mean number of photons $\bar{n} \gg 1$ in the mode and refer to the eigenstates of \hat{H}_Q as field-dressed states. The field-dressed therefore represent the eigenstates of the interacting atom-radiation system. The transitions between the field-dressed states can be observed experimentally by probing them with a second weak field [109, 110]. The plots of the dressed state energies as functions of frequency, electric or magnetic fields can help to identify resonances and correctly determine channel energies of atoms in the collision of particles in the presence of ac fields. By truncating the number of photons n , we can approximate the eigenvalues of the infinite matrix with sufficient accuracy and build a consistent approximation to the exact solution.

3.2.3 $^1\Sigma$ molecules in a microwave cavity

In this section we discuss the application of the dressed field formalism for polar molecules in a microwave cavity. The rotational energy levels of a $^1\Sigma$ molecule in the absence of external fields are described by the Hamiltonian $B_e\hat{N}^2$ with the rotational angular momentum \hat{N} and the rotational constant B_e . The eigenstates of this Hamiltonian are spherical harmonics of rank N :

$$B_e\hat{N}^2|NM_N\rangle = B_eN(N+1)|NM_N\rangle, \quad (3.17)$$

where M_N is the projection of \hat{N} on a space-fixed quantization axis.

The microwave field is described by the number of photons $\bar{n} + n$ in a given frequency mode, where \bar{n} is a mean number of photons in the cavity and n is a small integer number. Here, we consider a single-mode field. The Hamiltonian of the single-mode field can be written as $\hbar\omega(\hat{a}^\dagger\hat{a} - \bar{n})$, where \hat{a}^\dagger and \hat{a} are the photon

creation and annihilation operators:

$$\begin{aligned}\hat{a}|\bar{n}+n\rangle &= \sqrt{\bar{n}+n}|\bar{n}+n-1\rangle, \\ \hat{a}^\dagger|\bar{n}+n\rangle &= \sqrt{\bar{n}+n+1}|\bar{n}+n+1\rangle.\end{aligned}\quad (3.18)$$

The energy of the field is given by:

$$\hbar\omega(\hat{a}^\dagger\hat{a} - \bar{n})|\bar{n}+n\rangle = n\hbar\omega|\bar{n}+n\rangle. \quad (3.19)$$

The wave function of the rigid rotor in a microwave field can be expanded in the basis of direct products

$$|NM_N\rangle|\bar{n}+n\rangle. \quad (3.20)$$

The energy levels of the molecule in the ac field can then be found by diagonalizing the following Hamiltonian in the basis set (3.20):

$$\hat{H}_{\text{as}} = B_e\hat{\mathbf{N}}^2 + \hbar\omega(\hat{a}^\dagger\hat{a} - \bar{n}) + \hat{H}_{\text{m,f}}, \quad (3.21)$$

where the operator $\hat{H}_{\text{m,f}}$ describes the molecule-field interaction. We consider linearly polarized light with the polarization along the space-fixed quantization z -axis. For such a field orientation, the projection of the total angular momentum of the system on z axis is conserved. The interaction of the dipole moment of the molecule with a linearly polarized ac field is described by

$$\hat{H}_{\text{m,f}} = -\frac{\Omega}{2\sqrt{\bar{n}}}(\hat{a} + \hat{a}^\dagger)\cos\phi, \quad (3.22)$$

where ϕ is the angle between the polarization axis and the molecular axis, $\Omega = \varepsilon d$ is the strength of the field-induced coupling, d is the permanent dipole moment of the molecule and ε is the electric field component of the laser light. We assume that $\bar{n} \gg n$. Under this condition $\sqrt{\bar{n}+n} \approx \sqrt{\bar{n}+n-1} \approx \sqrt{\bar{n}}$. Therefore, the matrix elements of the operator $H_{\text{m,f}}$ in the basis (3.20) have the following form:

$$\langle N'M'_N|\langle\bar{n}+n'|\hat{H}_{\text{m,f}}|NM_N\rangle|\bar{n}+n\rangle =$$

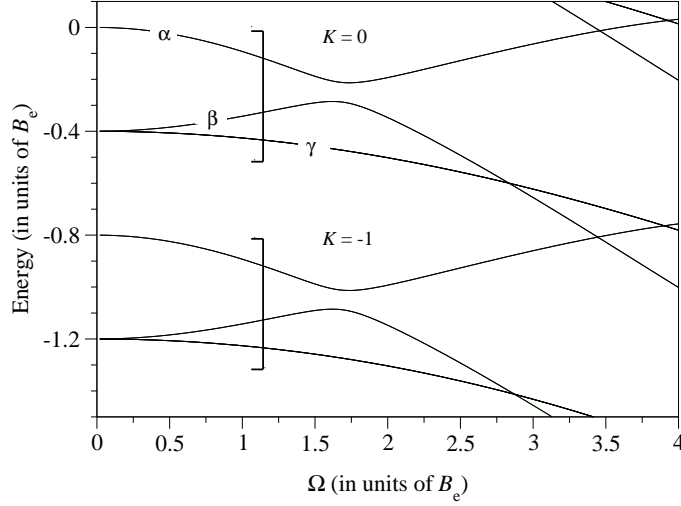


Fig. 3.1: Energy levels of a $^1\Sigma$ polar molecule in a microwave laser field as functions of the field-induced coupling strength Ω at a laser frequency $\hbar\omega/B_e = 0.8$. In the limit $\Omega \rightarrow 0$, the field-dressed states for $K = 0$ are: $(\alpha) - |N = 0 M_N = 0 n = 0\rangle$, $(\beta) - |N = 1 M_N = 0 n = -1\rangle$, $(\gamma) - |N = 1 |M_N| = 1 n = -1\rangle$.

$$-\frac{\Omega}{2}(\delta_{n',n-1} + \delta_{n',n+1})b_{N'M'_N, NM_N}, \quad (3.23)$$

where $b_{N'M'_N, NM_N} = \langle N'M'_N | \cos \phi | NM_N \rangle$. The matrix elements of $\cos \phi$ can be evaluated using the spherical harmonics addition theorem and the Wigner-Eckart theorem leading to the following expression:

$$b_{N'M'_N, NM_N} = \delta_{M'_N, M_N} (-1)^{M_N} \sqrt{(2N'+1)(2N+1)} \\ \times \begin{pmatrix} N' & 1 & N \\ 0 & 0 & 0 \end{pmatrix} \begin{pmatrix} N' & 1 & N \\ -M_N & 0 & M_N \end{pmatrix}, \quad (3.24)$$

where the parentheses denote $3j$ symbols. The first $3j$ symbol in Eq. (3.24) vanishes unless $N' = N \pm 1$. Therefore, $\hat{H}_{m,f}$ has no diagonal matrix elements and

it couples states with different photon numbers $n' = n \mp 1$ and rotational angular momentum quantum numbers $N' = N \pm 1$.

The eigenspectrum of the operator (3.21) can be divided into manifolds separated by multiples of the photon frequency, as illustrated in Fig. 3.1. Each state can be labeled by two quantum numbers: index K for the photon manifold and index ν for the field-dressed states within the manifold. An alternative way to label the quantum states could be to assign them the quantum numbers of the molecular state and the photon number state (N, M_N, n) which adiabatically correlate with a state of interest at zero Ω .

The field-dressed states can be generally written as

$$|\nu K\rangle = \sum_{NM_N} \sum_n C_{NM_N, n; \nu K} |NM_N\rangle |\bar{n} + n\rangle, \quad (3.25)$$

The transitions $|\nu K\rangle \rightarrow |\nu K'\rangle$ decrease (increase) for $K' = K - 1$ ($K' = K + 1$) the number of microwave photons in the cavity by one. Therefore, these transitions should be interpreted as accompanied by absorption (emission) of a photon. In the absence of the molecule - field interaction, the states (3.25) are direct products $|NM_N\rangle |\bar{n} + n\rangle$, representing the molecule in a particular rotational state and the quantized electromagnetic field with a given number of photons. When $\Omega > 0$, the field-dressed states are coherent superpositions of these product states. If the field is switched off adiabatically, the field-dressed states become the rotational states of the molecule in the $\Omega = 0$ limit. If the field is switched off rapidly, the molecule must remain in a coherent superposition of rotational states.

3.2.4 Scattering formalism

The interaction of a diatomic molecule with a structureless atom in the presence of external fields can be described by the following Hamiltonian:

$$\hat{H} = -\frac{1}{2\mu} \frac{d^2}{dR^2} + \frac{\hat{\mathbf{I}}^2}{2\mu R^2} + \hat{V}(R, r, \theta) + \hat{H}_{\text{as}}, \quad (3.26)$$

where μ is the reduced mass of the collision complex, R is the separation between the center of mass of the molecule and the atom, r is the interatomic distance in

the molecule and θ is the angle between \mathbf{R} and \mathbf{r} . The asymptotic Hamiltonian \hat{H}_{as} describes non-interacting atom and molecule in the presence of fields. The angular momentum operator \hat{l} describes the rotation of the collision complex in the space-fixed coordinate frame, and $\hat{V}(R, r, \theta)$ is the atom-molecule electrostatic interaction potential.

The total wave function of the collision complex is expanded in products of the field-dressed states (3.25) and the rotational functions of the collision complex $|lm_l\rangle$ as follows

$$\Psi = \sum_{\nu K l m_l} F_{\nu K l m_l}^M(R) |\nu K\rangle |l m_l\rangle. \quad (3.27)$$

The substitution of expansion (3.27) into the Schrödinger equation with Hamiltonian (3.26) leads to a system of coupled differential equations for the expansion coefficients $F_{\nu K l m_l}^M(R)$ parametrized by fixed values of the total angular momentum projection $M = M_N + M_s + m_l$ (for the case of parallel fields) and the total energy E_{tot} :

$$\left[\frac{d^2}{dR^2} + 2\mu(E_{\text{tot}} - E_{\nu, K}) - \frac{l(l+1)}{R^2} \right] F_{\nu K l m_l}^M(R) = \times 2\mu \sum_{\nu' K' l' m'_l} \langle \nu K l m_l | \hat{V}(R, r, \theta) | \nu' K' l' m'_l \rangle F_{\nu' K' l' m'_l}^M(R). \quad (3.28)$$

Here, $E_{\nu, K}$ is an eigenvalue of \hat{H}_{as} (given by Eq. (3.21) for $^1\Sigma$ molecules), i.e. the energy of a given $|\nu K\rangle$ field-dressed state. The matrix elements of the interaction potential $V(R, r, \theta)$ in the basis (3.27) can be written as follows:

$$\begin{aligned} \langle \nu K l m_l | \hat{V} | \nu' K' l' m'_l \rangle &= \sum_{n M_s N M_N N' M'_N} C_{N M_N n M_s, \nu K} \\ &\times C_{N' M'_N n M_s, \nu' K'} \langle N M_N l m_l | \hat{V} | N' M'_N l' m'_l \rangle, \end{aligned} \quad (3.29)$$

where the integrals $\langle N M_N l m_l | \hat{V} | N' M'_N l' m'_l \rangle$ can be evaluated by expanding the interaction potential in spherical harmonics

$$V(\mathbf{R}, \mathbf{r}) = \sum_{\lambda} \frac{4\pi}{2\lambda + 1} V_{\lambda}(R, r) \sum_{m_{\lambda}} (-1)^{m_{\lambda}} Y_{\lambda, -m_{\lambda}}(\hat{\mathbf{R}}) Y_{\lambda, m_{\lambda}}(\hat{\mathbf{r}}), \quad (3.30)$$

and applying the Wigner-Eckart theorem [111]. They have the form

$$\begin{aligned}
\langle NM_N l m_l | \hat{V} | N' M'_N l' m'_l \rangle &= \sum_{\lambda} V_{\lambda}(R, r) \\
&\times \begin{pmatrix} l & \lambda & l' \\ 0 & 0 & 0 \end{pmatrix} \begin{pmatrix} N & \lambda & N' \\ 0 & 0 & 0 \end{pmatrix} [(2l+1)(2l'+1)]^{1/2} \\
&\times [(2N+1)(2N'+1)]^{1/2} \sum_{m_{\lambda}} (-1)^{m_{\lambda}-m_l-M_N} \\
&\times \begin{pmatrix} l & \lambda & l' \\ -m_l & -m_{\lambda} & m'_l \end{pmatrix} \begin{pmatrix} N & \lambda & N' \\ -M_N & m_{\lambda} & M'_N \end{pmatrix}. \quad (3.31)
\end{aligned}$$

The coupled-channel equations (3.28) are integrated using the log-derivative method. The numerical solutions subject to the scattering boundary conditions yield the scattering matrix $S_{vKlm_l;v'K'l'm'_l}^M$ or the probability amplitudes for transitions between different scattering channels labeled by v, K, l, m_l .

The state-resolved cross sections for elastic and inelastic collision processes in a microwave cavity are computed from the S -matrix as

$$\sigma_{v,K \rightarrow v',K'} = \left(\frac{\pi}{k_{vK}^2} \right) \sum_M \sum_{l m_l} \sum_{l' m'_l} |\delta_{l m_l, l' m'_l} \delta_{vK, v'K'} - S_{vKlm_l;v'K'l'm'_l}^M|^2, \quad (3.32)$$

where $k_{vK}^2 = 2\mu(E_{\text{tot}} - E_{v,K})$.

3.2.5 Coupled-channel calculations for atom-molecule scattering in a microwave field

We consider collisions of CaH molecules with ^3He atoms. We neglect the spin structure of CaH molecule and therefore treat it as $^1\Sigma$ molecule. The interaction potential for the CaH-He system was calculated by Groenenboom and Balakrishnan [112].

Figure 3.2 shows the energy levels of CaH (or any other polar molecule) in a microwave field as functions of the Rabi frequency at $\hbar\omega/B_e = 1.9$. We consider collisions of CaH molecules in the state $|v = \alpha, K = 0\rangle$, which correlates with the ground rotational state $N = 0$ of CaH at zero field. The states of different K may

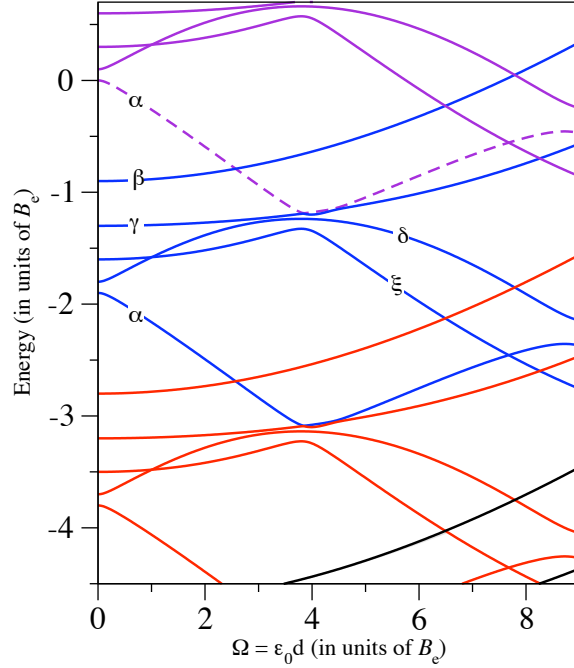


Figure 3.2: Energy levels of a polar molecule in a microwave cavity as functions of the Rabi frequency at $\hbar\omega/B_e = 1.9$. The levels are grouped in manifolds labeled by K . The initial state for scattering calculations is shown by the dashed line. At $\Omega \rightarrow 0$, the field-dressed states for $K = -1$ are: $|N = 0, n = -1\rangle$ (α), $|N = 4, n = -11\rangle$ (β), $|N = 3, n = -7\rangle$ (γ), $|N = 1, n = -2\rangle$ (ξ), and $|N = 2, n = -4\rangle$ (δ).

interact when $\Omega \geq 3B_e$. We consider moderate Rabi frequencies $0 < \Omega < B_e$ [102].

Figure 3.3 shows the cross sections for elastic scattering and inelastic relaxation in CaH-He collisions as functions of Ω at a collision energy of 0.3 cm^{-1} . In order to obtain converged results, we included in the total wave function expansion 5 rotational states of the molecule, 14 photon number states and 4 angular momenta l , which yields a system of 1744 differential equations for zero total angular momentum projection. The probabilities for inelastic collisions increase with decreasing the detuning from resonance $\Delta = 2B_e - \hbar\omega$. For the off-resonant microwave frequencies of 0.01 and $1.1B_e$, the inelastic cross sections increase monotonically with increasing Ω . At a near-resonant frequency of $1.9B_e$, the cross sections increase by a factor of ~ 50 and show broad oscillations. The difference between the cross

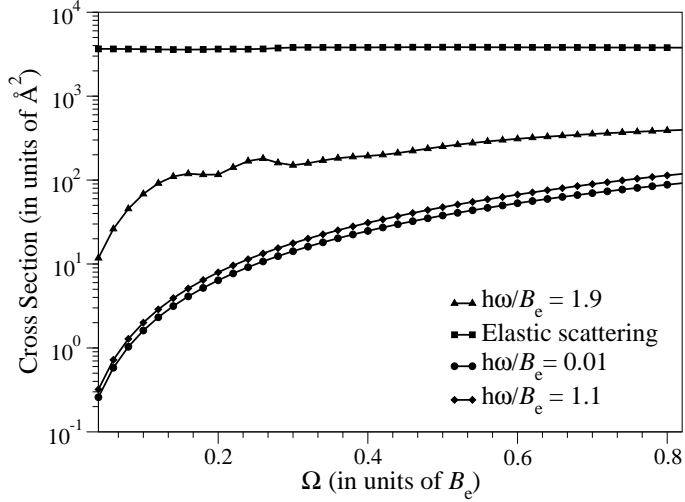


Figure 3.3: Cross sections for elastic scattering (squares) and inelastic relaxation of CaH molecules induced by collisions with He in a microwave field with $\hbar\omega/B_e = 1.9$ (triangles), 1.1 (diamonds), and 0.01 (circles) as functions of the field intensity. The elastic cross section is for the microwave field frequency of $1.9B_e$. The inelastic cross sections are summed over all energetically accessible field-dressed states except the elastic channel. The collision energy is 0.3 cm^{-1} .

sections corresponding to different microwave frequencies becomes smaller with increasing the field strength. The elastic scattering cross section is insensitive to the field.

The propensities for collision-induced transitions in a microwave field can be elucidated from Fig. 3.4, which presents state-resolved cross sections for inelastic transitions to various final field-dressed states. As our initial state is the ground state in the $K = 0$ manifold, inelastic relaxation involves transitions between different photon manifolds. Figure 3.4 shows that the total relaxation probability is determined by two major transitions: $|\alpha, K = 0\rangle \rightarrow |\alpha, K' = -1\rangle$ and $|\alpha, K = 0\rangle \rightarrow |\xi, K = -1\rangle$. The field-dressed states $|\alpha, K = 0\rangle$ and $|\alpha, K' = -1\rangle$ differ exactly by one quantum of microwave field energy. Therefore, the transition $|\alpha, K = 0\rangle \rightarrow |\alpha, K' = -1\rangle$ should be interpreted as a collision process accompa-

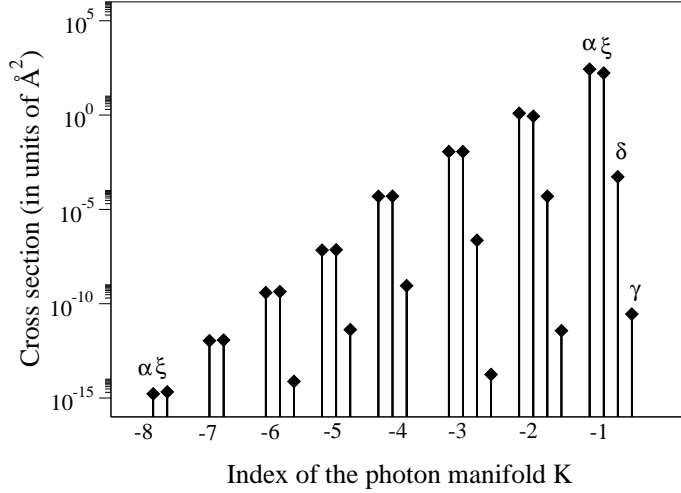


Figure 3.4: State-resolved cross sections for inelastic relaxation of CaH in a microwave field with $\hbar\omega/B_e = 1.9$ and $\Omega/B_e = 0.5$. The collision energy is 0.3 cm^{-1} . The inelastic channels are labeled according to Fig. 3.2.

nied by absorption of a microwave photon. The molecule-field interaction couples the product states with $\Delta N = \pm 1$ and $\Delta n = \mp 1$, so the strongest couplings occur between the field-dressed states in the adjacent photon manifolds ($\Delta K = \pm 1$). Figure 3.4 shows that the transitions with the minimal change of K are the most probable, and that the transition probabilities decrease rapidly with increasing ΔK .

The collision-induced transitions are induced by the matrix elements of the electrostatic interaction potential in the field-dressed basis Eq.(3.31). The anisotropic part of the interaction potential terms in this expansion ($\lambda \geq 1$) couples different $|NM_N\rangle$ states causing rotationally inelastic transitions. Although the interaction potential only couples the $|NM_N\rangle|\bar{n} + n\rangle$ states with the same n , the molecule-field Hamiltonian has the selection rules $\Delta N = \pm 1$ and $\Delta n = \mp 1$. A combination of the molecule - field and atom - molecule interactions thus leads to couplings between different K , inducing collisional absorption or emission of microwave photons. We have verified that if either the molecule-field interaction or

the anisotropy of the interaction potential are omitted, the different photon manifolds are uncoupled and the transitions $|vK\rangle \rightarrow |v'K'\rangle$ cannot occur unless $K' = K$.

To further elucidate the mechanism of molecular collisions in a microwave cavity, we have developed a simple model for the dominant relaxation channel $|\alpha, K = 0\rangle \rightarrow |\alpha, K' = -1\rangle$ based on the Born approximation. In the limit of small Rabi frequency, the initial and final field-dressed states can be expanded as where the coefficient a_1 is given to first order by

$$a_1 = \frac{\langle N = 0, \bar{n} | \hat{H}_{\text{mol.f}} | N = 1, \bar{n} - 1 \rangle}{\hbar\omega - 2B_e} \sim \frac{\Omega}{\Delta}. \quad (3.33)$$

The inelastic cross section in the Born approximation is given by the square of the matrix element in Eq. (3.29). Using Eq. (3.33) and assuming that $a_0 = \text{const}$, which is consistent with the smallness of Ω , we find

$$\sigma_{\text{inel}} \sim (\Omega/\Delta)^2. \quad (3.34)$$

This result shows that for large Δ , inelastic cross sections decrease quadratically with increasing detuning from resonance, similarly to the photon scattering probability in far-off-resonant optical dipole traps (FORTs).

Microwave fields may also modify the probability of elastic collisions near scattering resonances. Figure 3.5 presents the energy dependence of CaH-He elastic scattering. In the absence of a microwave field, the cross section increases by two orders of magnitude near a shape resonance at a collision energy of 0.04 cm^{-1} . The microwave field of $\Omega/B_e = 0.5$ suppresses the shape resonance. As the microwave detuning decreases from $1.5B_e$ to $0.1B_e$, the cross section maximum becomes smaller and shifts to higher collision energies. The interaction of the molecule with a microwave field leads to indirect couplings between different partial waves, which alter the shape of the centrifugal barrier and suppress shape resonances.

3.3 Conclusion

We have presented an accurate quantum mechanical study of low-temperature collisions of polar molecules in a microwave field using dressed-field approach to

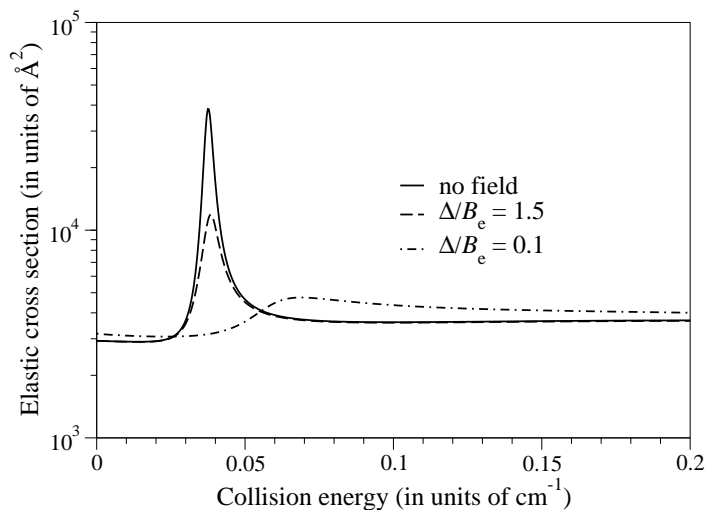


Figure 3.5: Modification of a shape resonance by microwave laser fields. The elastic cross section is plotted as a function of the collision energy for zero microwave field (full line), $\Delta/B_e = 1.5$ (dashed line), $\Delta/B_e = 0.1$ (dotted line). The Rabi frequency is $0.5B_e$.

describe interactions of the molecule with microwave field. Our results show that both elastic and inelastic collisions of molecules at temperatures below 1 Kelvin may be very sensitive to the photon field. In particular, we find that inelastic relaxation may occur through transitions between different photon manifolds even when the colliding molecules are in the absolute ground state. This process, driven by the anisotropy of the atom-molecule interaction potential, should be interpreted as collision-induced absorption of microwave photons followed by rotational de-excitation. It is sensitive to both the intensity and frequency of the electromagnetic field.

Chapter 4

Controlling spin-changing collisions of $^2\Sigma$ molecules with microwave field

4.1 Introduction

In this chapter we discuss the effects of microwave fields on spin-changing collisions of polar molecules in a magnetic field. We begin by reviewing recent work on spin-changing collisions of molecules in dc magnetic and electric fields. Next, we extend the field-dressed formalism introduced in the previous chapter to calculate the energy levels of $^2\Sigma$ molecules in the presence of dc magnetic and microwave fields. We discuss the effects of different field parameters. In particular, we are interested to explore the possibility of inducing avoided crossings between different field-dressed states, since the scattering dynamics of molecules is sensitive to small variations of the external fields near such avoided crossings. We derive simple analytical formulas to investigate the effects of the microwave and magnetic fields on the positions and splitting of the avoided crossings and show that the positions of the avoided crossings can be modified by varying the frequency and the intensity of the microwave field. We discuss the mechanisms of microwave field control of spin-dependent interactions in cold open-shell molecules. Finally, we present the

results of quantum scattering calculations of the cross sections for elastic and inelastic collisions of CaH molecules with He atoms in dc magnetic and microwave fields. We show that the microwave field enhances collision-induced spin relaxation. In particular, we demonstrate that collision dynamics of polar $^2\Sigma$ molecules are very sensitive to the field magnitude near the avoided crossings between different field-dressed states.

The complex structure of polar molecules with unpaired electrons (*e.g.*, $^2\Sigma$ radicals) can be used for a variety of applications. For example, ensembles of cold molecules prepared in a particular Zeeman state can be used to study the effects of spin-dependent interactions in chemical reactions. The rotational states of different parity of $^2\Sigma$ molecules exhibit an avoided crossing in the presence of magnetic and electric fields, which can be used to control molecular collisions [113] and collective spin excitation of molecules in an optical lattice [114]. The interferometric measurements of two spin states can be used for high-accuracy determination of the electron's dipole moment [21, 115, 116]. The precision spectroscopy of paramagnetic polar molecules would allow one to explore the time variation of fundamental constants [117, 118]. The imaging of electromagnetic field with cold $^2\Sigma$ molecules gives rise to enhancement of sensitivity and spatial resolution compared to atoms [119]. The hyperfine states of polar molecules are weakly dependent on the electric field fluctuation and therefore are good candidates for storing and processing quantum information (storage qubit) [55]. Exotic spin-lattice models can be simulated by tuning the energy levels of paramagnetic molecules trapped on a two dimensional optical lattice [53] with microwave fields. The inelastic spin-changing collisions of molecules in these schemes often lead to trap loss or decoherence. Molecules in a high-field seeking state can be trapped in a magnetic trap and buffer gas cooled to milli Kelvin temperatures [23]. The spin-changing collisions of molecules in a magnetic traps drive molecules to the untrappable high field-seeking state and result in trap loss [94, 120]. The modification of collisions of molecules in a magnetic trap, *e.g.* with microwave fields, would allow for more efficient cooling of molecular ensembles. On the other hand, the magnetic field can be used to tune Feshbach resonances in collisions of molecules trapped in a microwave or radio frequency trap and therefore the effects of magnetic and microwave fields on elastic and inelastic collisions need to be elucidated.

Collisions of molecules in magnetic fields have been studied by several authors in the context of trapping and cooling of molecules in magnetic traps. The theory of slow collisions was developed by Volpi and Bohn [85]. They demonstrated that collision-induced Zeeman relaxation in weak magnetic fields is suppressed due to the presence of the long-range centrifugal barriers in outgoing channels. Krems and Dalgarno [111] developed a formalism for calculating the collision cross sections in the presence of magnetic fields based on the fully uncoupled basis representation. The quantum scattering calculations for non-polar molecules O_2 - O_2 in magnetic fields were carried out by Tscherbil [121] and Perez-Rios [122]. The quantum scattering calculations for cold and ultracold NH-NH collisions in magnetic fields were performed by Janssen [123].

4.2 $^2\Sigma$ molecules in combined dc magnetic and microwave fields

4.2.1 Field-dressed states

In this section we generalize the dressed-state formalism described in the previous chapter to calculate the energy levels of paramagnetic polar diatomic molecules interacting with both dc magnetic and microwave fields. The Hamiltonian of a $^2\Sigma$ molecule in the presence of dc magnetic and microwave fields takes on the following form:

$$\hat{H}_{\text{as}} = B_e \hat{N}^2 + \gamma \hat{N} \cdot \hat{S} + 2\mu_B \mathbf{B} \cdot \hat{S} + \hbar\omega(\hat{a}^\dagger \hat{a} - \bar{N}) + \hat{H}_{\text{m,f}}, \quad (4.1)$$

where the additional interactions that were not described in the previous chapter are the interaction of the magnetic moment $2\mu_B \hat{S}$ (μ_B is the Bohr magneton and \hat{S} is the spin angular momentum) of the unpaired electron with the external magnetic field \mathbf{B} described by the Zeeman operator $2\mu_B \mathbf{B} \cdot \hat{S}$ and the spin-rotation coupling $\gamma \hat{N} \cdot \hat{S}$, where γ is a phenomenological spin-rotation coupling constant. The spin-rotation terms describe the interaction of the magnetic moment of the electron with the magnetic field created by the rotational motion of the molecule. We assume that the Z -axis of the space-fixed coordinate frame is oriented along the magnetic field.

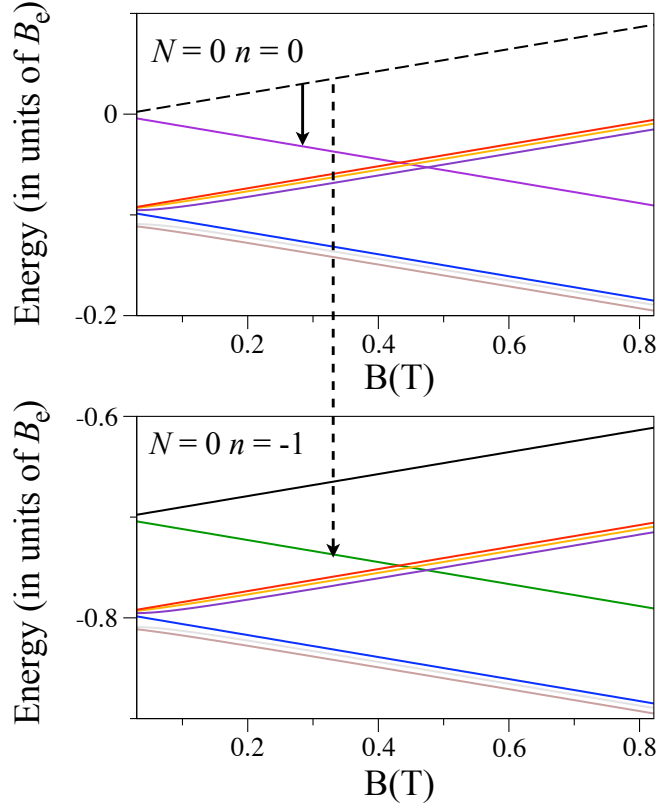


Fig. 4.1: The field-dressed states of the $\text{CaH}(^2\Sigma)$ molecule as function of magnetic field in a microwave field with photon frequency $\hbar\omega/B_e = 0.7$ and $\Omega/B_e = 0.2$. The initial magnetic low-field seeking state (black dashed curve) correlates with $N = 0, n = 0, M_S = 1/2$ state at zero Ω . The solid (dashed) arrows show the spin-relaxation transitions corresponding to $\Delta n = 0$ ($\Delta n = -1$).

Therefore, the Zeeman term takes on the form $2\mu_B M_Z \mathbf{B}$. The matrix elements of the spin-rotation interaction can be calculated using the following expression [124]:

$$\gamma \hat{\mathbf{N}} \cdot \hat{\mathbf{S}} = \gamma \left[\hat{N}_z \hat{S}_z + \frac{1}{2} (\hat{N}_- \hat{S}_+ + \hat{N}_+ \hat{S}_-) \right], \quad (4.2)$$

where N_{\pm} and S_{\pm} are the ladder operators. The explicit expression for the spin-rotation matrix elements is:

$$\begin{aligned} \langle N' M'_N S M'_S n' | \gamma \hat{\mathbf{N}} \cdot \hat{\mathbf{S}} | N M_N S M_S n \rangle &= \delta_{n',n} \delta_{N',N} \\ &\times \gamma \{ \delta_{M'_S, M_S} \delta_{M'_N, M_N} M_N M_S + \frac{1}{2} \delta_{M'_S, M_S \mp 1} \delta_{M'_N, M_N \pm 1} \\ &\times [N(N+1) - M_N(M_N \pm 1)]^{1/2} \times [S(S+1) - M_S(M_S \mp 1)]^{1/2} \}. \end{aligned} \quad (4.3)$$

The spin-rotation interaction is diagonal in the rotational angular momentum N and the photon numbers, and couples molecular states with different projections of spin M_S and rotational angular momentum M_N . The energy levels of the molecule inside the mw cavity in the presence of a dc magnetic field can be calculated by diagonalizing the matrix of \hat{H}_{as} in the basis of direct products of the molecular states and the photon number states $|NM_N\rangle |SM_S\rangle |\bar{N} + n\rangle$, where we have added the spin functions $|SM_S\rangle$ defined in the space-fixed coordinate frame.

Figure 4.1 shows the field-dressed energy levels of the CaH molecules as a function of magnetic field at a microwave field frequency $\hbar\omega/B_e=0.7$ and $\Omega/B_e=0.2$. The states which energy increase (decrease) with increasing magnetic field are called low-field (high-field) seeking states. The black dashed curve denotes the initial low-field seeking state correlating with $N=0$ $n=0$ $M_S=1/2$ state at zero Ω . The arrows indicate the spin-relaxation transitions between states of the same ($\Delta n=0$, solid curve) and different ($\Delta n=-1$, dashed curve) photon manifolds. The final field-dressed states for the spin relaxation transition are correlating with $N=0$ $n=0$ $M_S=-1/2$ and $N=0$ $n=-1$ $M_S=-1/2$ states at zero Ω .

Figure 4.2 shows the field-dressed energy levels of the CaH molecule as a function of the field-induced coupling strength Ω of the microwave field at a magnetic field of 0.1 T and a mw frequency of $\hbar\omega/B_e=0.7$. At non-zero fields, the rotational ground $N=0$ and first excited $N=1$ states split into two and six components respectively. The interaction with the magnetic field at $B=0.1$ T is stronger than the spin-rotation interaction in CaH with $\gamma=0.0415$ cm⁻¹ so M_S is a nearly conserved quantum number. The six states arising from the first rotationally excited state group into two Zeeman manifolds. All states within the manifold are characterized by the same value of M_S . At small coupling strength ($\Omega/B_e \ll 1$) the energy shifts are the same as the dc Stark shifts. At high field intensities we ob-

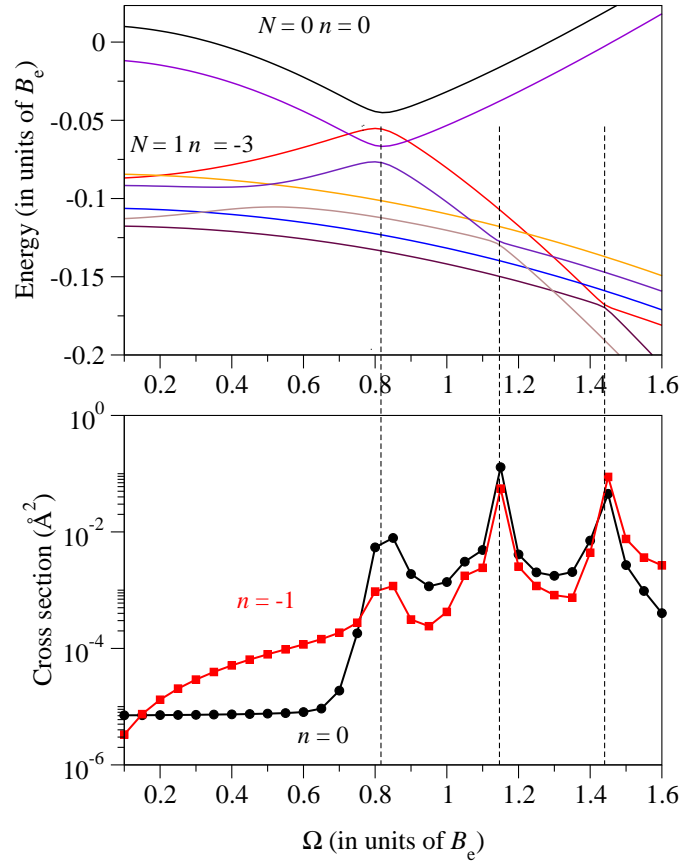


Fig. 4.2: Upper panel: The field-dressed states of the $\text{CaH}(^2\Sigma)$ molecule in a magnetic field of 0.1 T and a microwave field with the photon frequency $\hbar\omega/B_e = 0.7$ as functions of Ω . Lower panel: Cross sections for spin relaxation in $\text{CaH}(^2\Sigma)$ -He collisions at a magnetic fields of 0.1 T and mw frequency of $\hbar\omega/B_e = 0.7$. The curves are labeled by the photon number of the final magnetic high-field seeking state at zero Ω . The collision energy is 0.5 K.

serve a more complex behavior due to multiple avoided crossings. The spin-up and spin-down Zeeman states arising from the first rotationally excited state undergo an avoided crossing at $\Omega = 0.43 B_e$, where they are strongly mixed by a combination of the spin-rotation and Stark interactions. The avoided crossings of the ground $|N = 0 n = 0\rangle$ and first excited $|N = 1 n = -3\rangle$ rotational states shifted by three photon frequencies occur at the values $\Omega = 0.81, 1.15$, and $1.45 B_e$.

4.2.2 Avoided crossings of field-dressed states

The molecular Zeeman states corresponding to different rotational levels cross at a high magnetic field. In the presence of a microwave field these crossings become avoided crossings (see Fig. 4.3). Molecular properties such as orientation and alignment as well as collision cross sections should be very sensitive to the magnitudes of the fields near these avoided crossings [125, 126]. Our calculations show that the location of the avoided crossings can be manipulated by both microwave and magnetic fields. Figure 4.4 depicts the position of the avoided crossing between the $|N = 0 M_N = 0 M_S = \frac{1}{2} n = 0\rangle$ and $|N = 1 M_N = 1 M_S = -\frac{1}{2} n = -1\rangle$ states as a function of the magnetic field strength and the microwave field parameters. The avoided crossings occur at lower magnetic fields as the frequency of the mw field is increased. Increasing Ω shifts the positions of the avoided crossings to higher magnetic fields. The Zeeman levels $|a\rangle = |N = 0 M_N = 0 M_S = \frac{1}{2} n = 0\rangle$ and $|b\rangle = |N = 1 M_N = 1 M_S = -\frac{1}{2} n = -1\rangle$ cross at the magnetic field value B_c which can be defined to zeroth order by the equation $2\mu_B B_c = \Delta$, where $\Delta = 2B_e - \hbar\omega$ is the detuning from the resonance.

The energy levels near the avoided crossings can be described by an effective Hamiltonian [103]:

$$\hat{H}_{\text{eff}} = \begin{pmatrix} \mu_B B + \hat{R}_{aa}(\Delta/2) & \hat{R}_{ab}(\Delta/2) \\ \hat{R}_{ba}(\Delta/2) & \Delta - \mu_B B + \hat{R}_{bb}(\Delta/2) \end{pmatrix} \quad (4.4)$$

where $\hat{R}(\Delta/2)$ is a *level-shift operator* evaluated at the energy of the crossing $\Delta/2$. The level-shift operator $\hat{R}(z)$ can be represented by the following perturbative ex-

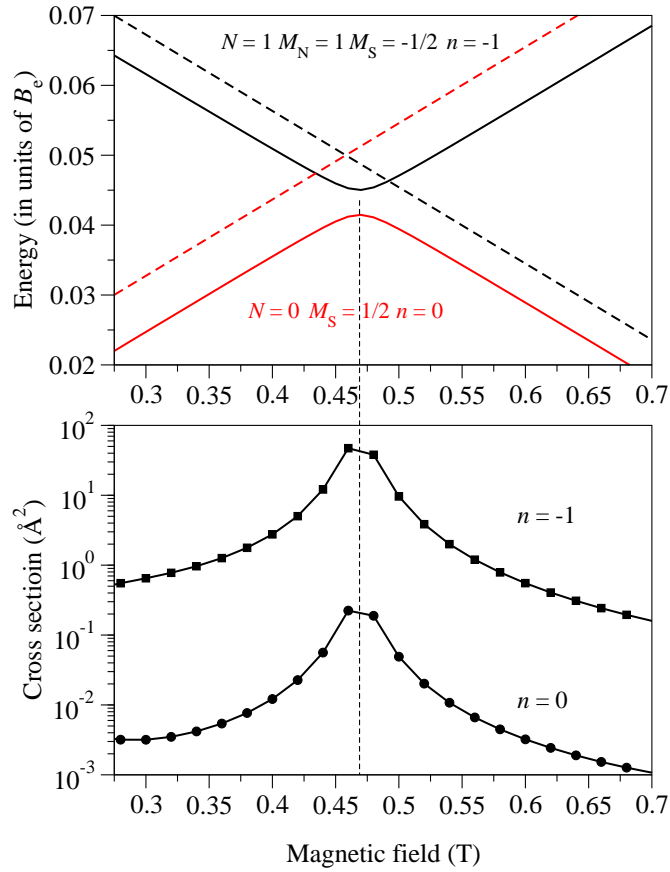


Fig. 4.3: Upper panel: The eigenvalues of \hat{H}_0 (dashed lines) and the Zeeman energy levels of the $\text{CaH}(^2\Sigma)$ molecule in combined magnetic and microwave mw field. The microwave field parameters are $\hbar\omega/B_e = 1.9$ and the field-induced coupling strength $\Omega/B_e = 0.1$. Lower panel: Cross sections for spin relaxation in $\text{CaH}(^2\Sigma)$ -He collisions at a mw frequency of $\hbar\omega/B_e = 1.9$ and the field-induced coupling strength $\Omega/B_e = 0.1$. The curves are labeled by the photon number of the final magnetic high-field seeking state at zero Ω . The collision energy is 0.5 K.

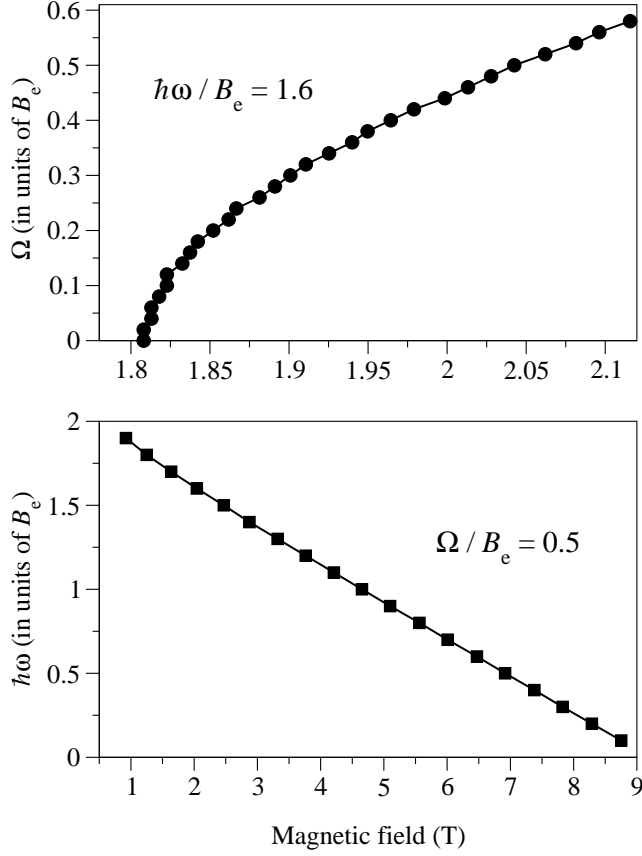


Fig. 4.4: The dependence of the position of the avoided crossing between the field-dressed states of $\text{CaH}(^2\Sigma)$ molecule in a microwave field with $\hbar\omega/B_e = 1.6$ (upper panel) and $\Omega/B_e = 0.5$ (lower panel).

pansion [103]:

$$\hat{R}(z) = \hat{V} + \hat{V} \frac{\hat{Q}}{z - \hat{H}_0} \hat{V} + \hat{V} \frac{\hat{Q}}{z - \hat{H}_0} \hat{V} \frac{\hat{Q}}{z - \hat{H}_0} \hat{V} + \dots, \quad (4.5)$$

where \hat{H}_0 and \hat{V} are parts of the Hamiltonian (4.1) ($\hat{H}_{\text{as}} = \hat{H}_0 + \hat{V}$) and \hat{Q} is a projector on the subspace spanned by noncrossing states. We include in \hat{V} the spin-rotation and the molecule-field interactions. At small field strengths $\Omega \ll \Delta$, it is sufficient to retain a few terms in the perturbative expansion (4.5). The diagonal

elements $\hat{R}_{aa}(\Delta/2) \sim -\Omega^2/12\Delta$ and $\hat{R}_{bb}(\Delta/2) \sim -\gamma/2 - \gamma^2/2\Delta$ give the shifts of the energy levels a and b upon the spin-rotation and the molecule-field interaction \hat{V} near the crossing point. The crossing of the shifted levels occurs at the magnetic field value B_c defined by the equation

$$2\mu_B B_c = \Delta + \Omega^2/12\Delta - \gamma/2 - \gamma^2/2\Delta. \quad (4.6)$$

The off-diagonal element of \hat{R} gives the separation between the levels ΔE .

$$\Delta E = 2|\hat{R}_{ab}(\Delta/2)| = \frac{\Omega\gamma}{\sqrt{6}\Delta}. \quad (4.7)$$

The crossing between the $|0\ 0\ \frac{1}{2}0\rangle$ and $|1\ 1\ -\frac{1}{2}-3\rangle$ levels is described by the equation

$$2\mu_B B_c = (2B_e - 3\hbar\omega) + \Omega^2/12(2B_e - \hbar\omega) - \gamma/2 - \gamma^2/2(2B_e - \hbar\omega). \quad (4.8)$$

The minimum energy difference between the adiabatic states is

$$\Delta E = \frac{\Omega^3\gamma}{72\sqrt{6}\hbar\omega(2B_e - \hbar\omega)(2B_e - 3\hbar\omega)}. \quad (4.9)$$

Note that no crossings occur in the absence of the mw field unlike in the case of dc electric fields where crossings are real in the absence of the electric field and become avoided in the presence of the electric field [127].

The crossings of the Zeeman states in the absence of the mw field occur at high magnetic fields ($B_c \sim 9.1$ T for CaH). The dc electric field can not shift these crossings significantly. As our analysis shows, microwave fields induce avoided crossings in a much wider range of magnetic field values, which suggests new mechanisms for controlling the dynamics of spin-dependent interactions in polar molecules.

The interaction of the molecule with the circularly σ_{\pm} polarized field defined by $(\hat{\epsilon} = (\hat{x} \pm i\hat{y})/\sqrt{2})$ can be described by the Hamiltonian:

$$\hat{H}_{m,f}^{\sigma_{\pm}} = -\frac{\Omega}{2\sqrt{N}}(4\pi/3)^{1/2}(\mp\hat{a}Y_{1\pm 1}(\hat{\mathbf{r}}) \pm \hat{a}^{\dagger}Y_{1\mp 1}(\hat{\mathbf{r}})). \quad (4.10)$$

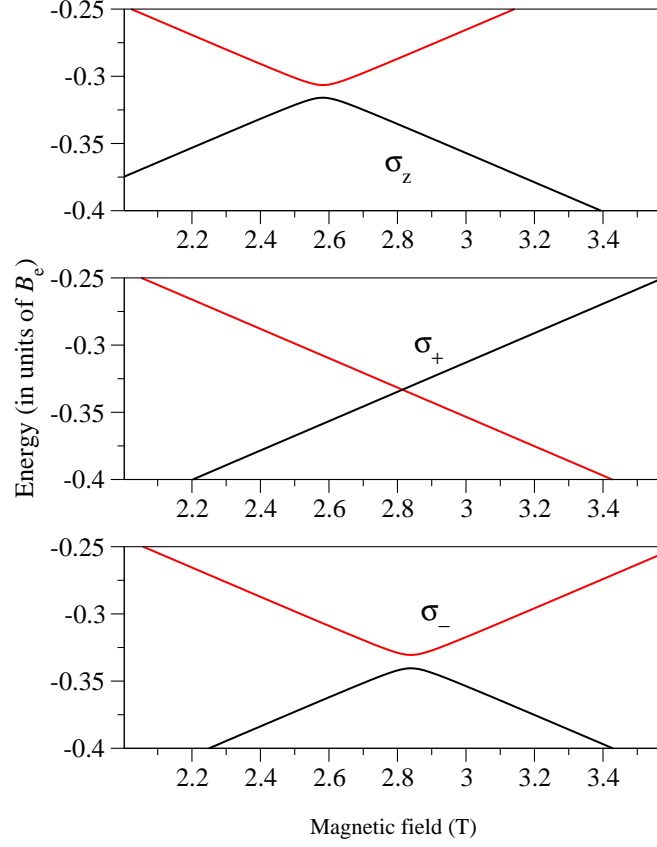


Fig. 4.5: Modification of avoided crossings with changing polarization of the microwave field. The graphs show the magnetic field dependence of the field-dressed states at $\hbar\omega/B_e = 1.9$ and $\Omega/B_e = 1$. The photon polarization is linear $\hat{\mathbf{e}} = \hat{z}$ (upper panel), $\hat{\mathbf{e}} = (\hat{x} + i\hat{y})/\sqrt{2}$ (middle panel), $\hat{\mathbf{e}} = (\hat{x} - i\hat{y})/\sqrt{2}$ (lower panel).

The matrix elements of $\hat{H}_{m,f}^{\sigma_{\pm}}$ have the following form:

$$\begin{aligned} \langle N'M'_N M'_S n' | \hat{H}_{m,f}^{\sigma_{\pm}} | NM_N M_S n \rangle &= -(\Omega/2) \delta_{M'_S, M_S} \\ &\times [\mp \delta_{n', n-1} b_{N'M'_N, NM_N}^{\pm 1} \pm \delta_{n', n+1} b_{N'M'_N, NM_N}^{\mp 1}], \end{aligned} \quad (4.11)$$

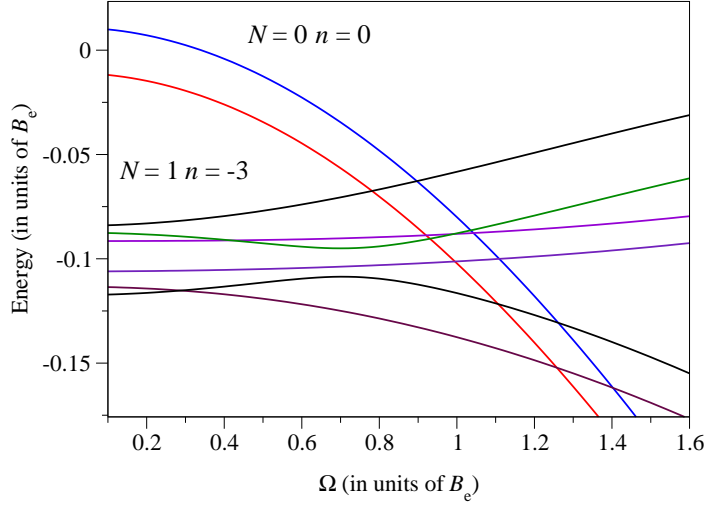


Fig. 4.6: The field-dressed states of the CaH($^2\Sigma$) molecule in a magnetic field of 0.1 T and a microwave field with circular polarization $\hat{\mathbf{e}} = (\hat{x} + i\hat{y})/\sqrt{2}$ and $\hbar\omega/B_e = 0.7$.

where $b_{N'M'_N, NM_N}^n$ are given by

$$b_{N'M'_N, NM_N}^n = (-1)^{M'_N} [(2N' + 1)(2N + 1)]^{1/2} \times \begin{pmatrix} N' & 1 & N \\ 0 & 0 & 0 \end{pmatrix} \begin{pmatrix} N' & 1 & N \\ -M'_N & n & M_N \end{pmatrix} \quad (4.12)$$

In the case of circularly polarized field, absorption and emission of photons is accompanied by a change in the rotational angular momentum projection of the molecule. For example, the σ_- (σ_+) polarized field couples the state $|N = 0 M_S = 1/2 n = 0\rangle$ with the states $|N = |m| M_N = m M_S = 1/2 n = -m\rangle$ ($|N = |m| M_N = -m n = m\rangle$), where m is an integer number. The σ_- light couples the same state to the rotationally excited state $|N = 1 M_N = -1 M_S = 1/2 n = -1\rangle$ which in turn is coupled by the spin-rotation interaction with the high-field-seeking states. The avoided crossings of the $|N = 0 M_S = 1/2 n = 0\rangle$ and $|N = 1 M_S = -1/2 n = -1\rangle$ levels in the presence of σ_- polarized field occur at different values of the magnetic

fields (see Fig. 4.5). The σ_+ polarized field couples the rotationally ground spin-up state to the maximally stretch state $|N = 1 M_N = 1 M_S = 1/2 n = -1\rangle$. Therefore there is no avoided crossings of the initial spin-up state with spin-down states (see Fig. 4.5) for the mw frequencies below resonance. Figure 4.6 shows the field-dressed energy levels as functions of the field-induced coupling for the σ_+ mw polarization. The spin-up and spin-down states do not exhibit avoided crossings at moderate field strength.

4.3 Scattering calculations

4.3.1 Microwave field dependence

We consider collisions of CaH molecules with ^3He atoms. The photon number basis is generated by fixing \bar{N} and varying n from $-n_{\text{max}}$ to n_{max} . We use $n_{\text{max}} = 5$, a total number of 6 rotational states ($N \leq 5$) and seven partial waves ($l \leq 6$) in the scattering basis set, which for $M = 0$ leads to the system of 3938 coupled differential equations.

The interaction of $^2\Sigma$ molecules with a magnetic field separates different M_S sublevels and the ac electric field lifts the degeneracy of the rotational states with different $|M_N|$. Our initial and final states correlate with the magnetic low-field-seeking $|N = 0, M_S = 1/2, n = 0\rangle$ and high-field-seeking $|N = 0, M_S = -1/2, n = 0\rangle$ states of the CaH molecule at zero mw field. In terms of v and K they are labeled as $|10\rangle$ and $|00\rangle$ correspondingly. The energy levels of the CaH($^2\Sigma$) molecule in a microwave field are shown in Figures 4.1 and 4.2. A linearly polarized microwave field couples states with $N' = N \pm 1$ and $n' = n \pm 1$ and conserves the angular momentum projection of the molecule, i.e. $M'_N = M_N$. The dependence of the cross sections for collision-induced spin relaxation $|N = 0, M_S = 1/2, n = 0\rangle \rightarrow |N = 0, M_S = -1/2, n = 0\rangle$ and $|N = 0, M_S = 1/2, n = 0\rangle \rightarrow |N = 0, M_S = -1/2, n = -1\rangle$ on the field-induced coupling strength Ω is shown in the lower panel of Fig. 4.2. For moderate $\Omega \ll B_e$ the cross section for transitions between different photon manifolds increases with increasing coupling strength. The cross section for processes conserving the number of photons has a weak dependence on Ω . The cross sections increase by three orders of magnitude near $\Omega/B_e = 0.81, 1.15$ and 1.45 , the

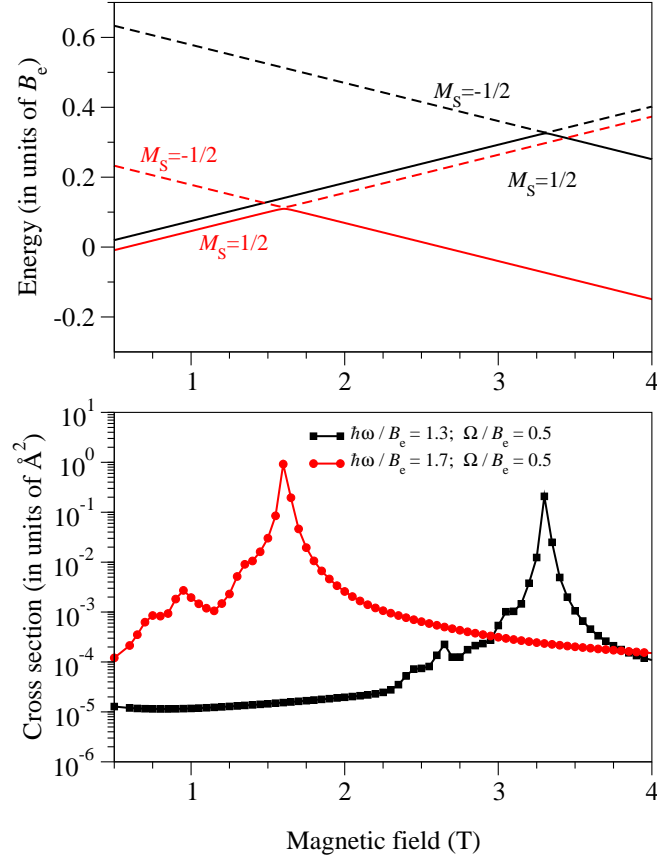


Fig. 4.7: Upper panel: Adiabatic energy levels of the CaH molecule in a microwave field at $\Omega/B_e = 0.5$, $\hbar\omega/B_e = 1.7$ (red) and $\hbar\omega/B_e = 1.3$ (black) correlating with $|N = 0M_S = 1/2n = 0\rangle$ (solid line) and $|N = 1M_N = 1M_S = -1/2n = -1\rangle$ (dashed line) at zero Ω . Lower panel: Magnetic field dependence of the cross sections for spin relaxation in CaH-He collisions near an avoided crossing of the field-dressed states correlating with $|N = 0, n = 0\rangle$ and $|N = 1, n = -1\rangle$ states at zero Ω . $\Omega/B_e = 0.5$, $\hbar\omega/B_e = 1.7$ (circles), $\hbar\omega/B_e = 1.3$ (squares).

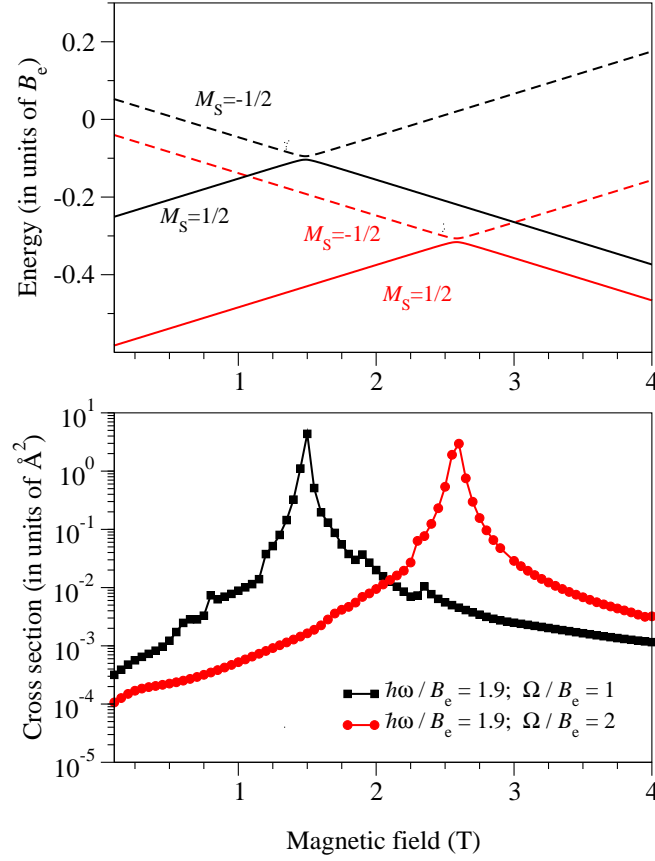


Fig. 4.8: Upper panel: Adiabatic energy levels of the CaH molecule in a microwave field at $\hbar\omega/B_e = 1.9$, $\Omega/B_e = 1$ (black) and $\Omega/B_e = 2$ (red) correlating with $|N = 0, M_S = 1/2, n = 0\rangle$ (solid line) and $|N = 1, M_N = 1, M_S = -1/2, n = -1\rangle$ (dashed line) at zero Ω . Lower panel: Magnetic field field dependence of cross sections for spin relaxation in CaH-He collisions near an avoided crossing of the field-dressed states correlating with $|N = 0, n = 0\rangle$ and $|N = 1, n = -1\rangle$ states at zero coupling. $\hbar\omega/B_e = 1.9$, $\Omega/B_e = 1$ (squares) and $\Omega/B_e = 2$ (circles).

values corresponding to the avoided crossings between the field-dressed states.

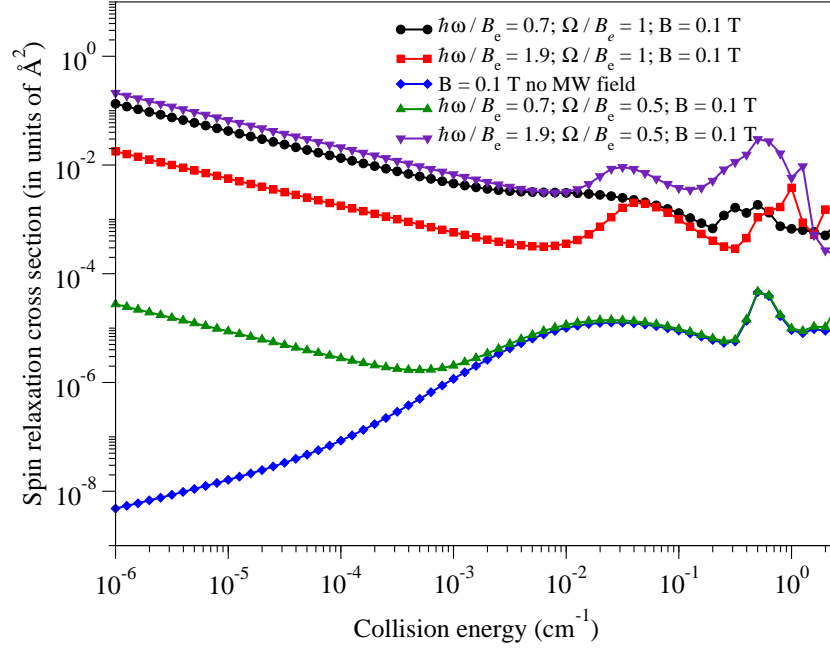


Fig. 4.9: Collision energy dependence of the cross sections for spin relaxation in CaH-He collisions at a magnetic field of 0.1 T and zero microwave field (diamonds); $\hbar\omega/B_c = 0.7$ and $\Omega/B_c = 0.5$ (triangles up); $\hbar\omega/B_c$ and $\Omega/B_c = 0.5$ (triangles down); $\hbar\omega/B_c = 0.7$ and $\Omega/B_c = 1$ (circles); $\hbar\omega/B_c = 1.9$ and $\Omega/B_c = 1$ (squares).

4.3.2 Resonances near avoided crossings

The lower panel of Figure 4.3 shows the cross sections for spin relaxation as a function of the magnetic field magnitude near the avoided crossing of the initial $|N = 0, M_S = 1/2, n = 0\rangle$ and excited $|N = 1, M_N = 1, M_S = -1/2, n = -1\rangle$ states at mw field parameters $\Omega = 0.1 B_e$ and $\hbar\omega = 1.9 B_e$. The crossing occurs at the magnetic field $B_c \sim 0.47 T$. The cross section for spin relaxation accompanied by absorption of the microwave photon is 100 times larger than for scattering within the same photon manifold. The cross sections increase by the factor of about 100 near the avoided crossing.

Figure 4.7 shows the cross sections for spin relaxation near the avoided crossing as functions of the magnetic field for different frequencies. The position of

the crossing shifts to lower magnetic field values B_c with increasing frequency. The cross sections increase by four orders of magnitude near the avoided crossings between the $|N = 0, M_S = 1/2, n = 0\rangle$ and $|N = 1, M_N = 1, M_S = -1/2, n = -1\rangle$ levels.

Figure 4.8 shows the cross sections for spin relaxation near the avoided crossing as functions of the magnetic field for different coupling strength Ω . The position of the crossing shifts to higher magnetic fields as the coupling strength increases. The magnitude of the cross sections increases by the factor of 10^3 near the avoided crossings.

4.3.3 Collision energy dependence

The collision energy dependence of the spin relaxation cross sections at a magnetic field of $B = 0.1$ T is shown in Figure 4.9. The cross sections for the spin-flipping transition follow the Wigner threshold law [65]. For small collision energies they are inversely proportional to the collision velocity $\sigma \sim 1/v$. For a weak magnetic field in the absence of the microwave field the spin-changing transition is nearly forbidden [128]. Microwave fields induce couplings between different Zeeman states and enhance the cross sections. The onset of the $1/v$ behavior is shifted to higher collision energies in the presence of the mw field.

4.4 Conclusion

We have presented a detailed study of inelastic spin-relaxation in collisions of $\text{CaH}(^2\Sigma)$ molecules with He atoms in superimposed magnetic and microwave fields. Our study demonstrates that the dynamics of molecular collisions may be sensitive to both the frequency and the intensity of the field. External fields modify the rotational structure of molecules and affect the spin-rotation interaction. Our study shows that microwave fields enhance collision-induced spin relaxation. Spin-changing transitions are dominated by the process accompanied with photon absorption. The structure of the molecules changes with varying magnetic field or mw field parameters. Variation of the mw fields may induce and shift avoided crossings between molecular Zeeman levels of different symmetry. Different spin states are strongly mixed and the dynamics of magnetic spin-relaxation is

extremely sensitive to external fields near the avoided crossings. Changing the polarization can significantly influence the dynamics of the spin-changing processes. The number of avoided crossings is reduced in the circularly polarized light. Circularly polarized light couples selectively the initial state of the molecule to the maximally stretched states that are not directly coupled by the spin-rotation interaction, which suppresses collisional spin-relaxation. For example, the use of σ_- polarization reduces the collisional spin-relaxation of molecules in the rotationally ground low-field-seeking state. Inelastic Zeeman transitions in collisions of molecules with atoms may thus be effectively controlled by varying the strength, the frequency and the polarization of the microwave field.

Chapter 5

Feshbach resonances in the presence of a microwave field

5.1 Introduction

In this chapter we discuss the effects of the microwave field on magnetic Feshbach resonances in collisions of polar molecules. The goal of this study is to explore the possibility of tuning elastic and inelastic collisions of molecules in a microwave trap by controlling magnetic Feshbach resonances. We start by reviewing recent work on Feshbach resonances in molecular collisions. Next, we discuss magnetic Feshbach resonances in collisions of NH molecules with He in the presence of microwave fields and in a pure dc magnetic field. After this, we present the results of coupled channel calculations for elastic and inelastic cross sections. We present a simple analytical expression for S -matrix elements describing scattering in the presence of several open channels and discuss the observed results. We show that magnetic Feshbach resonances of ultracold molecules can be modified by non-resonant microwave fields. The two important results of this study are: (i) the probability of collision-induced absorption of microwave photons is dramatically enhanced near a Feshbach resonance, which suggests a new method for detecting Feshbach resonances in collisions of molecules; and (ii) the scattering length of ultracold molecules can be tuned by varying the frequency and intensity of microwave field, i.e. the scattering properties of ultracold molecules can be tuned in

a wide range of microwave field intensities and frequencies.

5.2 Feshbach resonances

Magnetic Feshbach resonances play an important role in experiments with ultracold atoms and molecules. As we discussed in Chapter 1, they provide a mechanism for controlling effective interparticle interactions [57, 58] and can be used for the creation of weakly bound ultracold molecules [58–60]. Using magnetic fields for tuning ultracold gases, however, has two limitations: it is difficult to tune dc magnetic fields fast; and magnetic Feshbach resonances are usually very narrow, i.e. the scattering length of ultracold atoms can be tuned in a narrow range of magnetic fields. As a result, magnetic Feshbach resonances are often difficult to detect and the applications of magnetic field control of ultracold gases are limited to dynamical processes with the time scale of > 0.1 ms [62]. Many experiments have recently focused on the production of ultracold molecules in the ground internal energy state, successfully achieved by several research groups [97]. Like ultracold atoms, ultracold molecules with non-zero magnetic moments can be controlled by means of magnetic Feshbach resonances [121]. However, the ro-vibrational structure of molecules allows for new possibilities of controlling molecular gases.

5.2.1 Feshbach resonances in a single scattering channel

For one open channel the scattering description of the resonance is rather simple [129]. The scattering S matrix has a single element

$$S_{00}(k_0) = \exp(i2\delta_0(k_0)), \quad (5.1)$$

where k_0 is a wavevector in the incoming channel and δ_0 is a phase shift describing the additional phase acquired by the wavefunction due to the scattering interaction. In the presence of scattering resonance it can be parameterized by the Breit-Wigner form [124]

$$\delta(B) = \delta_{bg} + \arctg \frac{\Gamma_B}{2(B_{\text{res}} - B)}, \quad (5.2)$$

where δ_{bg} is a slowly varying background phase shift in the absence of the scattering resonance, and Γ_B and B_{res} are the width and position of the resonance. The

phase changes by π and the S -matrix element follows a circle of radius 1, in the complex plane, when the magnetic field changes across the resonance. In the limit of low collision energies Γ_B goes to zero as a linear function of k . The cross section is given by the following expression

$$\sigma_{00} = \frac{\pi}{k_0^2} |1 - S_{00}|^2 \quad (5.3)$$

The S -matrix element goes to -1 and the cross section grows up to $\frac{4\pi}{k_0^2}$ at the Feshbach resonance ($B = B_{\text{res}}$).

To illustrate the system with a single open channel Feshbach resonance consider collisions of NH molecules trapped in a magnetic field with He atoms. The Hamiltonian for the NH molecule in a magnetic field has the following form

$$\hat{H}_{\text{mol}} = \hat{H}_{\text{rot}} + \hat{H}_Z + \hat{H}_{\text{sr}} + \hat{H}_{\text{ss}}, \quad (5.4)$$

where \hat{H}_{rot} , \hat{H}_Z and \hat{H}_{sr} are, as discussed in the previous chapters, the rotational, Zeeman and spin-rotational Hamiltonians and \hat{H}_{ss} is the spin-spin Hamiltonian. The explicit expression for \hat{H}_{ss} in the space-fixed coordinate frame is

$$\hat{H}_{\text{ss}} = \frac{2}{3} \lambda_{\text{SS}} \left(\frac{4\pi}{5} \right)^{1/2} \sqrt{6} \sum_q (-1)^q Y_{2-q}(\hat{\mathbf{r}}) [\hat{S} \otimes \hat{S}]_q^{(2)}. \quad (5.5)$$

The eigenfunctions of the molecule can be expanded in products of rotational and spin functions $|NM_N\rangle|SM_S\rangle$ and the scattering wave function in products of molecular and rotational angular momentum functions of the complex. For collisions in magnetic fields the projection of the total angular momentum $M_J = M_N + M_L + M_S$ and the total parity $(-1)^{N+L+S}$ are conserved. The spin-spin Hamiltonian couples different molecular states with $\Delta N = \pm 2$. The absolute ground state of the complex in a magnetic field corresponds to the magnetic high-field seeking state $|N=0, M_N=0\rangle|S=1, M_S=-1\rangle$ of the molecule and s-wave partial wave ($L=0$). The intermolecular potential and the spin-spin interaction couple the initial state in second order to the $|N=0, M_N=0\rangle|S=1, M_S=1\rangle|L=2, M_L=-2\rangle$ bound state. For NH- ^3He collisions the initial $M_S = -1$ state crosses the $M_S = 1$ threshold at $B = 7168.750\text{G}$. Due to parity conservation the initial $L=0$ can be coupled only

to the states with $L = 0, 2, 4$. The collisions with $L > 0$ are suppressed, leaving only one open channel with $L = 0$.

5.2.2 Feshbach resonances in the presence of multiple open channels

Consider a magnetic Feshbach resonance with several decay channels [129]. The phase shift becomes a complex function. The sum of the phases of eigenvalues of S -matrix is real and obeys the Breit-Wigner relation. In the presence of several open channels the magnetic field dependence of the scattering S -matrix elements near resonance is given by the following expression:

$$S_{ii'}(B) = S_{bg,ii'} - \frac{i g_{Bi} g_{Bi'}}{B - (B_0 + \Delta) + i\Gamma_B/2}, \quad (5.6)$$

where $S_{bg,ii'}$ is a slowly varying background scattering matrix element, B_0 is the resonance position in the absence of the microwave field, Δ is the shift of the position of the resonant level caused by the interaction with a microwave field, the energy dependent width of the resonance Γ_B is given by the sum over the partial widths Γ_{Bi} in accessible decay channels i : $\Gamma_B = \sum_i \Gamma_{Bi}$, and g_{Bi} is a complex function so that $\Gamma_{Bi} = |g_{Bi}|^2$. In the absence of all inelastic channels except one the energy dependent width of the resonance is reduced to the single term $\Gamma_B = \Gamma_{B0} = 2k_0\gamma_{B0}$, where k_0 is an incoming wave vector and γ_{B0} is an energy-independent reduced width, which determines the variation of the scattering length as a function of the magnetic field. The matrix element of the S -matrix is equal to -1 exactly at the resonance ($B = B_{res}$), as predicted by single channel theory for suppressed inelastic transitions. The value of Γ_B includes contributions from decay channels $\Gamma_B^{inel} = \sum_{i>0} \Gamma_{Bi}$, which increase with the increasing field strength. The S -matrix element describes a circle in a complex plane with radius $|g_{Bi} g_{Bi'}|^2 / \Gamma_B$ as B is tuned across the resonance. The contribution from inelastic decay channels Γ_B^{inel} does not go to zero at resonance and therefore the S -matrix element does not pass through a pole. With the increasing field strength the radius of the circle is decreasing or in other words the denominator becomes larger and the oscillations of the cross section become weaker (the cross section does not reach its maximum value $4\pi/k_0^2$).

5.2.3 Feshbach resonances in the presence of a microwave field

In the previous chapters we considered interaction of polar molecules with a microwave field in the dressed field formalism. Consider an ensemble of polar diatomic molecules prepared in the absolute ground state and irradiated with microwave field far detuned from the molecular resonance. The dressed states form an infinite ladder of states above and below the ground molecular state. The interaction potential couples different field-dressed states. As a result, during collision molecules may undergo transitions to the lower energy field-dressed states. This leads to collision-induced absorption of microwave photons leading to the formation of a collision complex, in which one or both molecules are in a rotationally excited state. The molecules then undergo rotational relaxation, releasing energy, and the collision complex decays. This process is driven by the anisotropy of the intermolecular interaction potential [130]. The interaction with microwave fields thus induces inelastic decay channels, which suppress elastic scattering near Feshbach resonances [129].

To illustrate this by numerical calculations, we consider collisions of $\text{NH}(^3\Sigma)$ molecules with He atoms near a Feshbach resonance induced by a magnetic field. We will show that the strength of the interaction with microwave field can be always adjusted to compensate for the effects of the interaction anisotropy, so the microwave field can be effectively used to manipulate with Feshbach resonances. We focus on low-energy collisions ($E_{\text{kin}} = 1 \mu\text{K}$) of NH molecules prepared in the rotationally ground state $N = 0$ and the lowest-energy Zeeman level $M_S = -1$ with ^3He atoms near a Feshbach resonance at ~ 7150 G identified by González-Martínez and Hutson [131]. The collision problem of molecules in the presence of a microwave field is best described using the field-dressed-state formalism described in the previous chapters. The molecular Hamiltonian \hat{H}_{mol} describes the rotational and fine structure of the molecule [129, 132] and is given by Eq.(5.4). We represent the total wave function of the system as a close coupling expansion in terms of the products of the eigenfunctions of field-dressed Hamiltonian and the rotational wave functions of the collision complex (partial waves). The substitution of this expansion in the Schrödinger equation leads to a system of coupled differential equations, which we solve numerically to obtain the scattering S -matrix, elastic

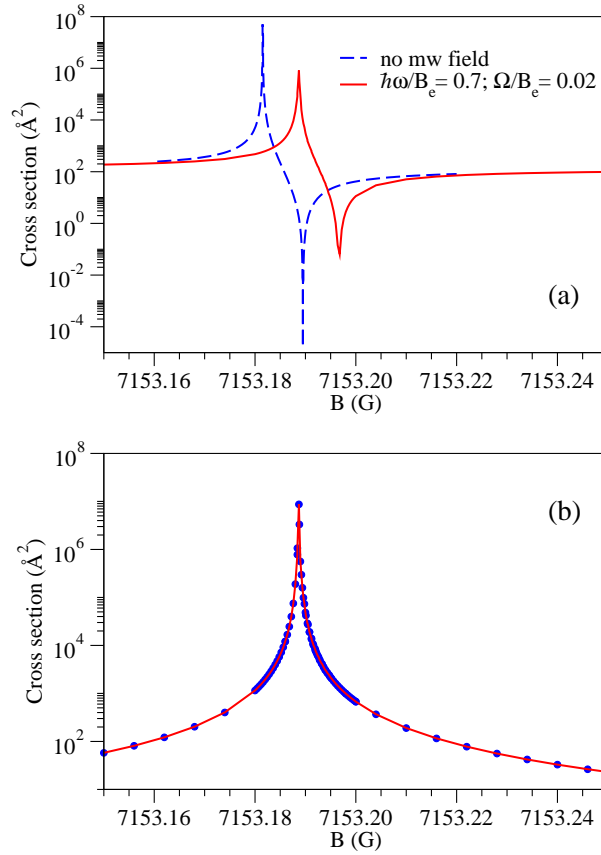


Fig. 5.1: Cross sections for elastic collisions (panel a) and collisions accompanied by absorption of microwave photons (panel b) in NH – He scattering as functions of the magnetic field: broken line – no microwave field; solid lines – in the presence of a microwave field with $\Omega = 0.02B_e$ and $\hbar\omega = 0.7B_e$, where $B_e = 16.343 \text{ cm}^{-1}$ is the rotational constants of NH. The line in panel (b) represents a sum of the transitions to all field-dressed states and the symbols represent the cross sections for the dominant single-photon transition $|N = 0, M_S = -1, \bar{N}\rangle \rightarrow |N = 0, M_S = 1, \bar{N} - 1\rangle$.

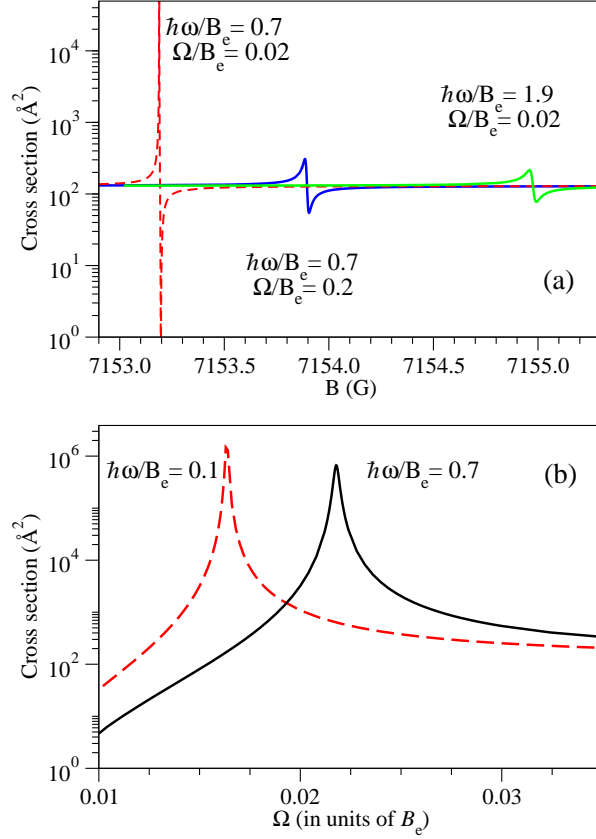


Fig. 5.2: Cross sections for elastic collisions in NH – He scattering as functions of the magnetic field (panel a) and as functions of the microwave field strength (panel b) for different parameters of the microwave field. The magnetic field in panel (b) is $B = 7153.19$ G.

and inelastic cross sections [130, 133]. Four rotational levels of the molecule, four photon number states and five partial waves were included in the basis set expansion, which leads to a system of 2880 equations for the total angular momentum projection equal to zero. We used the potential energy surface for the He - NH collision complex calculated in Ref. [132]. Figure 5.1 shows the magnetic field dependence of the cross sections for NH - He collisions near the Feshbach resonance. The line in panel (b) is a sum of the cross sections for transitions to all field-dressed states except the initial state. The analysis of the state-resolved tran-

sitions shows that the cross section shown in panel (b) of Fig. 5.1 is dominated by a single transition $|\psi_i\rangle \rightarrow |\psi_f\rangle$, where $|\psi_i\rangle = a|N = 0, M_S = -1, \bar{N}\rangle + b|\dots\bar{N}\dots\rangle$ and $|\psi_f\rangle = a|N = 0, M_S = +1, \bar{N} - 1\rangle + b|\dots\bar{N} - 1\dots\rangle$. The ket $|\dots\bar{N}\dots\rangle$ denotes collectively the states mixed in the ground rotational state of the molecule due to molecule - field and fine-structure interactions. For weak, non-resonant microwave fields considered here, a is very close to 1. The cross section in panel (b) of Fig. 5.1 thus represents the probability of a process, in which the collision complex absorbs a photon, the molecule undergoes the spin flip and the rotational relaxation and the collision complex releases energy by decaying into the collision products.

Figure 5.1 demonstrates two important observations: (i) the position of the resonance in the presence of a microwave field is shifted up to a few Gauss; and (ii) the probability of collision-induced absorption of microwave photons (panel b) is dramatically enhanced near the Feshbach resonance. As predicted by Hutson [129], the presence of strong inelastic transitions must suppress elastic scattering near a Feshbach resonance. This is indeed what we observe for collisions in microwave fields of higher intensity and lower detuning. The upper panel of Figure 5.2 shows that resonant enhancement of the elastic scattering cross section is suppressed, as the strength of the microwave field increases.

The shift of the Feshbach resonances can be exploited for tuning the scattering properties of ultracold molecules with microwave fields. Figures 5.2 and 5.3 show the scattering cross sections near the Feshbach resonance as functions of the microwave field strength and frequency. The Feshbach resonance depicted in Figure 5.1 is very narrow, leading to the variation of the scattering cross section in a very small interval of magnetic fields ~ 0.05 G. While not impossible, it is technologically challenging to tune the dc magnetic field with such a high resolution. Figures 5.2 and 5.3 show that the same resonance gives rise to the variation of the scattering cross sections over wide ranges of the microwave field strength and frequencies.

5.3 Conclusion

The interaction with non-resonant microwave fields induces inelastic losses of molecules due to collision-induced absorption of microwave photons. This leads to

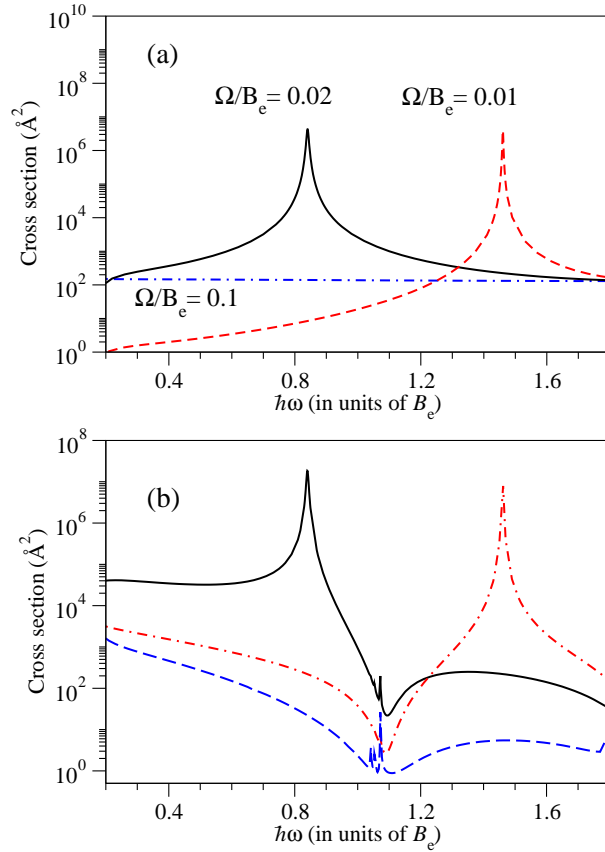


Fig. 5.3: Cross sections for elastic collisions (panel a) and collisions accompanied by absorption of microwave photons (panel b) in NH – He scattering as functions of the microwave field frequency. The magnetic field is $B = 7153.19$ G.

suppression of Feshbach resonances and allows for tuning Feshbach resonances by varying both the intensity and frequency of the microwave field. This suggests that measuring the microwave field absorption or loss of molecules as a function of microwave field parameters can be used as a method of detecting Feshbach resonances in an ultracold gas of molecules. Our calculations demonstrate that magnetic Feshbach resonances can be shifted in the presence of microwave fields by up to a few G. Feshbach resonances (including extremely narrow resonances) can therefore be located by varying the dc magnetic field with a step of a few G and scanning the

intensity of a non-resonant microwave field at a fixed magnetic field. Laser fields can be tuned much faster than dc magnetic fields. For example, the collapse of a BEC can be induced in experiments with ultracold atoms by varying the magnetic field near a Feshbach resonance on the time scale of 0.1 ms [62]. The variation of the microwave fields depicted in Figures 5.2 and 5.3 can be achieved on the time scale of nanoseconds. This can be used for new studies of BEC dynamics with instabilities induced on a much shorter time scale or BEC dynamics with instabilities oscillating on the time scale of intermolecular interactions. Finally, because the absorption of microwave field is enhanced near a Feshbach resonance, our results suggest that a combination of a Feshbach resonance and microwave fields can be used for photo association of atom - molecule or molecule - molecule collision complexes to produce ultracold trimers and tetramers. This technique would be analogous to the technique of Feshbach-enhanced photo association of ultracold atoms.

Chapter 6

Sensitive imaging of electromagnetic fields with paramagnetic polar molecules

6.1 Introduction

In this chapter we discuss the method for the parallel detection of low-frequency electromagnetic fields based on the fine structure interactions in paramagnetic polar molecules. First, we discuss the method based on the ultracold ^{87}Rb atoms, proposed by Böhi *et al.* [63], which was used for the imaging of the microwave field distribution over a chip. Next, we discuss an analogous method based on ultracold paramagnetic molecules instead of Rb atoms. In particular, we show that using molecules instead of atoms gives rise to the 100-fold increase in sensitivity, while allowing the detection of electromagnetic fields in a wider range of frequencies from a few kHz to THz.

Sensitive detection of weak electromagnetic fields is important for various applications ranging from fundamental physical measurements [134] and detection of explosive materials [135] to biomagnetic imaging [134] of brain and heart [136, 137]. A significant progress in sensing of magnetic fields has been achieved during the last decade and led to the development of numerous devices

such as Hall effect sensors [138], SQUID sensors [139], force sensors [140], sensors based on microelectromechanical systems [141], and NV centers in diamond [142], as well as atomic magnetometers [143, 144], making it possible to achieve the magnetic field sensitivity of $0.1 \text{ fT Hz}^{-1/2}$ and to detect the magnetic field of a single electron, with steps being taken towards the detection of the magnetic field of a single nuclear spin [145, 146]. The electric field sensing techniques advanced to the level of probing individual charges with the development of scanning capacitance microscopy [147], scanning Kelvin probe [148], and electric field-sensitive atomic force microscopy [149]. An unprecedented accuracy of 10^{-6} electron charge was achieved with the use of single-electron transistors [150]. The nitrogen-vacancy defects allow for very local highly spatially resolved measurements of electric fields of single electron charge [151]. However, both high spatial resolution and sensitivity is desirable, for example, for measuring of electromagnetic fields near nanosize structures.

6.2 Detection of weak radio-frequency fields with ultracold ^{87}Rb atoms

The method of highly sensitive imaging of microwave fields with ultracold atoms of frequencies in the range $2.5 - 14 \text{ GHz}$ was proposed by Böhi *et al.* [63]. The method relies on measuring the phase difference between two hyperfine states of ^{87}Rb , accumulated due to an interaction with the magnetic component of the microwave field. In particular, the magnetic component of the microwave field drives the Rabi oscillations between two hyperfine atomic states. The hyperfine splitting and therefore the measurable frequency can be tuned with an external magnetic field. The acquired phase difference is proportional to the evolution time, the magnetic moment of the atom, and the magnetic field amplitude. Changing the direction of the magnetic field allows one to measure the three different cartesian components of the magnetic field B_x , B_y and B_z . The relative phase can be reconstructed by observing transitions for different polarizations of the field. In the prototype experiment the cloud of initially magnetically trapped ultracold Rb atoms freely expands over time τ_{exp} . The microwave field of the microwave circuit is switched on for a time τ_{mw} . The density of atoms in an upper hyperfine state $n_2(\mathbf{r})$ is sub-

sequently measured by state-selective absorption imaging technique over time τ_{im} . The sensitivity of the method is proportional to the interrogation time τ_{mw} . However, long measurement times τ_{mw} lead to image blurring due to the atomic motion and decoherence, resulting in a compromise between field sensitivity and spatial resolution.

6.3 Detection of weak electromagnetic fields with polar molecules

Although measuring the electric component of an ac field is several orders of magnitude more efficient than detecting the magnetic component ¹, atoms possess no permanent electric dipole moments, rendering the detection of the Zeeman shift the only possible option. Here we describe a technique for parallel, noninvasive, and complete (amplitudes and phases) imaging of electromagnetic fields with an ensemble of polar open-shell molecules, many of which have been successfully cooled and trapped in experiments [94, 120, 152–154]. We show that the presence of permanent electric and magnetic dipole moments and the variety of molecular rotational constants allow for the detection of both electric and magnetic field components, in a wide range of frequencies from the dc limit through the radio and microwave to the THz frequency range. We show that measuring the electric component of an oscillating field must result in shorter measurement times compared to the atomic experiments, and consequently higher spatial resolution, which is mainly limited by the optical detection scheme and photon scattering.

6.3.1 Polar paramagnetic molecule in parallel electric and magnetic field

First, consider $^2\Sigma$ molecules with a dipole moment \mathbf{d} , subject to known dc magnetic and electric fields, \mathbf{B}_0 and \mathbf{E}_0 , both pointing along the laboratory Z axis. The

¹The electric, E , and magnetic, B , field amplitudes of the electromagnetic field are related as $E = Bc$ with c the speed of light, rendering the phase difference accumulated due to an electric dipole transition two orders of magnitude larger than for the transition between the atomic hyperfine states (for a given interaction time τ).

molecules are described by the following Hamiltonian:

$$\hat{H} = b_r \hat{\mathbf{N}}^2 + \gamma \hat{\mathbf{N}} \cdot \hat{\mathbf{S}} + g_S \mu_B \mathbf{B}_0 \cdot \hat{\mathbf{S}} - \mathbf{d} \cdot \mathbf{E}_0, (6.1)$$

where $\hat{\mathbf{N}}$ and $\hat{\mathbf{S}}$ are the rotational and spin angular momenta of the molecule, b_r and γ are the rotational and spin-rotation interaction constants, μ_B is the Bohr magneton, and $g_S = 2.0023$. In the absence of external fields, the states of a $^2\Sigma$ molecule are labeled by $|N, J, M\rangle$, where $\hat{\mathbf{J}} = \hat{\mathbf{N}} + \hat{\mathbf{S}}$ is the total angular momentum and M is the projection of $\hat{\mathbf{J}}$ on the Z axis. We use the same quantum numbers to label the molecular states in the presence of dc fields, bearing in mind that J is not conserved.

The effect of combined \mathbf{B}_0 and \mathbf{E}_0 fields on the rotational states of a $^2\Sigma$ molecule is shown in Fig. 6.1 (a) and (b) for the case of SrF ($^2\Sigma^+$) [153, 154]. We assume that the molecules are initially prepared in the magnetic low-field seeking M -component of the rotational ground state, state $|2\rangle \equiv |0, 1/2, 1/2\rangle$ in Fig. 6.1(a). This can be achieved by cooling molecules to subKelvin temperatures and confining a molecular cloud in a magnetic trap [120]. Alternatively, molecules can be confined in an electric or optical trap and transferred to state $|2\rangle$ by a sequence of microwave pulses [155]. Molecules can be cooled by a variety of recently developed experimental techniques such as buffer-gas cooling, Stark deceleration, or laser cooling [94, 120, 152–154].

State $|2\rangle$ exhibits an avoided crossing with the magnetic high-field seeking state $|3\rangle \equiv |1, 1/2, 1/2\rangle$ at the magnetic field $B^* = 659.5$ mT. The states $|2\rangle$ and $|3\rangle$ have the opposite parity and, due to the spin-rotation interaction, represent linear combinations of the states with spin projections $M_S = \pm 1/2$ [114, 126, 127]. Therefore the $|2\rangle \rightarrow |3\rangle$ transition is dipole-allowed and can be used to detect the electric component of a resonant rf or microwave field.

The measurement requires placing the molecular ensemble close to the source of the field to be measured, $\mathbf{E}(\mathbf{r}, t) = 1/2[\mathbf{E}(\mathbf{r})\exp(-i\omega t) + \mathbf{E}^*(\mathbf{r})\exp(i\omega t)]$, and an addition of background dc magnetic and electric fields, with magnitudes B_0 and E_0 . By adjusting B_0 and E_0 , the energy splitting between the states $|2\rangle$ and $|3\rangle$ can be tuned in resonance with the field frequency ω . The trapping field, if any, must be switched off in order to allow the field $\mathbf{E}(\mathbf{r}, t)$ to drive resonant oscillations

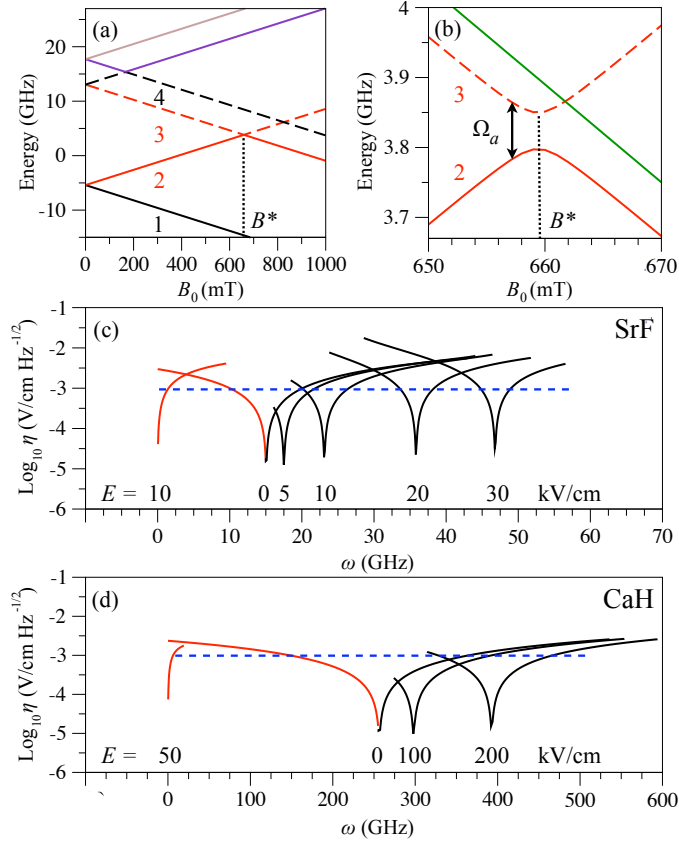


Figure 6.1: (a), (b) Energy levels of the SrF($2\Sigma^+$) molecule ($b_r = 7.53$ GHz, $\gamma = 74.7$ MHz) in an electric field of $E_0 = 10$ kV/cm as a function of magnetic field B_0 ; (c) Frequency dependence of the ac field sensitivity for SrF in a linearly polarized mw field for different electric fields; the red and black lines correspond to the $2 \rightarrow 3$ and $1 \rightarrow 4$ transitions respectively. The dashed line represents the sensitivity to the magnetic field component of the ac field that can be achieved in experiments with atoms; (d) Same as in (c) but for the CaH($2\Sigma^+$) molecule ($b_r = 128.3$ GHz, $\gamma = 1.24$ GHz)

between the states $|2\rangle$ and $|3\rangle$ during the free evolution time τ . The Rabi frequency of the oscillations is given by

$$\Omega_\alpha(B_0, E_0) = E_\alpha(\mathbf{r})d_\alpha(B_0, E_0)/\hbar, \quad (6.2)$$

where $\alpha = \{+; 0; -\}$ denotes the polarization of the oscillating field with respect to the laboratory Z axis, $E_\alpha(\mathbf{r})$ is the corresponding component of the field $\mathbf{E}(\mathbf{r}, t)$, and $d_\alpha(B_0, E_0)$ is the transition dipole moment between the two states. In order to compute $d_\alpha(B_0, E_0)$, we expand the molecular states $|n\rangle$ plotted in Fig. 6.1 as follows:

$$|n\rangle = \sum_{N, M_N, M_S} c_{NM_N M_S}^{(n)}(B_0, E_0) |NM_N\rangle |SM_S\rangle, \quad (6.3)$$

which gives

$$d_\alpha(B_0, E_0) = \sqrt{\frac{4\pi}{3}} \sum_{N, M_N, M_S} \sum_{N', M'_N, M'_S} c_{NM_N M_S}^{(2)*} c_{N' M'_N M'_S}^{(3)} \langle NM_N | Y_{1\alpha} | N' M'_N \rangle \delta_{M_S, M'_S}. \quad (6.4)$$

Here, M_N and M_S denote the projections of the angular momenta \mathbf{N} and \mathbf{S} on the Z axis, respectively.

After time τ the probability [63] to detect a molecule in the state $|3\rangle$ at the spatial point \mathbf{r} is

$$p_3(\mathbf{r}) = \frac{n_3(\mathbf{r})}{n_2(\mathbf{r}) + n_3(\mathbf{r})} = \sin^2 \left[\frac{\Omega_\alpha(\mathbf{r})\tau}{2} \right], \quad (6.5)$$

where n_2 and n_3 are the densities of the molecules in the states $|2\rangle$ and $|3\rangle$. From the measured value of $p_3(\mathbf{r})$ one can calculate $\Omega_\alpha(\mathbf{r})$ and, using Eq. (6.2), the components of the electric field. The amplitudes, $E_x(\mathbf{r})$, $E_y(\mathbf{r})$, and $E_z(\mathbf{r})$, and the relative phases can be reconstructed by measuring $E_\alpha(\mathbf{r})$ with the background magnetic field \mathbf{B}_0 pointing along the x , y , and z axes, by analogy with ref. [63]. From $\mathbf{E}(\mathbf{r})$, the spatial distribution of the magnetic field can be calculated using the Maxwell equations, while the amplitudes of the two fields are related as $E = cB$.

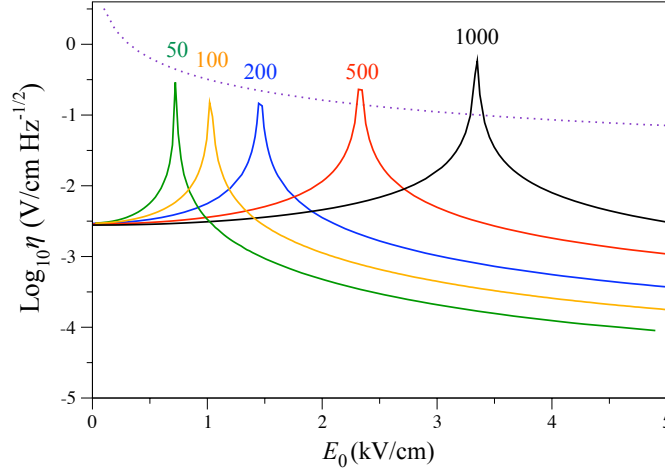


Figure 6.2: Sensitivity of the $|2\rangle \rightarrow |3\rangle$ transition in $\text{SrF}(^2\Sigma^+)$ to electromagnetic fields as a function of the dc electric field E_0 and the frequency of the microwave field. The peaks are labeled by the frequency of the ac field in MHz. The dotted line shows the sensitivity of the $|2\rangle \rightarrow |3\rangle$ transition in $\text{SrF}(^2\Sigma^+)$ to the magnetic field component of the microwave field.

6.3.2 Single-shot sensitivity

The single-shot sensitivity of the measurement to the ac electric fields is given by [63]:

$$\eta_E^{ac} [\text{V/cm Hz}^{-1/2}] = \frac{2\sqrt{3}\hbar}{100 d_\alpha(B_0, E_0) \sqrt{n V_{eff} \sqrt{\tau}}} \quad (6.6)$$

where n is the density of molecules, $V_{eff} = 2\pi\sigma_{eff}^2\rho$ is the effective imaging volume, σ_{eff} is the dispersion of the spatial coordinate, and ρ represents the $1/e$ radius of the cloud.

The dependence of the transition dipole moment d_α on the background fields \mathbf{B}_0 and \mathbf{E}_0 renders the sensitivity frequency dependent, $\eta_E^{ac} \equiv \eta_E^{ac}(\omega)$, as shown in Fig. 6.1 (c) by red curves for the $|2\rangle \rightarrow |3\rangle$ transition in $\text{SrF}(^2\Sigma^+)$. One can see that the frequency dependence exhibits sharp minima featuring the sensitivities on the order of $10^{-6} - 10^{-7} \text{ V/cm Hz}^{-1/2}$. The positions of the minima can be controlled by tuning the splitting of the levels $|2\rangle$ and $|3\rangle$ with the background

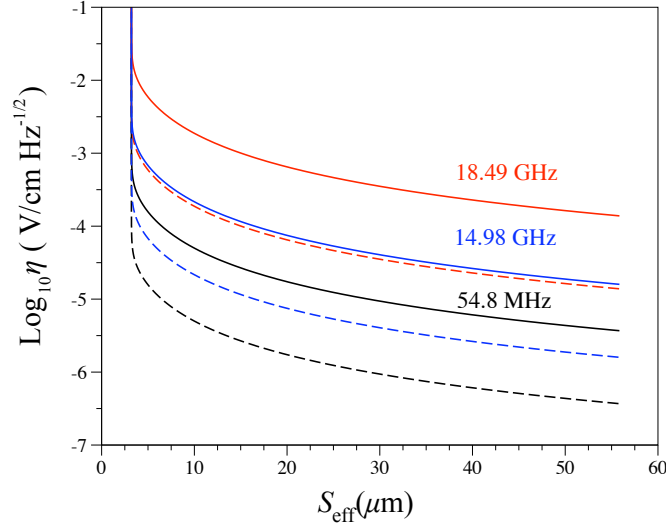


Figure 6.3: The ac electric field sensitivity for $\text{SrF}(^2\Sigma^+)$ as a function of the spatial resolution, for $n = 10^{10} \text{ cm}^{-3}$ (solid lines) and $n = 10^{12} \text{ cm}^{-3}$ (dashed lines). Different colors correspond to different ac field frequencies.

electrostatic field \mathbf{E}_0 , and thereby shifted towards smaller frequencies². The accessible frequency range can be extended by initially preparing the SrF molecules in the high-field seeking state, $|1\rangle \equiv |0, 1/2, -1/2\rangle$, and driving the transition to the state $|4\rangle \equiv |1, 3/2, -3/2\rangle$. The frequency dependence of the sensitivity corresponding to the $|1\rangle \rightarrow |4\rangle$ transition is shown in Fig. 6.1 (c) by black lines. Choosing a molecule with a different rotational constant allows for the detection of a completely different range of accessible frequencies. As an example, the rotational constant of $\text{CaH}(^2\Sigma^+)$ molecule [120] is about 17 times larger than that of SrF, which gives access to microwave fields of frequencies $\omega \sim 100 - 500 \text{ GHz}$, as shown in Fig. 6.1 (d).

Interestingly, the transition dipole moment $d_\alpha(B_0, E_0)$ for the $|2\rangle \rightarrow |3\rangle$ transition in $^2\Sigma$ molecules vanishes at certain combinations of E_0 and B_0 . At these par-

²The lowest detectable ac field frequency, ω_{min} , is limited by the linewidths of the dipole-dipole broadening, $\Gamma = 8/9\pi d^2 n$, and the Doppler broadening, $\sigma_\omega = \sqrt{kT/mc^2}\omega$, of the $|2\rangle \rightarrow |3\rangle$ transition. For a gas of SrF molecules with a density $n = 10^{10} \text{ cm}^{-3}$ the value of ω_{min} ranges from 0.26 kHz at $T = 1 \mu\text{K}$ to 8.28 kHz at $T = 1 \text{ K}$.

ticular combinations, the molecules become transparent to the resonant microwave field. This is demonstrated in Figure 6.2. The figure illustrates that the magnitude of the dc electric field E_0 , for which $d_\alpha(B_0, E_0) \sim 0$, depends sensitively on the frequency of the resonant transition (which can be tuned by varying B_0). This can be used for sensitive detection of the magnitude E_0 of a dc electric field, given the magnitude of B_0 and the frequency of the microwave field. Conversely, this can be also used for sensitive detection of the magnitude B_0 of the dc magnetic field, given the magnitude of E_0 and the resonant microwave frequency.

Longer interaction time τ results in increased sensitivity to electric fields. The sensitivity is, however, gained at the expense of the spatial resolution that decreases with τ due to the molecular motion and decoherence. The effective spatial resolution, $S_{eff} = 2(\sigma_\tau^2 + \sigma_{img}^2 + \sigma_{ps}^2)^{1/2}$, can be calculated from the displacements $\sigma_\tau = \tau\sqrt{2k_B T/m}$ during the measurement time (τ), $\sigma_{img} = \tau_{img}\sqrt{2k_B T/m}$ during the imaging pulse (τ_{img}), and $\sigma_{ps} = v_{rec}\tau_{img}\sqrt{2\Gamma\tau_{img}}/3$ due to the photon scattering. Here k_B is the Boltzmann constant, T is the temperature of the gas, m is the mass of a molecule, v_{rec} is the recoil velocity, and Γ is the scattering rate (for SrF, $\Gamma = 3$ MHz [153, 154]). Fig. 6.3 illustrates the relation between the sensitivity and the spatial resolution for an ensemble of SrF molecules and different frequencies of the field detected.

The energy level structure of paramagnetic molecules can also be used to probe sensitively static or off-resonant rf and microwave fields. This can be achieved by measuring the phase accumulation in a Ramsey-type sequence consisting of two $\pi/2$ pulses [5]. The first $\pi/2$ pulse prepares the molecules in the equal superposition of states $|2\rangle$ and $|3\rangle$, which acquire a relative phase proportional to the Stark shift, $\Delta\phi = d_{eff}(B_0, E_0)E\tau$, due to the effective dipole moment $d_{eff}(B_0, E_0) = \frac{d(\hbar\omega_{32})}{dE}$ during the evolution time τ . The second $\pi/2$ -pulse transforms the relative phase into a population difference. Because the states $|2\rangle$ and $|3\rangle$ become nearly degenerate at magnetic fields near $B = B^*$, the magnitude of d_{eff} is significantly enhanced near the avoided crossing depicted in Figure 1 (b). The sensitivity to a dc electric field is given by

$$\eta_E^{dc} = \frac{2\sqrt{3}\hbar}{100d_{eff}(B_0, E_0)\sqrt{nV_{eff}}\sqrt{\tau}}, \quad (6.7)$$

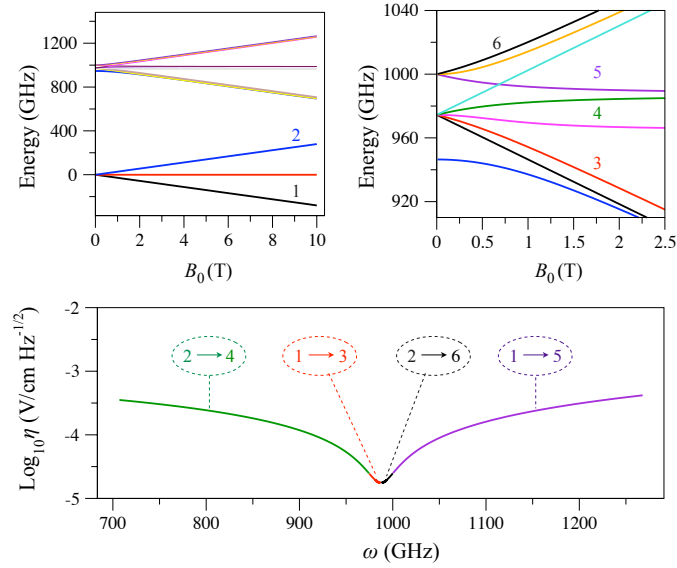


Figure 6.4: (a), (b) Energy levels of the $\text{NH}(^3\Sigma^-)$ molecule ($b_r = 490.0$ GHz, $\gamma = -1.65$ GHz, and $\lambda = 27.6$ GHz) as a function of the magnetic field B_0 ; (c) Frequency dependence of the ac field sensitivity. The background electric field $\mathbf{E}_0 = 0$.

and equals 1.58×10^{-5} V/cm Hz $^{-1/2}$ for SrF molecules with the density 10^{12} cm $^{-3}$ in a magnetic field of $B_0 = 545$ mT and electric field of $E_0 = 2.5$ kV/cm.

The range of detectable frequencies of electromagnetic fields can be extended by using paramagnetic molecules of higher spin multiplicity. For example, $^3\Sigma$ molecules offer a series of tunable transitions that can be used to probe ac electric fields in the same way as the transitions in the $^2\Sigma$ molecules described above. This is illustrated in Fig. 6.4 that shows the energy level structure of $\text{NH}(^3\Sigma^-)$ molecules, and the corresponding sensitivities. A large value of the rotational constant of NH and a series of tunable dipole-allowed transitions allow for the possibility to cover continuously a broad range of detectable ac fields in the THz frequency region, which is particularly interesting for a variety of practical applications [156].

6.4 Conclusion

We have described a technique for sensitive parallel measurements of electric and magnetic field components of electromagnetic fields, both dc and oscillating with frequencies ranging from a fraction of a kHz to THz. The method, based on tunable energy level structure of paramagnetic molecules in superimposed electric and magnetic fields, allows one to achieve the sensitivity on the order of V/cm Hz^{-1/2} and 100 fT Hz^{-1/2} for the ac fields and 10 V/cm Hz^{-1/2} and nT Hz^{-1/2} for dc fields. The sensitivity to the magnetic component of an ac field can be calculated as η_B^{ac} [T Hz^{-1/2}] = η_E^{ac} [V/cm Hz^{-1/2}] $\times 3.336^{-7}$. The ratio of the minimal detectable magnetic fields in experiments with cold atoms [63] and molecules is given by $B_{\min}^{\text{at}}/B_{\min}^{\text{mol}} = 2cd_\alpha^{12}/(\sqrt{3}\mu_B)$ (assuming the same interaction time τ , the same number of particles and the same detection efficiency in both cases), which for typical molecules with $d \sim 1$ a.u. amounts to ~ 100 -fold higher sensitivity using the proposed scheme. Finally, the method proposed here can be used for detecting weak dc and ac fields in the presence of high background dc magnetic and electric field.

Chapter 7

Conclusion

7.1 Overall conclusions of the dissertation

The field of cold and ultracold molecules is at the beginning of its development. Current research is focused on obtaining a large sample of ultracold polar molecules in the ground state [157], laser cooling of molecules [158] and the creation of optical lattices with cold polar molecules [159]. The complex structure of molecules, long-range anisotropic dipole-dipole intermolecular interactions and the overall enhanced controllability at low temperatures make cold and ultracold molecules attractive for various applications. The crucial step towards these applications is the understanding of the collisional properties of ultracold molecules.

The research presented in this work explores ultracold molecular collisions in electromagnetic fields, and describes new mechanisms for controlling the collision dynamics of atoms and molecules confined in a 2D geometry and collisions of molecules in microwave fields. We also propose a method for sensitive detection of weak electromagnetic fields in the low frequency regime. The results presented in this Thesis are of general interest for researches of ultracold molecules and important for particular applications, e.g. the development of methods for evaporative cooling of molecules and for the detection of weak electromagnetic fields with cold polar molecules.

7.2 Contributions of the dissertation

The research described in this Thesis can be divided in three parts.

First, we studied how confinement of molecular gases to 2D and quasi 2D geometries changes the energy dependence of the elastic and inelastic scattering cross sections. We derived the Wigner's threshold laws for collisions in confined gases and showed that inelastic angular momentum changing collisions are suppressed. This can be used to control the angular momentum changing collisions such as Zeeman and Stark relaxation by varying the direction of the external electric or magnetic fields. Recently the confinement of atoms and molecules in a quasi-2D geometry and effects of an electric field on chemical reactions were studied both theoretically [160–164] and experimentally [165].

In Chapters 3-5, we explored the effects of the microwave field on collision properties of ultracold molecules. We developed the scattering theory for molecular collisions in a microwave field based on the field-dressed formalism for molecule-field interactions. We found that in the presence of a microwave field collisions may lead to the absorption of the microwave photons. We showed that microwave fields can be used to enhance the inelastic spin-changing collisions and to shift and suppress the Feshbach resonances in collisions of ultracold molecules. We analyzed the effects of the anisotropy of the intermolecular potential and parameters of the microwave fields on collisions of polar molecules in a microwave cavity to investigate the possibility of evaporative cooling of polar molecules in a microwave trap. This is a first description of molecular collisions in the presence of a microwave field using the field-dressed approach and quantum scattering theory. The quantum scattering calculations based on the numerical solution of the close coupling equations is the most accurate method for performing calculations of the scattering cross sections from first principles. The field-dressed approach accurately and consistently describes the coupling of molecules with electromagnetic fields. The combination of the two approaches allows one to accurately describe molecular scattering in an electromagnetic field and incorporate the processes of photon absorption and emission in the scattering formalism. This work is important because of the large number of possible applications of microwave fields in the field of cold molecules, ranging from external field control of spin-forbidden

chemical reactions to manipulation with molecular qubits.

In Chapter 6, we suggested a method for sensitive detection of weak electromagnetic fields with ultracold polar molecules. This method can be used to detect both dc and ac electromagnetic fields in a large frequency range and is predicted to have a sensitivity of two orders of magnitude larger than the analogous method using ultracold Rb atoms [63]. The detection of weak electromagnetic fields is important for many applications ranging from biomagnetic imaging to chip design. The most sensitive methods are using alkali atoms to detect weak magnetic and microwave fields. Polar paramagnetic molecules provide controllability, which may result in a wide range of detectable frequencies due to the presence of both electric and magnetic moments and a large coupling of the permanent dipole moment to the electromagnetic field, which may enhance the sensitivity significantly. Our work is a first attempt to analyse the advantage of using molecules for sensing electromagnetic fields.

7.3 Future research directions

Understanding the effects of electromagnetic fields on collision dynamics of cold and ultracold polar molecules is very important for various applications and design of the experiments. There are many possible research directions for future work.

The developed method can be extended to consider the molecule-molecule collisions, collisions of more complex atoms or more complex molecules (e.g. molecules with three or more atoms) in microwave fields. The systematic investigation of the elastic and inelastic cross sections at different microwave field parameters would help to design the microwave traps suitable for trapping and evaporative or sympathetic cooling of polar molecules.

For an accurate description of the collision dynamics in the electromagnetic field it is important to include a large number of the angular momentum states and photon number states in the expansion of the wave function. The large number of the basis functions limits the accuracy of the quantum scattering calculations. The development of more efficient methods and algorithms for quantum scattering calculations for molecules in the electromagnetic fields, therefore, is of great importance.

The field-dressed state approach doesn't consider the probability of spontaneous emission of microwave photons during collision and it might overestimate the role of collision-induced photon absorption processes. The lifetime of the rotational states is very large and usually the spontaneous emission from the rotational state is not considered. However, the time of ultracold collisions is very long too and several transitions from the high rotational states become allowed in the presence of the other particle since the parity of the rotational state of the molecule is not conserved. Therefore, the development of methods that would allow the treatment of the spontaneous emission is necessary for more accurate calculations.

Another possible research direction is to explore the possibility of using cold and ultracold molecules as a quantum probe of weak electromagnetic fields or interaction potentials (e.g. the Casimir-Polder potential created by a surface). Collisions of molecules would lead to decoherence and limit such schemes. The development of methods for preserving quantum coherence in application to cold and ultracold molecules would advance the research in this direction.

As we showed in Chapter 6 the sensitivity of the method which uses molecules for sensing electromagnetic fields is fundamentally higher than the sensitivity of the method using Rb atoms. However, for practical applications it is important to develop a method that would work at high temperatures and would contain molecules in some sort of cell. For this purpose one needs to estimate the sensitivity taking into account the possibility of elastic and inelastic scattering of molecules that would lead to depletion of the initial state. The rate of such processes is expected to be much larger for molecules than for atoms, and therefore limiting the sensitivity of the molecule-based methods. However, the population of the initial state perhaps could be increased by optical pumping and a careful estimation is therefore required. The theory of optical pumping of atoms is well developed, compared to the theory of optical pumping of molecules. The development of the theory of optical pumping of molecular states is therefore necessary to extend the scheme for the detection of weak electromagnetic fields proposed in Chapter 6 from a single-shot experiment to a continuous measurement scheme. This, perhaps, could lead to the method with sensitivity higher than that of the atomic based sensors.

Bibliography

- [1] J. Doyle, B. Friedrich, R. V. Krems, and F. Masnou-Seeuws. Editorial: Quo vadis, cold molecules? *Eur. Phys. J. D*, 31:149–164, 2004. → pages 1, 20, 36
- [2] L. D. Carr, D. DeMille, R. V. Krems, and J. Ye. Cold and ultracold molecules: science, technology and applications. *New J. Phys.*, 11(5):055049, 2009. → pages 1, 20
- [3] G. K. Campbell and W. D. Phillips. Ultracold atoms and precise time standards. *Phil. Trans. R. Soc. A*, 369:4078–4089, Oct 2011. → pages 2
- [4] N. F. Ramsey. A new molecular beam resonance method. *Phys. Rev.*, 76:996–996, Oct 1949. → pages 2
- [5] N. F. Ramsey. *Molecular Beams*. Oxford, UK: Clarendon Press, 1956. → pages 2, 7, 88
- [6] L. Essen and J. V. L. Parry. An atomic standard of frequency and time interval: a caesium resonator. *Nature*, 176:280–282, 1955. → pages 2
- [7] T. W. Hänsch and A. L. Schawlow. Cooling of gases by laser radiation. *Opt. Commun.*, 13(1):68 – 69, 1975. → pages 2
- [8] D. J. Wineland and T. H. Dehmelt. Proposed $10^{14} \delta\varepsilon < \varepsilon$ laser fluorescence spectroscopy on Tl+mono-ion oscillator. *Bull. Am. Phys. Soc.*, 20:637, 1975. → pages 2
- [9] D. J. Wineland, R. E. Drullinger, and F. L. Walls. Radiation-pressure cooling of bound resonant absorbers. *Phys. Rev. Lett.*, 40:1639–1642, Jun 1978. → pages 2
- [10] W. Neuhauser, M. Hohenstatt, P. Toschek, and T. H. Dehmelt. Optical-sideband cooling of visible atom cloud confined in parabolic well. *Phys. Rev. Lett.*, 41:233–236, Jul 1978. → pages 2

- [11] S. Chu, L. Hollberg, J. E. Bjorkholm, A. Cable, and A. Ashkin. Three-dimensional viscous confinement and cooling of atoms by resonance radiation pressure. *Phys. Rev. Lett.*, 55:48–51, Jul 1985. → pages 3
- [12] P. D. Lett, R. N. Watts, C. I. Westbrook, W. D. Phillips, P. L. Gould, and H. J. Metcalf. Observation of atoms laser cooled below the doppler limit. *Phys. Rev. Lett.*, 61:169–172, Jul 1988. → pages 3
- [13] P. Verkerk, B. Lounis, C. Salomon, C. Cohen-Tannoudji, J.-Y. Courtois, and G. Grynberg. Dynamics and spatial order of cold cesium atoms in a periodic optical potential. *Phys. Rev. Lett.*, 68:3861–3864, Jun 1992. → pages 3
- [14] P. S. Jessen, C. Gerz, P. D. Lett, W. D. Phillips, S. L. Rolston, R. J. C. Spreeuw, and C. I. Westbrook. Observation of quantized motion of Rb atoms in an optical field. *Phys. Rev. Lett.*, 69:49–52, Jul 1992. → pages 3
- [15] A. L. Migdall, J. V. Prodan, W. D. Phillips, T. H. Bergeman, and H. J. Metcalf. First observation of magnetically trapped neutral atoms. *Phys. Rev. Lett.*, 54:2596–2599, Jun 1985. → pages 3
- [16] S. Chu, J. E. Bjorkholm, A. Ashkin, and A. Cable. Experimental observation of optically trapped atoms. *Phys. Rev. Lett.*, 57:314–317, Jul 1986. → pages 3
- [17] E. L. Raab, M. Prentiss, A. Cable, S. Chu, and D. E. Pritchard. Trapping of neutral sodium atoms with radiation pressure. *Phys. Rev. Lett.*, 59:2631–2634, Dec 1987. → pages 3
- [18] M. H. Anderson, J. R. Ensher, M. R. Matthews, C. E. Wieman, and E. A. Cornell. Observation of Bose-Einstein condensation in a dilute atomic vapor. *Science*, 269(5221):198–201, 1995. → pages 3
- [19] K. B. Davis, M. O. Mewes, M. R. Andrews, N. J. van Druten, D. S. Durfee, D. M. Kurn, and W. Ketterle. Bose-Einstein condensation in a gas of sodium atoms. *Phys. Rev. Lett.*, 75:3969–3973, Nov 1995. → pages 3
- [20] C. C. Bradley, C. A. Sackett, J. J. Tollett, and R. G. Hulet. Evidence of Bose-Einstein condensation in an atomic gas with attractive interactions. *Phys. Rev. Lett.*, 75:1687–1690, Aug 1995. → pages 3
- [21] J. J. Hudson, B. E. Sauer, M. R. Tarbutt, and E. A. Hinds. Measurement of the electron electric dipole moment using YbF molecules. *Phys. Rev. Lett.*, 89:023003, Jun 2002. → pages 5, 53

- [22] H. L. Bethlem, J. van Veldhoven, M. Schnell, and G. Meijer. Trapping polar molecules in an ac trap. *Phys. Rev. A*, 74:063403, Dec 2006. → pages 5
- [23] J. M. Doyle, B. Friedrich, J. Kim, and D. Patterson. Buffer-gas loading of atoms and molecules into a magnetic trap. *Phys. Rev. A*, 52:R2515–R2518, Oct 1995. → pages 6, 53
- [24] J. K. Messer and F. C. De Lucia. Measurement of pressure-broadening parameters for the CO-He system at 4 K. *Phys. Rev. Lett.*, 53:2555–2558, Dec 1984. → pages 6
- [25] Z. Hadzibabic, C. A. Stan, K. Dieckmann, S. Gupta, M. W. Zwierlein, A. Görlitz, and W. Ketterle. Two-species mixture of quantum degenerate Bose and Fermi gases. *Phys. Rev. Lett.*, 88:160401, Apr 2002. → pages 6
- [26] W. Petrich, M. H. Anderson, J. R. Ensher, and E. A. Cornell. Stable, tightly confining magnetic trap for evaporative cooling of neutral atoms. *Phys. Rev. Lett.*, 74:3352–3355, Apr 1995. → pages 6
- [27] E. Tiesinga, B. J. Verhaar, and H. T. C. Stoof. Threshold and resonance phenomena in ultracold ground-state collisions. *Phys. Rev. A*, 47:4114–4122, May 1993. → pages 6, 10
- [28] Z. Li and R. V. Krems. Electric-field-induced Feshbach resonances in ultracold alkali-metal mixtures. *Phys. Rev. A*, 75:032709, Mar 2007. → pages 6
- [29] P. O. Fedichev, Yu. Kagan, G. V. Shlyapnikov, and J. T. M. Walraven. Influence of nearly resonant light on the scattering length in low-temperature atomic gases. *Phys. Rev. Lett.*, 77:2913–2916, Sep 1996. → pages 6
- [30] D. Jaksch, C. Bruder, J. I. Cirac, C. W. Gardiner, and P. Zoller. Cold bosonic atoms in optical lattices. *Phys. Rev. Lett.*, 81:3108–3111, Oct 1998. → pages 6
- [31] H. Sakai, S. Minemoto, H. Nanjo, H. Tanji, and T. Suzuki. Controlling the orientation of polar molecules with combined electrostatic and pulsed, nonresonant laser fields. *Phys. Rev. Lett.*, 90:083001, Feb 2003. → pages 6
- [32] R. V. Krems. Breaking van der Waals molecules with magnetic fields. *Phys. Rev. Lett.*, 93:013201, Jun 2004. → pages 6

- [33] M. A. Kasevich, E. Riis, S. Chu, and R. G. DeVoe. rf spectroscopy in an atomic fountain. *Phys. Rev. Lett.*, 63:612–615, Aug 1989. → pages 7
- [34] A. Clairon, C. Salomon, S. Guellati, and W. D. Phillips. Ramsey resonance in a Zacharias fountain. *EPL (Europhysics Letters)*, 16(2):165, 1991. → pages 7
- [35] M. D. Swallows, M. Bishof, D. Lin, S. Blatt, M. J. Martin, A. M. Rey, and J. Ye. Suppression of collisional shifts in a strongly interacting lattice clock. *Science*, 331:1043, 2011. → pages 7
- [36] C. Braxmaier, O. Prndl, H. Müller, A. Peters, J. Mlynek, V. Loriette, and S. Schiller. Proposed test of the time independence of the fundamental constants α and m_e/m_p using monolithic resonators. *Phys. Rev. D*, 64:042001, Jul 2001. → pages 7
- [37] J. D. Prestage, R. L. Tjoelker, and L. Maleki. Atomic clocks and variations of the fine structure constant. *Phys. Rev. Lett.*, 74:3511–3514, May 1995. → pages 7
- [38] V. A. Dzuba, V. V. Flambaum, and J. K. Webb. Calculations of the relativistic effects in many-electron atoms and space-time variation of fundamental constants. *Phys. Rev. A*, 59:230–237, Jan 1999. → pages 7
- [39] P. Fritschel, G. González, B. Lantz, P. Saha, and M. Zucker. High power interferometric phase measurement limited by quantum noise and application to detection of gravitational waves. *Phys. Rev. Lett.*, 80:3181–3184, Apr 1998. → pages 7
- [40] P. D. D. Schwindt, S. Knappe, V. Shah, L. Hollberg, J. Kitching, Li-A. Liew, and J. Moreland. Chip-scale atomic magnetometer. *Appl. Phys. Lett.*, 85(26):6409–6411, 2004. → pages 8
- [41] E. Salim, J. DeNatale, D. Farkas, K. Hudek, S. McBride, J. Michalchuk, R. Mihailovich, and D. Anderson. Compact, microchip-based systems for practical applications of ultracold atoms. *QIP*, 10:975–994, 2011. 10.1007/s11128-011-0300-8. → pages
- [42] M. Horikoshi and K. Nakagawa. Atom chip based fast production of Bose-Einstein condensate. *Appl. Phys. B*, 82:363–366, 2006. 10.1007/s00340-005-2083-z. → pages 8

- [43] M. Greiner, O. Mandel, T. Esslinger, T. W. Hänsch, and I. Bloch. Quantum phase transition from a superfluid to a Mott insulator in a gas of ultracold atoms. *Nature*, 415:39–49, 2002. → pages 8
- [44] M. W. Zwierlein, C. A. Stan, C. H. Schunck, S. M. F. Raupach, A. J. Kerman, and W. Ketterle. Condensation of pairs of Fermionic atoms near a Feshbach resonance. *Phys. Rev. Lett.*, 92:120403, Mar 2004. → pages 8
- [45] B. Paredes, P. Fedichev, J. I. Cirac, and P. Zoller. $\frac{1}{2}$ -Anyons in small atomic Bose-Einstein condensates. *Phys. Rev. Lett.*, 87:010402, Jun 2001. → pages 8
- [46] F. Schreck, L. Khaykovich, K. L. Corwin, G. Ferrari, T. Bourdel, J. Cubizolles, and C. Salomon. Quasipure Bose-Einstein condensate immersed in a Fermi sea. *Phys. Rev. Lett.*, 87:080403, Aug 2001. → pages 8
- [47] D. S. Hall, M. R. Matthews, J. R. Ensher, C. E. Wieman, and E. A. Cornell. Dynamics of component separation in a binary mixture of Bose-Einstein condensates. *Phys. Rev. Lett.*, 81:1539–1542, Aug 1998. → pages 8
- [48] P. Bouyer and M. A. Kasevich. Heisenberg-limited spectroscopy with degenerate Bose-Einstein gases. *Phys. Rev. A*, 56:R1083–R1086, Aug 1997. → pages 8
- [49] A. Gorlitz, J. M. Vogels, A. E. Leanhardt, C. Raman, T. L. Gustavson, J. R. Abo-Shaer, A. P. Chikkatur, S. Gupta, S. Inouye, T. Rosenband, and W. Ketterle. Realization of Bose-Einstein condensates in lower dimensions. *Phys. Rev. Lett.*, 87:130402, Sep 2001. → pages 8, 9, 20
- [50] V. Bagnato and D. Kleppner. Bose-Einstein condensation in low-dimensional traps. *Phys. Rev. A*, 44:7439–7441, Dec 1991. → pages 8
- [51] D. S. Petrov, M. Holzmann, and G. V. Shlyapnikov. Bose-Einstein condensation in quasi-2D trapped gases. *Phys. Rev. Lett.*, 84:2551–2555, Mar 2000. → pages 9, 20
- [52] H. P. Büchler, E. Demler, M. Lukin, A. Micheli, N. Prokof'ev, G. Pupillo, and P. Zoller. Strongly correlated 2D quantum phases with cold polar molecules: Controlling the shape of the interaction potential. *Phys. Rev. Lett.*, 98:060404, Feb 2007. → pages 9, 21, 36
- [53] A. Micheli, G. K. Brennen, and P. Zoller. A toolbox for lattice-spin models with polar molecules. *Nature Phys.*, 2(5):341, 2006. → pages 9, 21, 53

- [54] D. DeMille. Quantum computation with trapped polar molecules. *Phys. Rev. Lett.*, 88:067901, Jan 2002. → pages 9
- [55] A. Andre, D. DeMille, J. M. Doyle, M. D. Lukin, S. E. Maxwell, P. Rabl, R. J. Schoelkopf, and Zoller P. A coherent all-electrical interface between polar molecules and mesoscopic superconducting resonators. *Nature Phys.*, 2(5):636–642, 2006. → pages 9, 53
- [56] J. C. Allred, R. N. Lyman, T. W. Kornack, and M. V. Romalis. High-sensitivity atomic magnetometer unaffected by spin-exchange relaxation. *Phys. Rev. Lett.*, 89:130801, Sep 2002. → pages 9, 17
- [57] S. Inouye, M. R. Andrews, J. Stenger, H.-J. Miesner, D. M. Stamper-Kurn, and W. Ketterle. Observation of Feshbach resonances in a Bose-Einstein condensate. *Nature*, 392:151–154, March 1998. → pages 10, 71
- [58] C. A. Regal, M. Greiner, and D. S. Jin. Lifetime of molecule-atom mixtures near a Feshbach resonance in ^{40}K . *Phys. Rev. Lett.*, 92:083201, Feb 2004. → pages 10, 71
- [59] F. Lang, K. Winkler, C. Strauss, R. Grimm, and J. H. Denschlag. Ultracold triplet molecules in the rovibrational ground state. *Phys. Rev. Lett.*, 101:133005, Sep 2008. → pages 10
- [60] M. W. Zwierlein, C. A. Stan, C. H. Schunck, S. M. F. Raupach, S. Gupta, Z. Hadzibabic, and W. Ketterle. Observation of Bose-Einstein condensation of molecules. *Phys. Rev. Lett.*, 91:250401, Dec 2003. → pages 10, 71
- [61] C. Chin, M. Bartenstein, A. Altmeyer, S. Riedl, S. Jochim, J. H. Denschlag, and R. Grimm. Observation of the pairing gap in a strongly interacting Fermi gas. *Science*, 305(5687):1128–1130, 2004. → pages 10
- [62] C. A. Sackett, J. M. Gerton, M. Welling, and R. G. Hulet. Measurements of collective collapse in a Bose-Einstein condensate with attractive interactions. *Phys. Rev. Lett.*, 82:876–879, Feb 1999. → pages 10, 71, 79
- [63] P. Böhi, M. F. Riedel, T. W. Hänsch, and P. Treutlein. Imaging of microwave fields using ultracold atoms. *Apl. Phys. Lett.*, 97:051101, 1995. → pages 15, 80, 81, 85, 86, 90, 93
- [64] L. M. C. Janssen, P. S. Zuchowski, Ad van der Avoird, J. M. Hutson, and G. C. Groenenboom. Cold and ultracold NH-NH collisions: The field-free case. *J. Chem. Phys.*, 134(12):124309, 2011. → pages 17

- [65] E. P. Wigner. On the behavior of cross sections near thresholds. *Phys. Rev.*, 73(9):1002–1009, May 1948. → pages 18, 24, 26, 29, 30, 68
- [66] L. D. Landau and E. M. Lifshitz. *Quantum Mechanics (Non-Relativistic Theory)*. Butterworth-Heinemann, 3 edition, 1981. → pages 19, 28, 31, 32
- [67] T. F. O’Malley. Low-energy expansion of the scattering amplitude for long-range quadrupole potentials. *Phys. Rev.*, 134:A1188–A1197, Jun 1964. → pages 19
- [68] I. I. Fabrikant. Effective-range analysis of low-energy electron scattering by non-polar molecules. *J. Phys. B: At. Mol. Opt. Phys.*, 17(20):4223, 1984. → pages
- [69] O. Hinckelmann and L. Spruch. Low-energy scattering by long-range potentials. *Phys. Rev. A*, 3:642–648, Feb 1971. → pages
- [70] R. Shakeshaft. Low energy scattering by the r^{-3} potential. *J. Phys. B: At. Mol. Opt. Phys.*, 5(6):L115, 1972. → pages 19
- [71] P. Soltan-Panahi, J. Struck, P. Hauke, A. Bick, W. Plenkers, G. Meineke, C. Becker, P. Windpassinger, M. Lewenstein, and K. Sengstock. Multi-component quantum gases in spin-dependent hexagonal lattices. *Phys. Rev. Lett.*, 7:595–602, 2011. → pages 20
- [72] G.-B. Jo, J. Guzman, C. K. Thomas, P. Hosur, A. Vishwanath, and D. M. Stamper-Kurn. Ultracold atoms in a tunable optical Kagome lattice. *Phys. Rev. Lett.*, 108:045305, Jan 2012. → pages 20
- [73] P. C. Hohenberg. Existence of long-range order in one and two dimensions. *Phys. Rev.*, 158:383–386, Jun 1967. → pages 20
- [74] A. A. Burkov, M. D. Lukin, and E. Demler. Decoherence dynamics in low-dimensional cold atom interferometers. *Phys. Rev. Lett.*, 98:200404, May 2007. → pages
- [75] D. Rychtarik, B. Engeser, H.-C. Nägerl, and R. Grimm. Two-dimensional Bose-Einstein condensate in an optical surface trap. *Phys. Rev. Lett.*, 92:173003, Apr 2004. → pages
- [76] V. Schweikhard, I. Coddington, P. Engels, V. P. Mogendorff, and E. A. Cornell. Rapidly rotating Bose-Einstein condensates in and near the lowest Landau level. *Phys. Rev. Lett.*, 92:040404, Jan 2004. → pages 20

- [77] D. S. Petrov and G. V. Shlyapnikov. Interatomic collisions in a tightly confined Bose gas. *Phys. Rev. A*, 64(1):012706, Jun 2001. → pages 21, 28, 30, 32
- [78] M. Abramowitz and I. A. Stegun. *Handbook of Mathematical Functions with Formulas, Graphs, and Mathematical Tables*. Dover Publications, 1 edition, 1964. → pages 24, 28, 29
- [79] E. P. Wigner and L. Eisenbud. Higher angular momenta and long range interaction in resonance reactions. *Phys. Rev.*, 72(1):29–41, Jul 1947. → pages 24, 26
- [80] M. S. Child. *Molecular Collision Theory*. Dover Publications, 1 edition, 1974. → pages 31
- [81] Z. Li, S. V. Alyabyshev, and R. V. Krems. Ultracold inelastic collisions in two dimensions. *Phys. Rev. Lett.*, 100:073202, Feb 2008. → pages 32
- [82] G. Quéméner and J. L. Bohn. Strong dependence of ultracold chemical rates on electric dipole moments. *Phys. Rev. A*, 81:022702, Feb 2010. → pages 32
- [83] A. Micheli, Z. Idziaszek, G. Pupillo, M. A. Baranov, P. Zoller, and P. S. Julienne. Universal rates for reactive ultracold polar molecules in reduced dimensions. *Phys. Rev. Lett.*, 105:073202, Aug 2010. → pages 32
- [84] G. Quéméner and J. L. Bohn. Dynamics of ultracold molecules in confined geometry and electric field. *Phys. Rev. A*, 83:012705, Jan 2011. → pages 32
- [85] A. Volpi and J. L. Bohn. Magnetic-field effects in ultracold molecular collisions. *Phys. Rev. A*, 65:052712, May 2002. → pages 33, 54
- [86] Z. Li and R. V. Krems. Electric-field-induced Feshbach resonances in ultracold alkali-metal mixtures. *Phys. Rev. A*, 75(3):032709, Mar 2007. → pages 33
- [87] M. Shapiro and P. Brumer. *Principles of Quantum Control of Molecular Processes*. Wiley-Interscience, 1 edition, 2003. → pages 35
- [88] S. A. Rice and M. Zhao. *Optical Control of Molecular Dynamics*. Wiley-Interscience, 1 edition, 2000. → pages
- [89] A. Stolow and D. M. Jonas. Multidimensional snapshots of chemical dynamics. *Science*, 305(5690):1575–1577, 2004. → pages 35

- [90] B. J. Sussman, D. Townsend, M. Y. Ivanov, and A. Stolow. Dynamic stark control of photochemical processes. *Science*, 314(5797):278–281, 2006. → pages 35
- [91] R. N. Zare. Laser control of chemical reactions. *Science*, 279(5358):1875–1879, 1998. → pages 35
- [92] J. J. Larsen, I. Wendt-Larsen, and H. Stapelfeldt. Controlling the branching ratio of photodissociation using aligned molecules. *Phys. Rev. Lett.*, 83:1123–1126, Aug 1999. → pages 35
- [93] R. V. Krems. Cold controlled chemistry. *Phys. Chem. Chem. Phys.*, 10:4079–4092, 2008. → pages 35
- [94] W. C. Campbell, E. Tsikata, H.-I. Lu, L. D. van Buuren, and J. M. Doyle. Magnetic trapping and zeeman relaxation of $\text{NH}(X^3\Sigma^-)$. *Phys. Rev. Lett.*, 98:213001, May 2007. → pages 35, 53, 82, 83
- [95] S. Y. T. van de Meerakker, H. L. Bethlem, and G. Meijer. Taming molecular beams. *Phys. Rev. Lett.*, 4:595–602, 2008. → pages
- [96] J. G. Danzl, E. Haller, M. Gustavsson, M. J. Mark, R. Hart, N. Bouloufa, O. Dulieu, H. Ritsch, and H.-C. Nägerl. Quantum gas of deeply bound ground state molecules. *Science*, 321(5892):1062–1066, 2008. → pages
- [97] K.-K. Ni, S. Ospelkaus, M. H. G. de Miranda, A. Pe'er, B. Neyenhuis, J. J. Zirbel, S. Kotochigova, P. S. Julienne, D. S. Jin, and J. Ye. A high phase-space-density gas of polar molecules. *Science*, 322(5899):231–235, 2008. → pages 35, 71
- [98] A. V. Gorshkov, P. Rabl, G. Pupillo, A. Micheli, P. Zoller, M. D. Lukin, and H. P. Büchler. Suppression of inelastic collisions between polar molecules with a repulsive shield. *Phys. Rev. Lett.*, 101:073201, Aug 2008. → pages 36
- [99] H. P. Büchler, A. Micheli, and P. Zoller. Three-body interactions with cold polar molecules. *Nature Phys.*, 3:726, Oct. 2007. → pages 36
- [100] C. C. Agosta, I. F. Silvera, H. T. C. Stoof, and B. J. Verhaar. Trapping of neutral atoms with resonant microwave radiation. *Phys. Rev. Lett.*, 62:2361–2364, May 1989. → pages 36
- [101] R. J. C. Spreeuw, C. Gerz, L. S. Goldner, W. D. Phillips, S. L. Rolston, C. I. Westbrook, M. W. Reynolds, and I. F. Silvera. Demonstration of neutral

- atom trapping with microwaves. *Phys. Rev. Lett.*, 72:3162–3165, May 1994. → pages 36
- [102] D. DeMille, D. R. Glenn, and J. Petricka. Microwave traps for cold polar molecules. *Eur. Phys. J. D*, 31:375–384, 2004. → pages 36, 47
- [103] C. Cohen-Tannoudji, J. Dupont-Roc, and G. Grynberg. *Atom-Photon Interactions: Basic Processes and Applications*. Wiley-VCH, 1 edition, 1992. → pages 37, 40, 58, 60
- [104] P. S. Julienne. Laser modification of ultracold atomic collisions in optical traps. *Phys. Rev. Lett.*, 61:698–701, Aug 1988. → pages 37
- [105] H. M. J. M. Boesten and B. J. Verhaar. Simple quantum-mechanical picture of cold optical collisions. *Phys. Rev. A*, 49:4240–4242, May 1994. → pages 37
- [106] A. J. Moerdijk, B. J. Verhaar, and T. M. Nagtegaal. Collisions of dressed ground-state atoms. *Phys. Rev. A*, 53:4343–4351, Jun 1996. → pages 37
- [107] T. V. Tscherbul, T. Calarco, I. Lesanovsky, R. V. Krems, A. Dalgarno, and J. Schmiedmayer. rf-field-induced Feshbach resonances. *Phys. Rev. A*, 81:050701, May 2010. → pages 37
- [108] J. H. Shirley. Solution of the Schrödinger equation with a Hamiltonian periodic in time. *Phys. Rev.*, 138:B979–B987, May 1965. → pages 37, 38
- [109] S. H. Autler and C. H. Townes. Stark effect in rapidly varying fields. *Phys. Rev.*, 100:703–722, Oct 1955. → pages 41
- [110] W. Happer. Observations of transitions between stationary states in a rotating magnetic field. *Phys. Rev.*, 136:A35–A42, Oct 1964. → pages 41
- [111] R. V. Krems and A. Dalgarno. Quantum-mechanical theory of atom-molecule and molecular collisions in a magnetic field: Spin depolarization. *J. Chem. Phys.*, 120(5):2296–2307, 2004. → pages 46, 54
- [112] G. C. Groenenboom and N. Balakrishnan. The He-CaH ($^2\Sigma^+$) interaction. i. three-dimensional ab initio potential energy surface. *J. Chem. Phys.*, 118(16):7380–7385, 2003. → pages 46
- [113] T. V. Tscherbul and R. V. Krems. Quantum theory of chemical reactions in the presence of electromagnetic fields. *J. Chem. Phys.*, 129(3):034112, 2008. → pages 53

- [114] J. Perez-Rios, F. Herrera, and R. V. Krems. External field control of collective spin excitations in an optical lattice of $^2\Sigma$ molecules. *New J. Phys.*, 12(10):103007, 2010. → pages 53, 83
- [115] D. DeMille, S. B. Cahn, D. Murphree, D. A. Rahmlow, and M. G. Kozlov. Using molecules to measure nuclear spin-dependent parity violation. *Phys. Rev. Lett.*, 100:023003, Jan 2008. → pages 53
- [116] J. J. Hudson, D. M. Kara, I. J. Smallman, B. E. Sauer, M. R. Tarbutt, and E. A. Hinds. Enhanced sensitivity to the time variation of the fine-structure constant and m_p/m_e in diatomic molecules. *Nature*, 473:493, 2011. → pages 53
- [117] V. V. Flambaum. Enhanced effect of temporal variation of the fine-structure constant in diatomic molecules. *Phys. Rev. A*, 73:034101, Mar 2006. → pages 53
- [118] V. V. Flambaum and M. G. Kozlov. Enhanced sensitivity to the time variation of the fine-structure constant and m_p/m_e in diatomic molecules. *Phys. Rev. Lett.*, 99:150801, Oct 2007. → pages 53
- [119] S. V. Alyabyshev, M. Lemeshko, and R. V. Krems. Sensitive imaging of electromagnetic fields with paramagnetic polar molecules. *Phys. Rev. A*, 86:013409, Jul 2012. → pages 53
- [120] J. D. Weinstein, R. deCarvalho, T. Guillet, B. Friedrich, and J. M. Doyle. Magnetic trapping of calcium monohydride molecules at millikelvin temperatures. *Nature*, 395:148, Jan 1998. → pages 53, 82, 83, 87
- [121] T. V. Tscherbul, Y. V. Suleimanov, V. Aquilanti, and R. V. Krems. Magnetic field modification of ultracold molecule-molecule collisions. *New J. Phys.*, 11(5):055021, 2009. → pages 54, 71
- [122] J. Perez-Rios, J. Campos-Martinez, and M. I. Hernandez. Ultracold $O_2 + O_2$ collisions in a magnetic field: On the role of the potential energy surface. *J. Chem. Phys.*, 134(12):124310, 2011. → pages 54
- [123] L. M. C. Janssen, P. S. Żuchowski, Ad van der Avoird, G. C. Groenenboom, and J. M. Hutson. Cold and ultracold NH-NH collisions in magnetic fields. *Phys. Rev. A*, 83:022713, Feb 2011. → pages 54
- [124] R. N. Zare. *Angular Momentum: Understanding Spatial Aspects in Chemistry and Physics*. Wiley-Interscience, 2.5 edition, 1988. → pages 55, 71

- [125] E. Abrahamsson, T. V. Tscherbul, and R. V. Krems. Inelastic collisions of cold polar molecules in nonparallel electric and magnetic fields. *J. Chem. Phys.*, 127(4):044302, 2007. → pages 58
- [126] B. Friedrich and D. Herschbach. Steric proficiency of polar $^2\Sigma$ molecules in congruent electric and magnetic fields. *Phys. Chem. Chem. Phys.*, 2:419–428, 2000. → pages 58, 83
- [127] T. V. Tscherbul and R. V. Krems. Controlling electronic spin relaxation of cold molecules with electric fields. *Phys. Rev. Lett.*, 97:083201, Aug 2006. → pages 61, 83
- [128] R. V. Krems, A. Dalgarno, N. Balakrishnan, and G. C. Groenenboom. Spin-flipping transitions in $^2\Sigma$ molecules induced by collisions with structureless atoms. *Phys. Rev. A*, 67:060703, Jun 2003. → pages 68
- [129] J. M. Hutson. Feshbach resonances in ultracold atomic and molecular collisions: threshold behaviour and suppression of poles in scattering lengths. *New J. Phys.*, 9(5):152, 2007. → pages 71, 73, 74, 77
- [130] S. V. Alyabyshev, T. V. Tscherbul, and R. V. Krems. Microwave-laser-field modification of molecular collisions at low temperatures. *Phys. Rev. A*, 79(5):060703, 2009. → pages 74, 76
- [131] M. L. Gonzalez-Martinez and J. M. Hutson. Ultracold atom-molecule collisions and bound states in magnetic fields: Tuning zero-energy Feshbach resonances in He-NH($^3\Sigma^-$). *Phys. Rev. A*, 75:022702, Feb 2007. → pages 74
- [132] L. M. C. Janssen, G. C. Groenenboom, Ad van der Avoird, P. S. Zuchowski, and R. Podeszwa. Ab initio potential energy surfaces for NH($^3\Sigma^-$)-NH($^3\Sigma^-$) with analytical long range. *J. Chem. Phys.*, 131(22):224314, 2009. → pages 74, 76
- [133] S. V. Alyabyshev and R. V. Krems. Controlling collisional spin relaxation of cold molecules with microwave laser fields. *Phys. Rev. A*, 80:033419, Sep 2009. → pages 76
- [134] J. M. Brown, S. J. Smullin, T. W. Kornack, and M. V. Romalis. New limit on Lorentz- and CPT-violating neutron spin interactions. *Phys. Rev. Lett.*, 105:151604, Oct 2010. → pages 80
- [135] W. P. Delaney and D. Etter. Report of the defense science board task force on unexploded ordinance, 2003. → pages 80

- [136] H. Xia, A. Ben-Amar Baranga, D. Hoffman, and M. V. Romalis. Magnetoencephalography with an atomic magnetometer. *Appl. Phys. Lett.*, 89:211104, 2006. → pages 80
- [137] G. Bison, R. Wynands, and A. Weis. Dynamical mapping of the human cardiomagnetic field with a room-temperature, laser-optical sensor. *Opt. Exp.*, 11:904, 2003. → pages 80
- [138] E. Ramsden. *Hall-Effect Sensors*. Newnes, Oxford, UK, 2006. → pages 81
- [139] M. E. Huber, N. C. Koshnick, H. Bluhm, L. J. Archuleta, T. Azua, P. G. Björnsson, B. W. Gardner, S. T. Halloran, E. A. Lucero, and K. A. Moler. Gradiometric micro-SQUID susceptometer for scanning measurements of mesoscopic samples. *Rev. Sci. Instrum.*, 79:053704, 2008. → pages 81
- [140] M. Poggio and C. L. Degen. Force-detected nuclear magnetic resonance: recent advances and future challenges. *Nanotechnology*, 21:342001, 2010. → pages 81
- [141] B. Gojdka, R. Jahns, K. Meurisch, H. Greve, R. Adelung, E. Quandt, R. Knöchel, and F. Faupel. Fully integrable magnetic field sensor based on delta-E effect. *Appl. Phys. Lett.*, 99:223502, 2011. → pages 81
- [142] J. M. Taylor, P. Cappellaro, L. Childress, L. Jiang, D. Budker, P. R. Hemmer, A. Yacoby, R. Walsworth, and M. D. Lukin. High-sensitivity diamond magnetometer with nanoscale resolution. *Nature Phys.*, 4:810, 2008. → pages 81
- [143] D. Budker and M. Romalis. Optical magnetometry. *Nature Phys.*, 3:227, 2007. → pages 81
- [144] H. B. Dang, A. C. Maloof, and M. V. Romalis. Ultrahigh sensitivity magnetic field and magnetization measurements with an atomic magnetometer. *Appl. Phys. Lett.*, 97:151110, 2010. → pages 81
- [145] N. Zhao, J.-L. Hu, S.-W. Ho, J. T. K. Wan, and R. B. Liu. Atomic-scale magnetometry of distant nuclear spin clusters via nitrogen-vacancy spin in diamond. *Nature Nanotech.*, 6:242, 2011. → pages 81
- [146] M. Schaffry, E. Gauger, J. Morton, and S. Benjamin. Proposed spin amplification for magnetic sensors employing crystal defects. *Phys. Rev. Lett.*, 107:207210, 2011. → pages 81

- [147] C. C. Williams, J. Slinkman, W. P. Hough, and H. K. Wickramasinghe. Lateral dopant profiling with 200 nm resolution by scanning capacitance microscopy. *Appl. Phys. Lett.*, 55:1662, 1989. → pages 81
- [148] A. K. Henning, T. Hochwitz, J. Slinkman, J. Never, S. Hoffmann, P. Kaszuba, and C. Daghljan. Two-dimensional surface dopant profiling in silicon using scanning kelvin probe microscope. *J. Appl. Phys.*, 77:1888, 1995. → pages 81
- [149] C. Schönenberger and S. F. Alvarado. Observation of single charge carriers by force microscopy. *Phys. Rev. Lett.*, 65:3162–3164, Dec 1990. → pages 81
- [150] M. H. Devoret and R. J. Schoelkopf. Amplifying quantum signals with the single-electron transistor. *Nature*, 406:1039, 2000. → pages 81
- [151] F. Dolde, H. Fedder, M. W. Doherty, T. Nöbauer, F. Rempp, G. Balasubramanian, T. Wolf, F. Reinhard, L. C. L. Hollenberg, F. Jelezko, and J. Wrachtrup. Electric-field sensing using single diamond spins. *Nature Phys.*, 7:459, 2011. → pages 81
- [152] S. van de Meerakker, P. Smeets, N. Vanhaecke, R. Jongma, and G. Meijer. Deceleration and electrostatic trapping of OH radicals. *Phys. Rev. Lett.*, 94:023004, 2005. → pages 82, 83
- [153] E. S. Shuman, J. F. Barry, and D. DeMille. Laser cooling of a diatomic molecule. *Nature*, 467:820, 2010. → pages 83, 88
- [154] E. S. Shuman, J. F. Barry, D. R. Glenn, and D. DeMille. Radiative force from optical cycling on a diatomic molecule. *Phys. Rev. Lett.*, 103:223001, Nov 2009. → pages 82, 83, 88
- [155] S. Ospelkaus, K.-K. Ni, G. Quémener, B. Neyenhuis, D. Wang, M. H. G. de Miranda, J. L. Bohn, J. Ye, and D. S. Jin. Controlling the hyperfine state of rovibronic ground-state polar molecules. *Phys. Rev. Lett.*, 104:030402, Jan 2010. → pages 83
- [156] W. L. Chan, J. Deibel, and D. M. Mittleman. Imaging with terahertz radiation. *Rep. Prog. Phys.*, 70(8):1325, 2007. → pages 89
- [157] J. Deiglmayr, A. Grochola, M. Repp, K. Mörtlbauer, C. Glück, J. Lange, O. Dulieu, R. Wester, and M. Weidemüller. Formation of ultracold polar molecules in the rovibrational ground state. *Phys. Rev. Lett.*, 101:133004, Sep 2008. → pages 91

- [158] J. F. Barry, E. S. Shuman, E. B. Norrgard, and D. DeMille. Laser radiation pressure slowing of a molecular beam. *Phys. Rev. Lett.*, 108:103002, Mar 2012. → pages 91
- [159] A. Chotia, B. Neyenhuis, S. A. Moses, Bo Yan, J. P. Covey, M. Foss-Feig, A. M. Rey, D. S. Jin, and J. Ye. Long-lived dipolar molecules and Feshbach molecules in a 3D optical lattice. *Phys. Rev. Lett.*, 108:080405, Feb 2012. → pages 91
- [160] A. Micheli, Z. Idziaszek, G. Pupillo, M. A. Baranov, P. Zoller, and P. S. Julienne. Universal rates for reactive ultracold polar molecules in reduced dimensions. *Phys. Rev. Lett.*, 105:073202, Aug 2010. → pages 92
- [161] P. S. Julienne, T. M. Hanna, and Z. Idziaszek. Universal ultracold collision rates for polar molecules of two alkali-metal atoms. *Phys. Chem. Chem. Phys.*, 13:19114–19124, 2011. → pages
- [162] C. Ticknor. Two-dimensional dipolar scattering with a tilt. *Phys. Rev. A*, 84:032702, Sep 2011. → pages
- [163] J. P. D’Incao and C. H. Greene. Collisional aspects of bosonic and fermionic dipoles in quasi-two-dimensional confining geometries. *Phys. Rev. A*, 83:030702, Mar 2011. → pages
- [164] G. Quéméner and J. L. Bohn. Dynamics of ultracold molecules in confined geometry and electric field. *Phys. Rev. A*, 83:012705, Jan 2011. → pages 92
- [165] M. H. G. de Miranda, A. Chotia, B. Neyenhuis, Wang. D, G. Quemener, S. Ospelkaus, J. L. Bohn, J. Ye, and D.S. Jin. Controlling the quantum stereodynamics of ultracold bimolecular reactions. *Nature Phys.*, 7:502, Oct. 2011. → pages 92